NASA CR-66378

CONCEPTUAL MECHANIZATION STUDIES FOR A HORIZON DEFINITION SPACECRAFT ELECTRICAL POWER SUBSYSTEM

Horizon Definition Study

May 1967

Prepared under Contract No. NAS 1-6010 by

HONEYWELL INC., Systems & Research Division, Minneapolis, Minn.; GULTON INDUSTRIES INC.; and TEXTRON ELECTRONICS INC.; Spectrolab Division

for

NATIONAL AERONAUTICS AND SPACE ADMINISTRATION

May 1967

NASA CR-66378

CONCEPTUAL MECHANIZATION STUDIES FOR A HORIZON DEFINITION SPACECRAFT ELECTRICAL POWER SUBSYSTEM

By Otto L. Jourdan, Honeywell Inc.
Jay A. Cox, Gulton Industries, Inc.
John D. Gum, Spectrolab
Karl Preusse, Gulton Industries, Inc.
James J. Baltes, Honeywell Inc.
David J. Hartman, Honeywell Inc.
Fred E. Betz, Gulton Industries, Inc.
Burton J. McComb, Gulton Industries, Inc.

ABSTRACT

A solar cell-battery electrical power subsystem was developed which is compatible with the Horizon Definition Study spacecraft. This subsystem is capable of delivering 70 watts ot continuous electrical power for one year in a sun-synchronous, 3 o'clock nodal crossing, 500 km orbit.

NASA CR - 66378

CONCEPTUAL MECHANIZATION STUDIES FOR A HORIZON DEFINITION SPACECRAFT ELECTRICAL POWER SUBSYSTEM

By Otto L. Jourdan, Honeywell Inc.
Jay A. Cox, Gulton Industries Inc.
John D. Gum, Spectrolab
Karl Preusse, Gulton Industries Inc.
James J. Baltes, Honeywell Inc.
David J. Hartman, Honeywell Inc.
Fred E. Betz, Gulton Industries Inc.
Burton J. McComb, Gulton Industries Inc.

HORIZON DEFINITION STUDY

MAY 1967

Prepared under Contract No. NAS 1-6010 by
Honeywell Inc.
Systems and Research Division
Minneapolis, Minnesota;
Gulton Industries Inc.; and
Textron Electronics Inc., Spectrolab Division

for

NATIONAL AERONAUTICS AND SPACE ADMINISTRATION

FOREWORD

This report documents Phase A, Part II of An Analytical and Conceptual Design Study for an Earth Coverage Infrared Horizon Definition Study performed under National Aeronautics and Space Administration Contract NAS 1-6010 for Langley Research Center.

The Horizon Definition Study was performed in two parts. Part I, which was previously documented, provided for delineation of the experimental data required to define the infrared horizon on a global basis for all temporal and spatial periods. Once defined, the capabilities of a number of flight techniques to collect the experimental data were evaluated. The Part II, documented in this report, provides a measurement program plan which satisfies the data requirements established in the Part I study. Design requirements and the conceptual design for feasibility of the flight payload and associated subsystems to implement the required data collection task are established and documented within this study effort.

Honeywell Inc., Systems and Research Division, performed this study program under the technical direction of Mr. L. G. Larson. The program was conducted from 28 March 1966 to 10 October 1966 (Part I) and from 10 October 1966 to 29 May 1967 (Part II). This Part II portion of the study was the joint effort of Gulton Industries Inc.; Textron Electronics Inc., Spectrolab Division; and Honeywell Inc.

Gratitude is extended to NASA Langley Research Center for their technical guidance, under the program technical direction of Messrs. L. S. Keafer and J. A. Dodgen with direct assistance from Messrs. W. C. Dixon, Jr., E. C. Foudriat, H. J. Curfman, Jr., and G. A. Haynes, Jr., as well as the many people within their organization.

CONTENTS

ILLUSTRATIONS

TABLES

CONCEPTUAL MECHANIZATION STUDIES FOR A HORIZON DEFINITION SPACECRAFT ELECTRICAL POWER SUBSYSTEM

By Otto L. Jourdan, Honeywell Inc.
Jay A. Cox, Gulton Industries Inc.
John D. Gum, Spectrolab
Karl Preusse, Gulton Industries Inc.
James J. Baltes, Honeywell Inc.
David J. Hartman, Honeywell Inc.
Fred E. Betz, Gulton Industries Inc.
Burton J. McComb, Gulton Industries Inc.

SUMMARY

This report describes the electrical power utilization of a spacecraft system concept which satisfies the requirements of the Horizon Definition Study. A feasible electrical power subsystem capable of supplying the required electrical power is recommended.

The recommended electrical power subsystem is capable of deliverying 70 watts of continuous electrical power for one year in a sun-synchronous, 3 o'clock nodal crossing, 500 km orbit. The subsystem basically consists of six passively oriented solar panels, two nickel-cadmium electrical storage batteries, battery charge regulators, system controls, and two bus regulators. System protection and isolation of redundant loads are provided.

INTRODUCTION

The electrical power subsystems study documented herein is a portion of the Horizon Definition Study (HDS) conducted for NASA Langley Research Center, Contract NAS 1-6010, Part II. The purpose of the Horizon Definition Study is to develop a complete horizon radiance profile measurement program to provide data which can be used to determine the earth's atmospheric state, especially at high altitudes. These data can then be effectively used in many atmospheric sciences studies and in the design of instruments and measurement systems which use the earth's horizon as a reference.

Part I of the HDS resulted in the following significant contributions to the definition of the earth's radiance in the infrared spectrum:

- The accumulation of a significant body of meteorological data covering a major portion of the Northern Hemisphere.
- Computation of a large body of synthesized horizon radiance profiles from actual temperature profiles obtained by rocket soundings.
- Generation of a very accurate analytical model and computer program for converting the temperature profiles to infrared horizon profiles (as a function of altitude).
- An initial definition of the quantity, quality, and sampling methodology required to define the earth's infrared horizon in the CO_2 absorption band for all temporal and spatial conditions.
- An evaluation of the cost and mission success probabilities of a series of flight techniques which could be used to gather the radiance data. A rolling-wheel spacecraft was selected in a nominal 500 km polar orbit.

The Part II study effort was directed toward the development of a conceptually feasible measurement system, which includes a spacecraft to accomplish the measurement program developed in Part I. In the Part II HDS, a number of scientific and engineering disciplines were exercised simultaneously to design conceptually the required system. Accomplishments of Part II of the study are listed below:

- The scientific experimenter refined the sampling methodology used by the measurement system. This portion of the study recommends the accumulation of approximately 380 000 radiance profiles taken with a sampling rate that varies with the spacecraft's latitudinal position.

- A conceptual design was defined for a radiometer capable of resolving the earth's radiance in the 15-micron spectrum to 0.01 watt/meter^2-steradian with an upper level of response of 7.0 watt/meter^2-steradian.

- A starmapper and attitude determination technique were defined capable of determining the pointing direction of the spacecraft radiometer to an accuracy of 0.25 km in tangent height at the earth's horizon.

  The combination of the radiometer and starmapper instruments is defined as the mission experiment package.

- A solar cell-battery electrical power subsystem conceptual design was defined which is completely compatible with the orbital and experiment constraints. This system is capable of delivering 70 watts of continuous electrical power for one year in the sun-synchronous, 3 o'clock nodal crossing, 500 km orbit.

- A data-handling subsystem conceptual design was defined which is capable of processing in digital form all scientific and status data from the spacecraft. This subsystem is completely solid state and is designed to store the 515 455 bits of digital information obtained in one orbit of the earth. This subsystem also includes command verification and execute logic.

- A communications subsystem conceptual design was defined to interface between the data-handling system of the spacecraft and the STADAN network. The 136 MHz band is used for primary data transmission and S band is used for the range and range-rate transponder.

- A spacecraft structural concept was evolved to contain, align, and protect the spaceborne subsystems within their prescribed environmental constraints. The spacecraft is compatible with the Thor-Delta launch vehicle.

- An open-loop, ground-commanded attitude control subsystem conceptual design was defined utilizing primarily magnetic torquing which interacts with the earth's field as the force for correcting attitude and spin rates.

- The Thor-Delta booster, which provides low cost and adequate capability, was selected from the 1972 NASA "stable".

- Western Test Range was selected as the launch site due to polar orbit requirements. This site has adequate facilities, except for minor modifications, and is compatible with the polar orbital requirements.

This report contains documentation of those areas of study directly related to the conceptual design of the electrical power subsystem on the vehicle. The objectives of these studies were as follows:

- To determine the electrical power utilization of all on-board electrical subsystems.

- To define design requirements for an electrical power subsystem and develop a feasible concept which would realize the program objectives and achieve compatibility with the overall spacecraft concept, experiment requirements, and all the constraints which have evolved during both phases of the Horizon Definition Study.

The detailed study performed to meet these objectives is presented in the following pages.

STUDY REQUIREMENTS AND OBJECTIVES

Basic system requirements are those defined by the original statement of work, Phase A Part I results, and NASA instructions.

The following list itemizes the primary and secondary requirements of the Horizon Definition Study.

BASIC REQUIREMENTS

Radiance Profile Measurements

- Spectral interval: 615 to 715 cm^{-1} (14.0 to 16.28μ)
- Profile accuracy
  - ► Tangent height range: +80 km to -30 km
  - ► Instantaneous value of radiance measured must be assignable to a tangent height value to within ±0.25 km.
  - ► Radiance characteristics and resolution:

    Maximum peak radiance = 7.0 W/m^2 - sr.

    Minimum peak radiance = 3.0 W/m^2 - sr.

    Maximum slope = 0.6 W/m^2 - sr - km.

    Minimum slope = 0.02 W/m^2 - sr - km.

    Maximum slope change = 0.15 W/m^2 - sr - km^2.

    Radiance magnitude resolution = 0.01 W/m^2 - sr.
  - ► Horizontal resolution: 25 km
- Data requirements - Data requirements for the Horizon Definition Study (HDS) experiment, as refined during the study, are as follows:

  Minimum requirements. --
  - ► One-year continuous coverage
  - ► "Uniform" time sampling in each space cell over each time cell, i.e., no more than two samples/space cell/day
  - ► 13 time cells (28 days/cell)
  - ► 408 space cells

Latitude (60°S to 60°N)	320
Latitude (60°N to 90°N)	44
Latitude (60°S to 90°S)	44

- Samples per cell

Latitude (0° to 60°)	16
Latitude (60° to 90°)	38

- Total samples (one year) 110 032

Recommended requirements. --

- One-year continuous coverage
- Maximum of 10° latitude separation between successive samples
- 13 time cells (28 days/cell)
- 588 space cells:

Latitude (30°S to 30°N)	128
Latitude (30°N to 60°N)	134
Latitude (60°N to 82.6°N)	96
Latitude (30°S to 60°S)	134
Latitude (60°S to 82.6°S)	96

- Average number of samples per cell:

Latitude (30°S to 30°N)	45
Latitude (30°N to 60°N)	39
Latitude (60°N to 82.6°N)	67
Latitude (30°S to 60°S)	39
Latitude (60°S to 82.6°S)	67

- Total samples (one year) 378 508

Mission Profile

Nominal circular, polar orbit of approximately 500 km altitude.

Tracking and Data Acquisition

Limited to the existing Satellite Tracking And Data Acquisition Network (STADAN) with minimum modification.

Experiment Package

- Passive radiometric and attitude measurements with redundancy (more than one unit) in the research package for the radiometer and attitude determination device.
- Minimum scan rate >0. 5 scans/min average.
- Maximum scan angle with respect to orbit plane ≤5°.

Spacecraft

- Rolling-wheel configuration (spin axis normal to the orbit plane).
- Weight in less than 800 pound class mandatory.

State of the Art

Proven subsystems shall be employed wherever possible.

Mission Effectiveness/Reliability

Reliability shall be approached on the basis of "designing in" successful performance of the one-year, data-collection mission, i.e., the effort is to be biased strongly toward mission effectiveness. Consequently, the mission effectiveness/reliability effort should involve continuing tradeoffs in each subfunction area against the criteria of maximum effectiveness. A numerical estimate of the probable system MTBF shall be made on the final configured system.

Strong consideration should be given to the use of reserve spacecraft as a "backup" means rather than as a continuously ready standby. Specifically, the "backup" concept (as opposed to continuously ready) is of more significance on a Thor-Delta sized vehicle than on a Scout vehicle.

ELECTRICAL POWER SUBSYSTEM REQUIREMENTS

The electrical power subsystem requirements are the result of the functional analysis and other Part II studies. These subsystem requirements state what is necessary to satisfy the mission and basic requirements and are listed below.

- Provide spacecraft electrical power source - The solar array must supply load plus system losses and charge battery under following conditions:

- ► Sun angle - 64 degrees maximum
  - 31 degrees minimum
- ► Shadow fraction - 0. 364 maximum
  - 0. 26 minimum
- ► Radiation - 270 nautical mile, near-polar orbit plus solar flares
- ► Orientation - Passive on spin-stabilized vehicle
- ► Configuration - Must not interfere with radiometer or starmapper field of view

- Store electrical energy - The battery must supply load plus system regulation and control losses under following conditions:
  - ► Charge - discharge cycles - 5600
  - ► Shadow fraction - 0. 364 maximum
    - 0. 26 minimum

- Regulate and control electrical power
  - ► Electrical load

    70 watts continuous for one year

    96 watt peak for 4 minutes every 94 minutes
  - ► Power characteristics

    50 watts, 28 volts dc ±2% regulation

    0. 25% peak-to-peak ripple

    20 watts, 5 volts dc ±5% regulation

    1. 0% peak-to-peak ripple

- Distribute electrical power
  - ► Provide electrical fault protection and isolation
  - ► Provide electromagnetic compatibility
  - ► Provide magnetic moment compatible with attitude control and determination

ELECTRICAL POWER UTILIZATION

The following section describes the electrical power utilization of the HDS spacecraft.

ELECTRICAL LOADS

Electrical Load Analysis

Average electrical energy requirements for the Horizon Definition Study (HDS) spacecraft do not display extreme variation from orbit to orbit or between spacecraft night and day, since the radiometer utilized in the experiment is required to make continuous measurements during the entire life of the spacecraft.

Possible variations in average energy requirements which must be considered are due to utilizing system redundancy, attitude control torquing modes, starmapper - sun sensor interface, and available and/or required spacecraft tracking time.

The maximum average electrical load which can occur during the HDS spacecraft lifetime is 63. 7 watts (Table 1). This maximum load occurs only during the several orbits when all redundant units are energized simultaneously to allow the outputs of the radiometer and redundant starmappers and sun sensors to be correlated.

Another maximum load condition will occur during the first day after spacecraft launch. During this first day, the attitude control system will be torquing to orient the spacecraft within the required tolerances, and the range and range-rate transponder will be operating for a maximum percentage of available time to determine accurately the orbit parameters. Orbit analysis has shown that the spacecraft will be in view of a ground station for as long as 20 minutes during a single orbit and that the transponder could be transmitting for two to three hours during the first day. Average power requirements during this mode of operation will be 60. 7 watts.

The nominal spacecraft operating mode, occurring for the highest number of spacecraft orbits, will require operation of only a single radiometer, starmapper, and sun sensor. The attitude control system will not be torquing, and the telemetry transmitter and range and range-rate transmitter will each transmit for an average of two minutes in this operating mode. Average electrical power requirements for the nominal orbit will be 56. 0 watts.

HDS power-utilizing equipment has been divided into 10 subsystems to facilitate analysis as shown in the electrical load analysis of Table 1. The power requirements of each subsystem are as follows:

TABLE 1. - ELECTRICAL LOAD ANALYSIS

Subsystem no.	Item	Standby power, watts	Peak power, watts	Peaks per orbit	Time per peak, minutes	Average watts/ item	Power /orbit/ subsystem, watts
1	Radiometer	11.0	11.0	--	--	--	11.0
2	Starmapper	10.0	10.0	--	--	--	10.0
3	Sun sensor	1.0	1.0	--	--	--	1.0
4	System timing and control	3.9	5.7	1	2	--	3.94
4A	Command verifier and decoder	0.2	2.0	1	2	0.24	--
4B	Timing oscillator	0.7	0.7	--	--	0.7	--
4C	Time register	1.0	1.0	--	--	1.0	--
4D	Timing and control	2.0	2.0	--	--	2.0	--
5	Storage	2.72	2.72	--	--	--	2.72
5A	Main storage	0.72	0.72	--	--	0.72	--
5B	Multiplexer and buffer storage	2.0	2.0	--	--	2.0	--
6	Formatter	2.0	2.0	--	--	--	2.0
7	Data collection and control	12.7	12.7	--	--	--	12.7
7A	10 bit A/D converter	3.0	3.0	--	--	3.0	--
7B	Starmapper digitization	4.0	4.0	--	--	4.0	--
7C	8-bit multiplexer	4.2	4.2	--	--	4.2	--
7D	Status A/D converter	1.5	1.5	--	--	1.5	--
8	Communications	9.22	--	--	--	--	9.6
8A	Command receiver	0.22	0.22	--	--	0.22	--
8B	Telemetry transmitter	--	5.0	1	2	0.12	--
8C	Tracking beacon	5.0	5.0	--	--	5.0	--
8D	Range and range-rate transponder	4.0	15.8	1	2	4.26	--
9	Attitude control	5.5	10.0	1	47.3	--	7.75
10	Miscellaneous control circuits	3.0	3.0	--	--	--	3.0
	Total						63.7

1) Radiometer - 11 watts average/orbit.

The radiometer utilizes redundant calibration sources, choppers, electronics, and detectors within a single optical system. Both radiometer detectors, detector preamplifiers, and telemetry input preamplifiers are normally energized along with a single chopper and a single calibration unit. The stepper for the calibration unit draws five three-watt-millisecond pulses of power each revolution of the spacecraft about its spin axis.

2) Starmapper - 5 watts average/orbit each.

Two starmappers are provided on the spacecraft, only one of which is normally energized. Power-utilizing components are the detector electronics and filters and the photomultipler high-voltage power supply. The starmapper operates only during the dark portions of each orbit; however, a reverse potential must be applied to the photomultiplier tube during the sunlit portion of the orbit. Therefore, input power requirements do not vary significantly between spacecraft day and night. The alternate starmapper is shuttered when it is de-energized.

3) Sun sensor - 0.5 watt average/orbit each.

Two sun sensors are provided on the spacecraft, only one is normally energized. Power is required for signal amplification.

4) System timing and control - 3.94 watts average/orbit.

The system timing and control subsystem verifies and decodes ground commands, provides the spacecraft time reference, and provides control commands from the time register. This subsystem requires 3.94 watts average per orbit and has a 5.7 watt peak for approximately two minutes each orbit.

5) Storage - 2.72 watts average/orbit.

This subsystem stores experiment and spacecraft status data. The subsystem requires 2.72 watts and is energized continuously.

6) Formatter - 2 watts average/orbit.

This subsystem adds synchronizing and parity checking bits to the data. The subsystem requires two watts and is energized continuously.

7) Data collection and control - 12.7 watts average/orbit.

This subsystem provides analog-to-digital conversion and selects the data source and formats for uniform storage words. This subsystem requires 12.7 watts and is energized continuously.

8) Communication subsystem - 9.6 watts average/orbit.

The communications subsystem provides a data link for transfer of experiment and engineering information between the spacecraft and ground stations, and it provides a means of determining the exact orbit of the spacecraft.

A vhf system basically consisting of a command receiver and a transmitter is used for the data link. The command receiver is on continuously and requires 0.22 watts of electrical power. The transmitter is used for two minutes each orbit and requires five watts of power while transmitting.

HDS spacecraft orbit determination is supplied by a tracking beacon and an S-band, range and range-rate transponder. The tracking beacon is supplied by a vhf transmitter, identical to the data-link transmitter, which is energized continuously. The tracking-beacon transmitter can also be used to transfer experiment and engineering data in the event of a failure of the data-link transmitter.

The range and range-rate transponder requires four watts of power in the standby mode and 15.8 watts during interrogation. The transponder can be transmitting as much as 20 minutes per orbit during early orbits; however, the average "on" time during the one-year operation will not exceed two minutes per orbit. The range and range-rate transponder can also be used as a spacecraft data link.

9) Attitude control subsystem - 7.75 watts average/orbit.

The attitude control subsystem controls the spin rate and attitude of the spacecraft. The spacecraft is initially spun up to approximately three rpm and oriented to the correct sun angle by the launch vehicle prior to separation. The spacecraft system then maintains the spin rate and correct sun angle.

The attitude control V-head horizon sensor, logic, and residual coil are energized continuously and require 5.5 watts of electrical power. The torquer and spin coils require an additional 4.5 watts and are energized for one-half orbit every 5 to 20 orbits.

10) Miscellaneous control circuits - 3 watts average/orbit.

Three watts have been allocated for control circuits which are not part of any specific subsystem. These circuits include system monitoring, magnetic compensation, system protection, etc.

Electrical Power Profile

Figure 1 shows a power utilization profile for the maximum load conditions shown by the load analysis. Peak system load is 73 watts.

Figure 2 shows a power utilization profile for the electrical load which will be typical for the greatest number of orbits during the year. Nominal peak load is 67. 5 watts.

Power system capacity at the load bus is also shown by the power profiles. The HDS electrical power system is configured to supply 70 watts of electrical power to the load continuously for one year and, in addition, to supply a 96-watt peak for four minutes every orbit.

The configured electrical system has a load capacity approximately 10 percent greater than the present maximum load requirements and 25 percent greater than present nominal power requirements. This reserve capacity is provided for distribution losses and contingency power.

ELECTRICAL POWER CHARACTERISTICS

Two bus voltages will be supplied: one at 28 volts for general purpose application and one at 5 volts primarily for systems utilizing integrated circuits. Regulation and power characteristics for the two buses have been chosen so as to provide the highest quality power consistent with a reliable power system.

From the power user's point of view, the ideal power system would supply perfectly regulated and noise-free voltage. Clearly, as soon as any line length is introduced between the power supply and the using subsystems, the effective power supply at the end of the line is degraded from the ideal by effects of the resistance and reactance of the lines. These factors set a fundamental lower limit to the effective output impedance of the power supply as seen by the subsystem.

The power system itself deviates from the ideal in two significant respects: first, it impresses a ripple upon the subsystem, and second, its output impedance is not zero; therefore, other using subsystems contribute an additional unwanted voltage to the output.

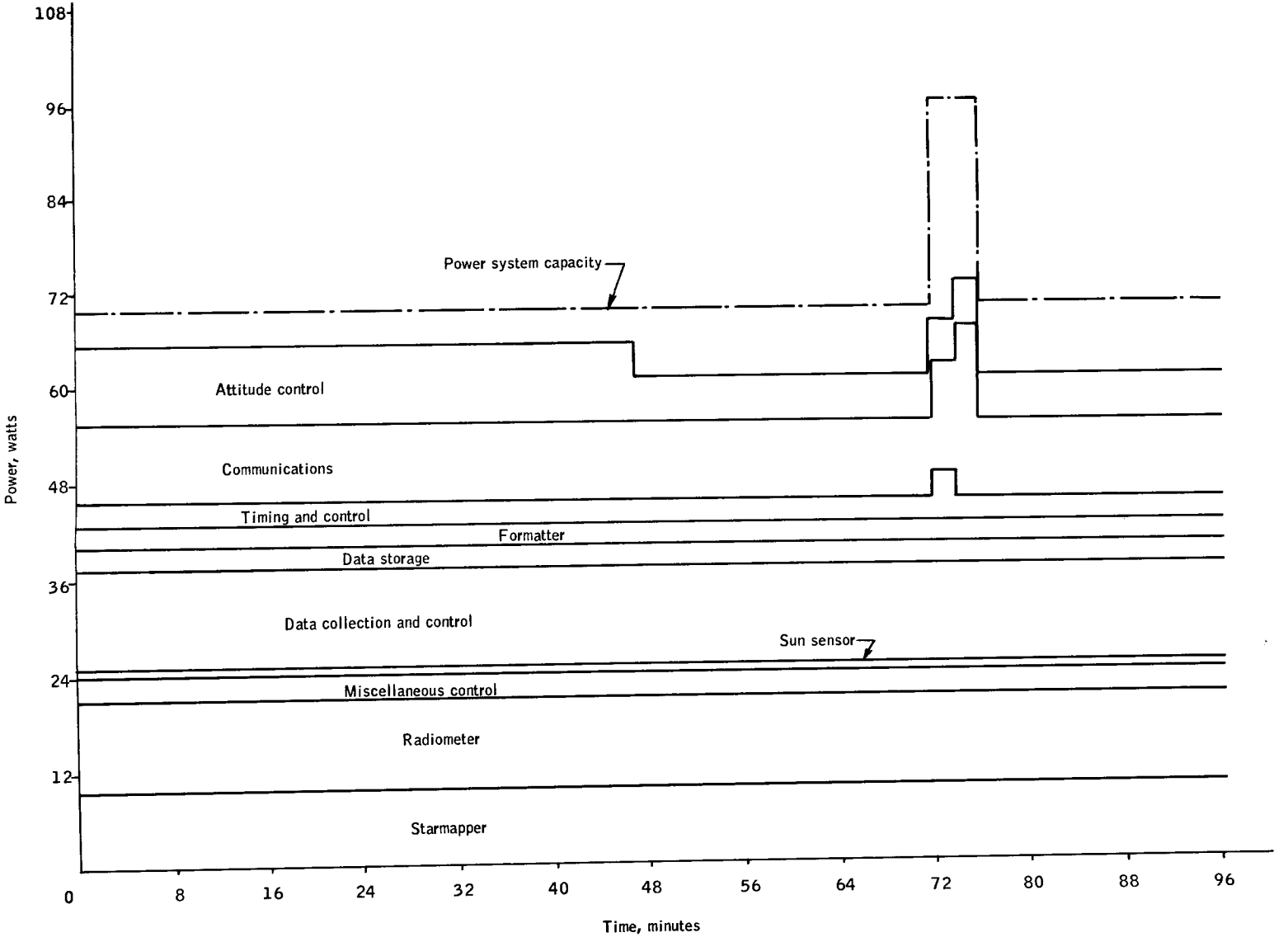

Figure 1. Power Utilization Profile for a Maximum Load Orbit

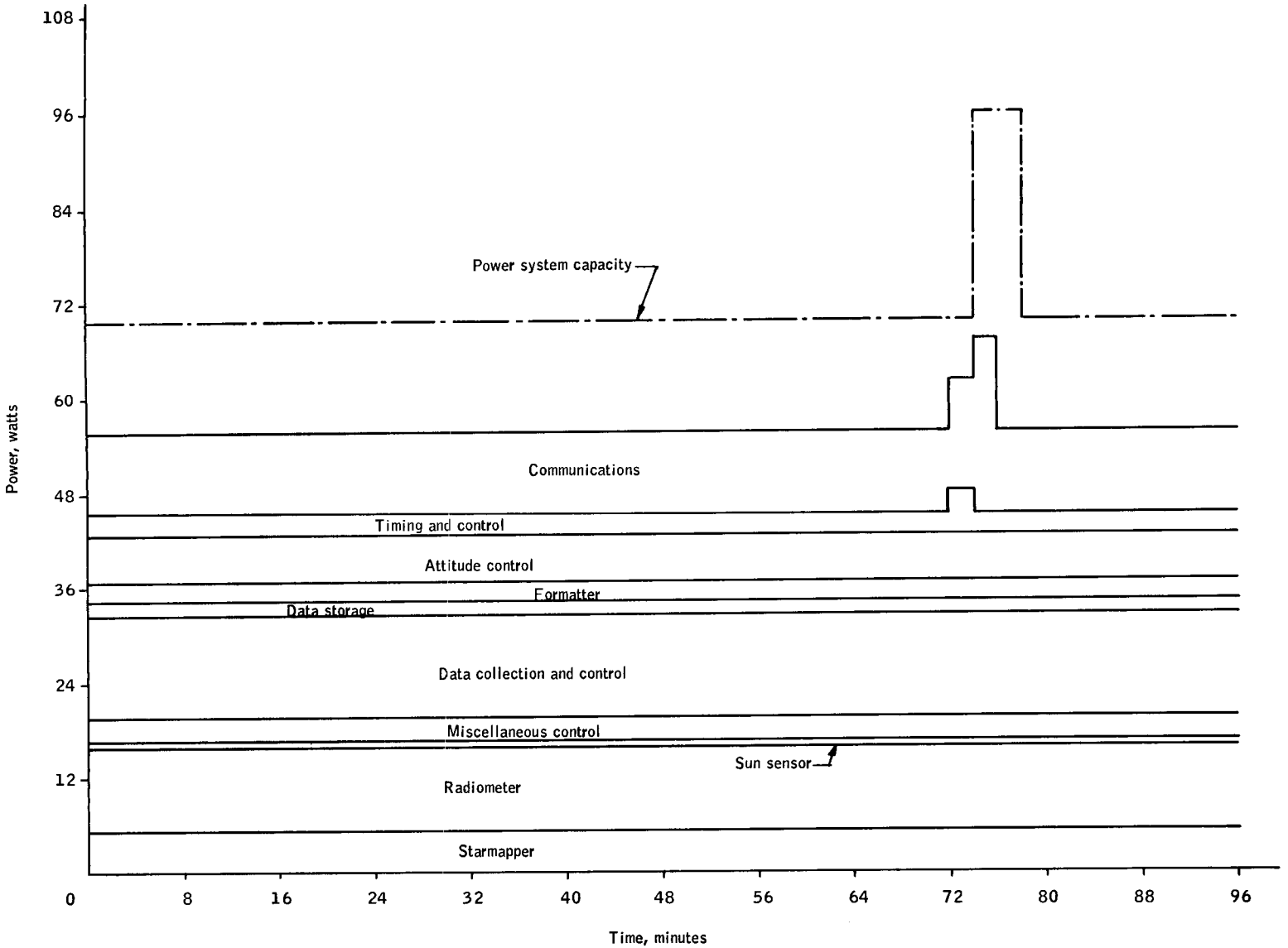

Figure 2. Power Utilization Profile for a Nominal Load Orbit

Constancy of the value of the output voltage is another question of interest to subsystem power users. In general, there are two levels of stability required. The most stable finds general applications in reference circuits where some comparison is made between a measurand and the reference. The stabilities are generally of the orders of fractions of a percent. The next order of stability required is that necessary to ensure that solid-state amplifier bias points are adequately stable. An adequate level here is of the order of a few percent. In view of the above-mentioned noise and common power supply difficulties, power of the reference quality should be regulated at the component level rather than at the general purpose bus.

The 28-volt power is recommended to be supplied directly from a three-terminal regulator and to have the following characteristics:

- Output impedance: 0.1 ohm maximum from dc to 5 kHz
  0.5 ohm from 5 kHz to 1 MHz
- Ripple: Less than 0.15 volt peak-to-peak
- Voltage stability: ±1 percent of nominal value over the complete temperature range

The five-volt power is recommended to be a four-terminal (that is, transformer isolated) source, the ground of which can be located as most desirable for the elimination of noise. Characteristics of this supply are:

- Output impedance: Less than 0.15 ohm from dc to 5 kHz
  Less than 0.5 ohm from 5 kHz to 1 MHz
- Ripple: Less than 0.1 volt peak-to-peak
- Voltage stability: Better than 0.15 volt from the room temperature value over the full temperature range.

ELECTRICAL POWER SYSTEM

This section describes the power system constraints, the tradeoff studies conducted to select a feasible concept, and a description of the recommended concept.

SYSTEM CONSTRAINTS

Orbit Constraints

The shadow fraction per orbit and the angle between the sun-line and the vehicle spin axis are shown in Figure 3 for the first year after launch. The angle of incidence relative to the vehicle spin axis will vary through the year on either side of the 45-degree nominal value. Taking into account the anticipated three-sigma limits for launch error, the angle of incidence from the sun-line to the spin axis can vary from a minimum of 31° to a maximum of 64° and is accompanied by variations in the magnitude of the shadow fraction. A limiting requirement for the power system is the 64-degree sun angle. The solar array must be approximately twice as large at a 64-degree sun angle (without active orientation) as the array required at a 31-degree sun angle and 1-1/2 times the size of the array required at a 45-degree sun angle. The one-year operation and the fact that the spacecraft enters the earth's shadow every orbit during the year also establishes the battery cycle life requirement at 5600 cycles. The orbit altitude, 500 km, establishes the radiation level and, consequently, the necessary allowance for solar cell degradation. The selected altitude is an optimum altitude as far as radiation degradation is concerned.

Spacecraft Constraints

The spacecraft is spin stabilized, rotating at 3 rpm, with the spin axis maintained in an orientation perpendicular to an earth radius and to the plane defined by the orbit.

The shape of the spacecraft is in the general form of a hexagonal right prism. This shape determines the number of solar panels (six) and the maximum width of each panel (27 inches).

The attitude of the spacecraft must be accurately known at all times. This prohibits the use of moving parts such as an actively oriented solar array. Also, the location and mounting angle of the solar array are restricted by the radiometer and starmapper field-of-view requirements. The attitude control system uses magnetic torquing. Attitude determination and control constraints also require an electrical power system whose magnetic moment is small and does not vary greatly during the life of the spacecraft.

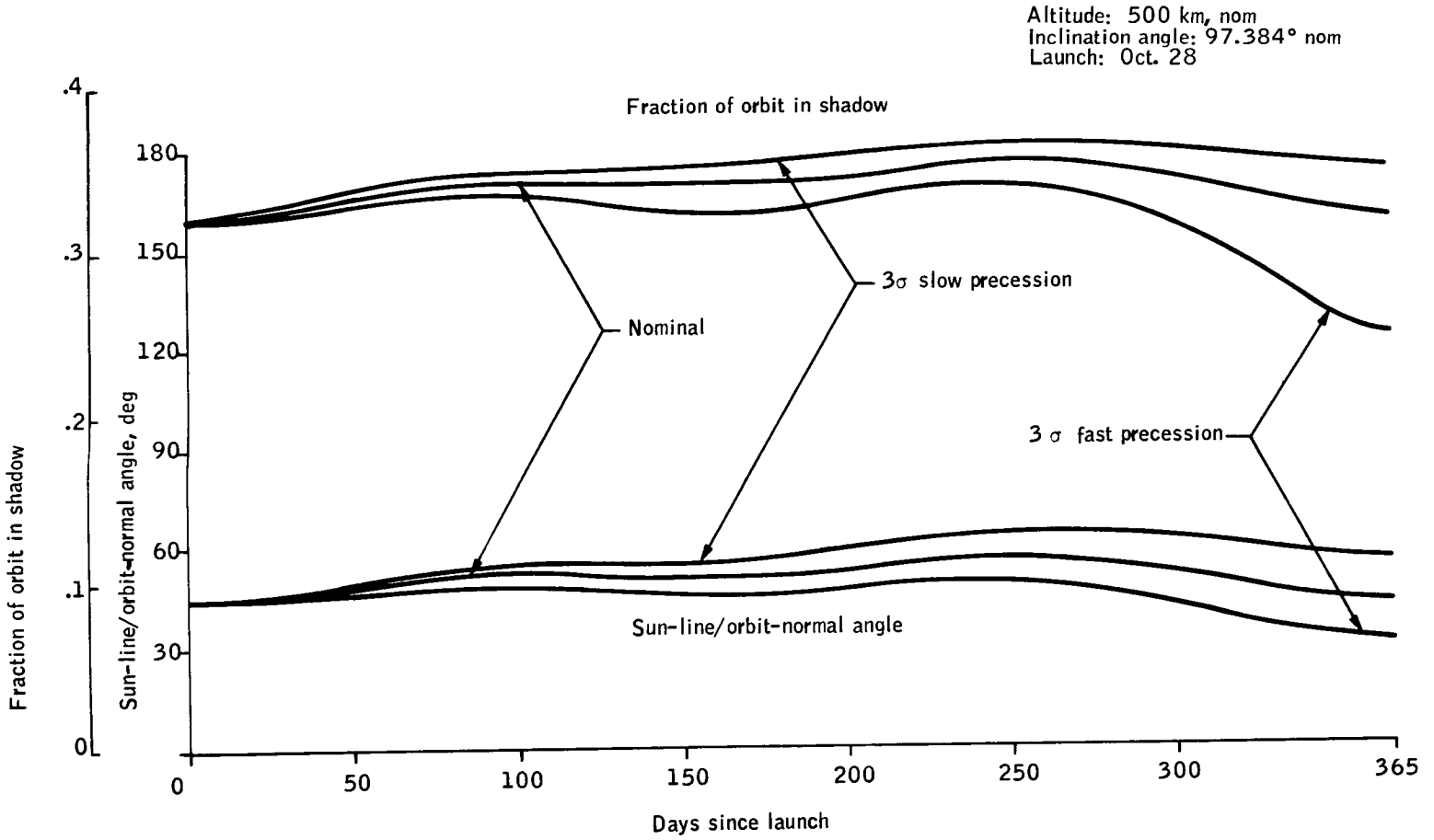

Figure 3. Sun-Synchronous 3 O'clock Orbit

Launch Vehicle Interface

The maximum spacecraft envelope is a cylinder 54 inches in diameter and 48 inches high. Maximum cylindrical diameter is limited by the Thor-Delta shroud. Cylindrical length is limited by spacecraft balance requirements and could be increased only in the event of an urgent conflicting design requirement. The above constraints determine the allowable length of the solar panels. The power system will also place a requirement on the launch vehicle for a signal to erect the solar panels prior to spin-up.

Environmental Effects

Environmental requirements for the power system are not severe. The temperature of internally mounted electrical power system components is being held to the relatively narrow 0° to 35° C range. The launch environment normally seen from the Thor-Delta system can be tolerated within the normal rating of standard aerospace components. The radiation environment, as previously noted, is low due to the low orbit. The most important environmental constraint will probably be the wiring and terminations to the experiment and low temperature baseplate, as well as the requirement that the electrical system shall not provide good heat conduction paths to these areas.

POWER SYSTEM TRADEOFFS

Energy Source

Three energy sources were considered to be potentially feasible for the HDS spacecraft. These three systems were: 1) fuel cell, 2) radioisotope-thermoelectric system, and 3) solar cell-battery. To be feasible, the system must meet technical performance requirements, be available in time to meet program flight schedules, and not add excessive costs to the program. Evaluation of the major characteristics of each system has led to the conclusion that a solar array-battery system is the best system for HDS.

Fuel cell. -- A cursory analysis immediately reveals that a fuel cell system is not technically feasible due to two factors:

- The life expectancy of available fuel batteries does not approach the one-year operational requirement.
- The weight of fuel and fuel tanks is prohibitive. For the HDS mission, fuel and fuel-tank weight would be in the range of 700 to 900 pounds, to which the weight of cells and system controls must be added to arrive at the total system weight.

Radioisotope. -- A radioisotope-thermoelectric source has the advantage of allowing complete flexibility in the choice of a spacecraft orbit. The isotope-thermoelectric system has the following interfaces with the spacecraft:

- A considerable amount of shielding is required to protect the spacecraft instruments from the isotope radiation.
- Special precautions are required to prevent the inherent high temperatures of the power system from limiting the life of the low temperature coolant associated with the radiometer.
- A battery charge control and regulator will be required to supply system peak loads to avoid sizing the system for the short duration peak load.

Results of the tradeoff study indicate that all of the foregoing interface problems can be solved within the power system weight allowances on the HDS spacecraft.

Cost and schedule considerations present more serious problems. As to delivery schedule, it seems clear that the development of a generator in time for an October 1969 launch is difficult although not impossible. Application of existing designs such as SNAP 19 or SNAP 27 do not seem feasible, since their existing configurations would impose restrictions on the design of the vehicle. Availability of the fuel is another consideration and is potentially limiting. Since the total fuel quantity is in short supply, program success would depend upon the allocation of an adequate priority in comparison to all other proposed programs competing for the fuel.

Development cost of an optimum generator is estimated at 10 million dollars; however, this cost probably would not be borne by the project.

Cost of the thermoelectric generator is estimated at $100 000 to $300 000. Based on Plutonium 238 as the probable fuel, fuel cost is estimated at $2 300 000 per charge. Most of this cost, however, could be recovered if the fuel system is returned from orbit. Any such reckoning of cost reduction must, of course, include the probability of failure to recover due to all possible causes.

Certain other costs would be incurred. It will be necessary to provide radiation shielding, special handling and cooling procedures, and equipment for prelaunch operations. This total cost is estimated to be $200 000. A major cost is that of providing for radioisotope re-entry and recovery. Existing recovery systems used by the military could probably be adapted for this program. Cost of the adaptation, to this program, is estimated to be $1 000 000.

Solar cells. -- The solar array-battery system has the most extensive flight history, the lightest weight, and the lowest cost. This system does have the disadvantage of requiring either restrictions on the allowable spacecraft orbits or use of active orientation of the solar panels with attendent solar array reliability and attitude control system interface problems. However, this disadvantage is not a limiting consideration since a 3 o'clock sun-synchronous orbit has been selected for the HDS experiment. With the selected orbit, the vehicle spin axis is always between 31 and 64 degrees from the sun-line; therefore, one vehicle face normal to the spin axis is continuously illuminated except during earth shadow. This permits the design of an array which can extract energy from solar radiation incident to surfaces which are always illuminated and avoids the necessity of orientation mechanisms with their adverse effects on reliability and vehicle stability.

A summary of the salient points of comparison is presented in Table 2. Evidently the solar cell-battery system is best for the HDS program, although an isotope-battery system is a feasible backup. Program requirements are beyond the present state of the art for fuel cell systems.

Control and Regulation

Bus regulator. -- A great variety of dc power regulation circuits, each with different characteristics, are available due to recent advances in semiconductors and magnetics. Available regulator circuit configurations must be evaluated for each specific power system application since no one of the regulation circuits has characteristics which are best for all applications. Analysis of system requirements and regulation circuits shows that a series pulse-width-modulated (PWM) regulator is the optimum bus regulator for the HDS spacecraft.

HDS electrical system performance requirements can be met with either the dissipative (Class A) or nondissipative (PWM) type. The dissipative type uses transistors operating as a series or shunt valve of varying "resistance". This type regulator characteristically has low weight, low output impedance, fast response, low efficiency (hence thermal problems), and straightforward design. EMI problems are minimized.

Operation of both types is based on comparison of the output to a reference and amplification of the difference to control the output (Figures 4 and 5).

With modern components, it is possible to design the series regulator such that shunt losses are negligibly small with respect to the load. In this case, the efficiency n of this regulator is approximately $n = \frac{E}{E_i}$ showing that for a range of E_i, the efficiency varies from $\frac{E_o}{E_{i\,min.}}$ to $\frac{E_o}{E_{i\,max.}}$. $E_{i\,min.}$ must be about E_o + 1 volt, so that for a 1.5: 1 input range and 28-volt output the efficiency varies from about 97 percent to about 64 percent.

TABLE 2. - ENERGY SYSTEM COMPARISON

Characteristic	Solar array-battery combination	Fuel cell	Isotope-battery
Flight history	Considerable	None for long missions	Some
Life	Limited by battery	500 to 1000 hours	Limited by battery
Limitations on mission growth capability	Some; growth is possible at moderate cost		Some; cost is high
Availability, schedule	Readily available		Marginally available
Relative cost	$1		$4
Weight	75 to 100 pounds depending on redundancy used	700 to 900 pounds fuel + cells, tanks	60 to 200 pounds
Intact recovery required	No	No	Yes

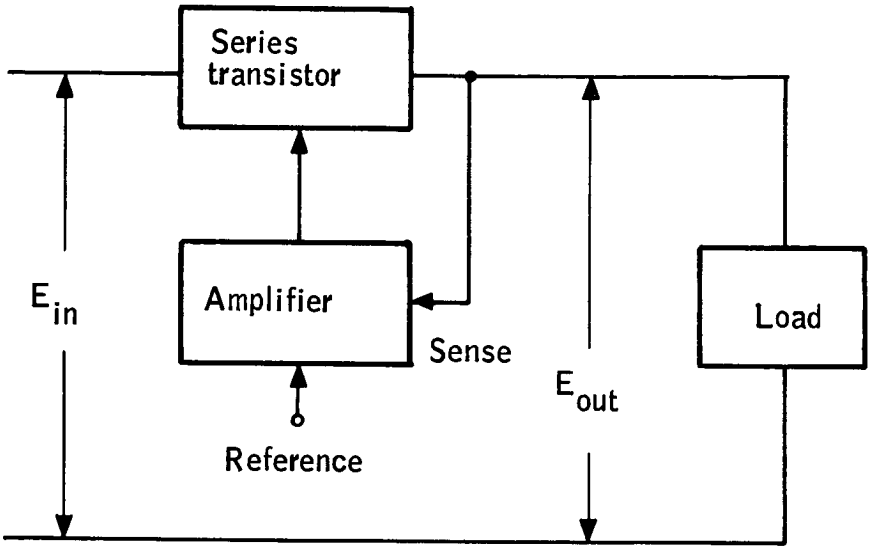

Figure 4. Series Regulator

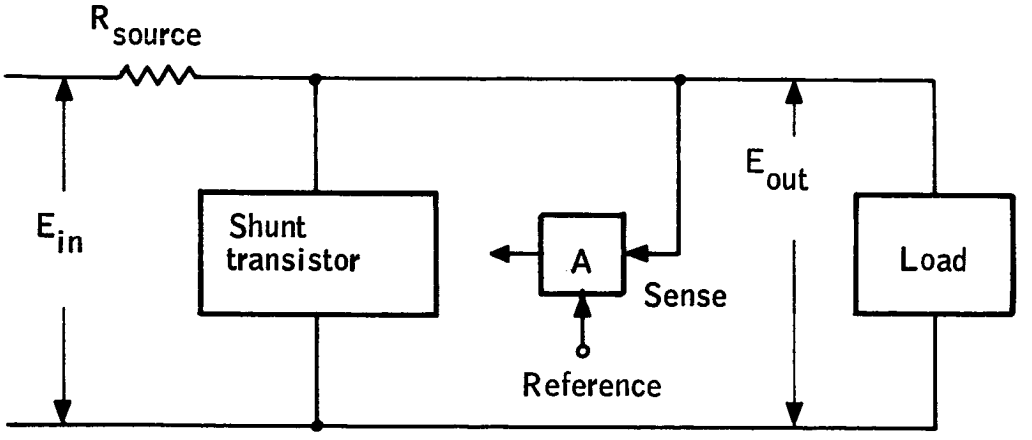

Figure 5. Shunt Regulator

For a shunt regulator, operation is based on attenuating the input voltage by causing a large current to flow through the source internal resistance or an added external resistance. In the case of a 28-volt battery of 0.5 ohm internal impedance with 1.5: 1 voltage variation, it would be impractical to draw $\frac{(1.5-1)(28)}{0.5}$ = 28 amperes shunt current solely for purposes of regulation. The situation is only slightly improved for the "optimum" shunt regulator (see Appendix A). (Note that these comments pertain only to the application of a shunt regulator to the bus regulation function.)

For a series nondissipative or switching regulator, modern designs exhibit low output impedance, fast response, and high efficiency but are more difficult to design and have a relatively fixed minimum ripple and greater weight due to the need for filtering. A regulator operating over the required 1.5 to 1 input range can have efficiency greater than 90 percent at all values of input voltage. (Note that the figure of 1.5 to 1 for the input voltage range is that which would exist while the battery is in use. Following completion of battery charging, the regulator input voltage rises even further, and there is a great deal of available array power which is unused. Hence a large drop in conversion efficiency at this time results in no penalty in increased array size.)

The modern series, nondissipative regulator operates in the "switching" mode, but the error signal controls the switch "connection" directly rather than the switching rate or duty cycle as in previous designs. The modern regulator, for instance, operates in such a way that the series switch is "off" if the output voltage as sensed by the amplifier is too high and is "on" if the output voltage is too low. Operation of this regulator is literally the analog of the so-called "bang-bang" control system. The old type regulator utilizes a self-oscillating circuit to perform the switching function, and control is exercised by virtue of the fact that the circuit is modulated by the output of a preamplifier. The process of modulating the oscillator is relatively slow, so that the output impedance of the old regulator is relatively high for any frequency appreciably above dc. Illustration of these modes of operation is shown in Figures 6 and 7.

Efficiency of both types can be very high, but the ac output impedance and response time of the Type I can be much superior. The penalty for these advantages is slight; the ripple cannot be reduced to quite as low a value as possible with the older types. No disadvantage is thus incurred for this power system as is explained in Audio and RF Filtering.

Reliability of modern switching regulators is about equal to that of dissipative types. Excluding filter components, parts counts are nearly equal, and the difference between regulator reliabilities is largely the difference between the reliability of the filter components versus the reliability of the series-pass transistor operating at high temperature with considerable loss.

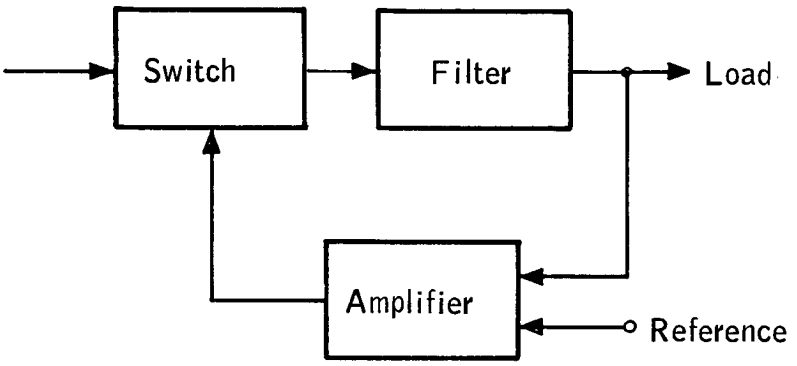

Figure 6. Modern Regulator, Type I

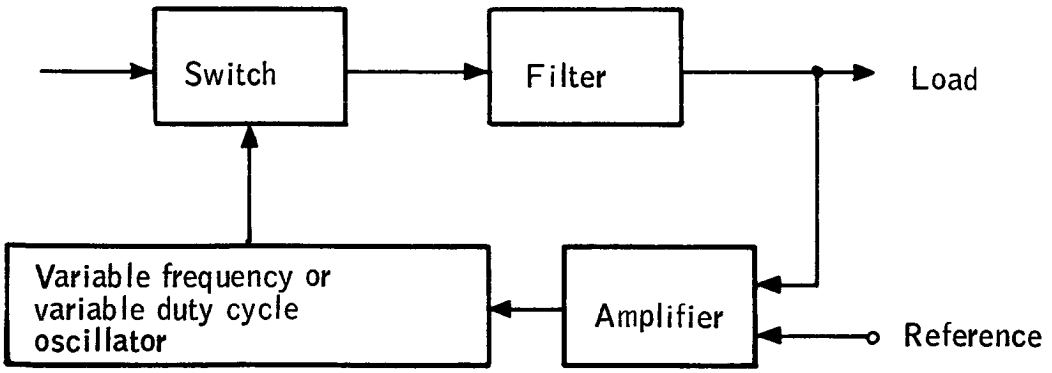

Figure 7. "Old" Regulator, Type II

Using the minimum efficiency figures of 0.64 and 0.90, it can be seen that the loss in the nondissipative regulator is $70\left(\frac{1}{0.90} - 1\right) = 7.7$ watts, and in the dissipative regulator is $70\left(\frac{1}{0.64} - 1\right) = 39.4$ watts, most of which is a single series element.

The difference between 39.4 and 7.7 watts, or 31.7 watts, must then be generated by an array of appreciably greater size and weight. The somewhat greater simplicity of the dissipative regulator is not worth the large size penalty imposed on the power system and the thermal problem imposed on the structure.

It is also possible to construct a nondissipative regulator which could be called a shunt type, in contrast to those which have been discussed above which could be called the series type. These regulators can also be quite efficient and are distinguished by the fact that the switching element operates with respect to ground so as to charge an inductance with a relatively high current, which is then discharged into the load through a series diode. This regulator is also called a boost regulator, since its operation is to provide a voltage step up from the output. This type of regulator would be best used for reducing the array voltage. For this type of regulator the array would be designed for a maximum voltage somewhat less than the minimum battery voltage, so that a step-up in voltage would always be required of the regulator. The chief advantage of this type of regulator is that the transistor voltage rating could be lower than that needed to place the transistor in the series mode. For the system in question, however, modern transistors are completely adequate to hold off the highest voltage to be encountered, so this is no longer a factor against the series type. In view of its lower efficiency and the fact that current limiting cannot be obtained, the shunt switching regulator is not considered to be a candidate.

Charge regulator. -- Requirements for the charge regulator differ from those for the bus regulator. Output of the charge regulator must be controlled so that the battery-charging requirements are observed. Failure to observe these requirements will result in either undercharge or damage due to overcharge. To meet these requirements, the reference must vary appropriately with battery temperature. A sensor located within the battery provides this function.

The element which directly controls charging current can be operated in either the dissipative or nondissipative mode. As with the bus regulator, there is appreciable heat loss associated with a dissipative regulator and a greatly reduced heat loss with the nondissipative regulator.

Following is a discussion of the factors which influence the size of the solar array for both types of regulators. It is assumed that 78-watts, continuous power output is required from each. Since the output voltage of these assumed configurations varies considerably from charge to discharge conditions, the constant-power assumption implies that the bus regulator

following this output is nondissipative. If, instead, the bus regulator is dissipative, the array size must be even larger to supply this additional loss as well as that incurred in the battery while it supplies the load. The following analysis compares the array power output required to deliver 78 watts with dissipative and nondissipative regulators.

Nondissipative regulator:

$$\text{Discharge } J_D = P_o T_D \tag{1}$$

$$\text{Required recharge} = J_c = K_R J_D = K_R P_o T_D \tag{2}$$

at a constant charge rate.

$$\text{Recharge power} = \frac{J_c}{T_c} \tag{3}$$

$$\text{Array power to charge battery} = \frac{1}{n_c} \frac{J_c}{T_c} \tag{4}$$

$$\text{Array power for load} = P_o$$

$$\text{Total array power} = P_o + \frac{1}{n_c} \times \frac{K_R P_o T_D}{T_c} = P_o \left(1 + \frac{K_R T_D}{n_c T_c}\right) \tag{5}$$

for $P_o = 78$ watts, $K_R = 1.57$ $T_D = 36$, $T_c = 54$

$$n_c = 0.90$$

$$\text{Array power} = 78 \left[1 + \frac{1.57(36)}{0.9(54)}\right] = 168 \text{ watts}$$

where:

P_o = power out (78 watts)

J_D = discharge energy

J_c = charge energy

T_D = discharge time

T_c = charge time

K_R = regulator control factor

n_c = battery charge efficiency

E_O = bus voltage

E_{BD} = battery discharge voltage

E_{BC} = battery charge voltage

To meet this requirement, the number of series solar cells must be sufficient to develop a voltage of $E_{BC} + 1$ or 44 volts at the 31° sun angle. Under conditions of 64° sun angle, the array voltage rises to about 55 volts due to drop in temperature. The number of parallel cells must then be such as to supply $\frac{168}{55} = 3.05$ amperes.

Dissipative regulator: Assume P_o is supplied at $E_O = E_{BD} - 1$ volt during battery discharge and at $E_O = E_{BC} + 1$ volt during battery charge (and before next dark cycle).

Discharge energy $J_D = P_o T_D$, and required recharge energy $J_c = K_R J_D = K_R(P_o)T_D$ at a constant charge rate (that of the worst-case orbit).

$$\text{Recharge I} = \frac{J_c}{T_c E_{BC}}$$

$$\text{Load current} = \frac{P_o}{E_{BC} + 1} \tag{6}$$

$$\text{Array current} = \frac{P_o}{E_{BC}+1} + \frac{K_R P_o T_D}{T_c E_{BC}} = \frac{78}{44} + \frac{1.57(78)(36)}{54(43)} \tag{7}$$

$$\text{Array voltage} = E_{BC} + 1 = 44$$

$$\text{Array power} = 161$$

Note that for this case the array must supply the values of current and voltage listed at all temperatures. This means that for the mission in question, the number of series solar cells must be determined so as to produce 44 volts at the 31° sun angle where the cells are at the highest temperature. The number of parallel paths must be determined so as to produce 3.67 amperes at the 64° sun angle where the reduced illumination cuts the amount of current available, but the lower temperature raises cell voltage. Because the system requirements for voltage and current are determined by non-simultaneous limitations, the array is actually capable of greater power. At 31° sun angle, the array maximum power is about (42V) (6.8) = 285 watts; and at 64° sun angle, the array maximum power is about 55(3.59) = 198 watts, even though power actually drawn is only 161

watts. In addition, it should be recognized that, since array size was based on extreme values of current and voltage which are not simultaneous, none of the apparently surplus power is available to the system. The array must thus be larger in order to supply a smaller amount of power, relative to the system utilizing "nondissipative" charge regulation.

Solar Cell Array

Two different basic configurations were considered: one in which the solar cells were mounted on the body of the spacecraft and the other where all or part of the cells are mounted on deployable panels. In addition, many alternatives of this latter arrangement were studied and three of the most promising are presented here.

The basic criteria for evaluation were 168 watts under the worst conditions of sun angle, simplicity, low weight, high reliability, and a minimum magnetic moment. These items are discussed for the various configurations, and a summary of the features is presented as Table 3. A comparison of the power available is presented in Table 4. It should be noted that basic power requirements increased to 189 watts and array temperatures increased as the design concept evolved and calculations were refined. All of these changes are reflected in the configuration selected.

Cylindrical - body-mounted cells. -- The simplest configuration from a mechanical standpoint is to mount the solar cells to the body of the spacecraft. Using the entire vehicle front face and cylindrical area (except for ports) for cells, it is possible to generate approximately 134 watts of array power in the worst case (sun-line spin-axis angle of 31°) using a little over 11 000 body-mounted 2 x 2 cm solar cells. Further system refinement might show that it is marginally possible to meet the power requirement without the need for any auxiliary solar array surfaces, but additional growth could be met only by lengthening the cylinder, and the cost would be relatively high because of the large number of cells needed.

This power was estimated assuming the mean effective temperature for the front face and cylindrical areas would be respectively 89° C and 2° C for the 31° sun-line to spin-axis angle, 75° C and 18° C for the 45° angle, and 40° C and 33° C for the 64° angle.

The body-mounted configuration analyzed is for a spacecraft concept which consists of a 44-inch long spacecraft with end-mounted starmappers and sunshaded radiometer. The present configuration, which is a spacecraft 40-inches long with rim-mounted starmappers and sunshaded radiometer, has sufficient cell mounting area for approximately 100-watts array power output at 64-degrees sun angle. The present configuration also would present cell connection problems since available rim area is not evenly divided between the six sides.

TABLE 3. - COMPARISON OF VARIOUS SOLAR CELL ARRAY CONFIGURATIONS

	Body mounted	Panel mounted					
		Hexagonal				Octagonal	
		6 panels only, 26" x 44" panels		6 panels + front face, 25" x 30" panels		8 panels + front face	
Power, worst case	134 watts, 31° incidence	208, 64° incidence		169, 64° incidence		178, 64° incidence	
Cell quantity	11 380	10 368		8400		8832	
Complexity	Simplest	Fair		Fair		Fair	
Reliability	Mechanically best Electrically poor	Mechanically fair Electrically good		-		-	
Weight, pounds	24.0[a]	20.1[b]	37.7[a]	34.3[b]	35.0[a]	32.3[b]	34.9[a]	32.0[b]
Watts/pound	5.6[a]	6.7[b]	6.2[a]	6.8[b]	4.8[a]	5.2[b]	5.1[a]	5.6[b]
Expansion capability	Poor	Poor	Good	Good	Good	Good		
Magnetic moment	Worst, impossible to balance		Good, symmetrical and can be balanced		Good, symmetrical and can be balanced		Good, symmetrical and can be balanced	

[a] Using solder-dipped cells

[b] Using solderless cells

TABLE 4. - POWER OUTPUT FROM SOLAR CELL ARRAY

Configuration	Sun angle, degrees		
	31°	45°	64°
	Power, watts		
Cylindrical - body-mounted, face and rim	134	149	146
Face	74	64	40
Rim	60	85	106
Hexagonal - 6 panels only, 26" x 44" panels	367	324	208
Hexagonal - panels and front face	301	261	169
Face	57	49	32
Panels	244	212	137
Octagonal - panels and front face	317	275	178
Face	57	49	32
Panels	260	226	146

The optimum design would utilize 133 cells in series on the front face and 106 cells in series on the cylindrical elements to provide the best overall balance for the requirement of 44 volts (after isolation diode drop). For the cases defined above, the maximum power voltages of these solar cell strings on the front face would be 44, 47.5, and 55.7 volts, respectively, for the 31°, 45°, and 64° cases. For the cylindrically mounted strings, the maximum power voltages would be 52.2, 49.0, and 46.0 volts, respectively, for the three spacecraft orientations.

For a typical body-mounted configuration, 8800 cells can be mounted on the cylindrical areas, based on 74 circuits of 106 cells in series and 10 of 105 cells in series. On the front face using full diameter less the prohibited areas, an absolute maximum number of cells could be as high as 3100; however, a more realistic number would be about 2500. Using the latter figure, the total quantity of cells is 11 380 resulting in a projected power of 134 watts at the 31° angle, 149 watts at the 45° angle, and 146 watts at the 64° angle. Figure 8 shows this power as a function of sun angle.

As can be seen from this analysis, the 189 watts cannot be achieved with the present thermal design basis and spacecraft geometry. From a reliability standpoint this method would appear to be good at first glance. Mechanically, this is true. Electrically, however, the relative reliability is lower than the panel mounted system. Since illumination on the cells mounted on the rim always varies from shadow to full illumination, isolation must be provided for each series string. As discussed later in the reliability section, paralleling of cells gives an increase in the reliability to be expected if a complete failure of a cell occurs. This would not be practical on the rim-mounted cells, and the added complexity of the isolation diodes for each string lowers the reliability even more.

Magnetic effects caused by currents through the panels can be minimized by careful layout. Techniques such as bringing the return lead under the cells do not lend themselves to this type of construction. In addition, since the power conversion takes place only on the lighted side of the spacecraft, the magnetic effects are unsymmetrical and cannot be balanced.

Panel-mounted configurations. -- Since even under the worst solar incidence case cells on the front face are more effective than those on the cylinder, a more efficient system would probably result if the rim-mounted cells are replaced by cells on panels which on deployment would be coplanar with the front face. During launch these panels could be folded back against the side. Under these circumstances, the cells are capable of producing about three times the power in the minimum case as cells mounted on a rim, since they are all simultaneously exposed.

The general case where panels are folded back along the cylinder at the edge of the front face and in deployment are extended to make any angle with the front face was examined. The optimum angle, ignoring temperature considerations, is that in which the entire array is coplanar. The analysis is included as Appendixes B and C. Any cup-shaped array (either inward or outward) is less efficient than the planar array, in spite of the high incidence angles.

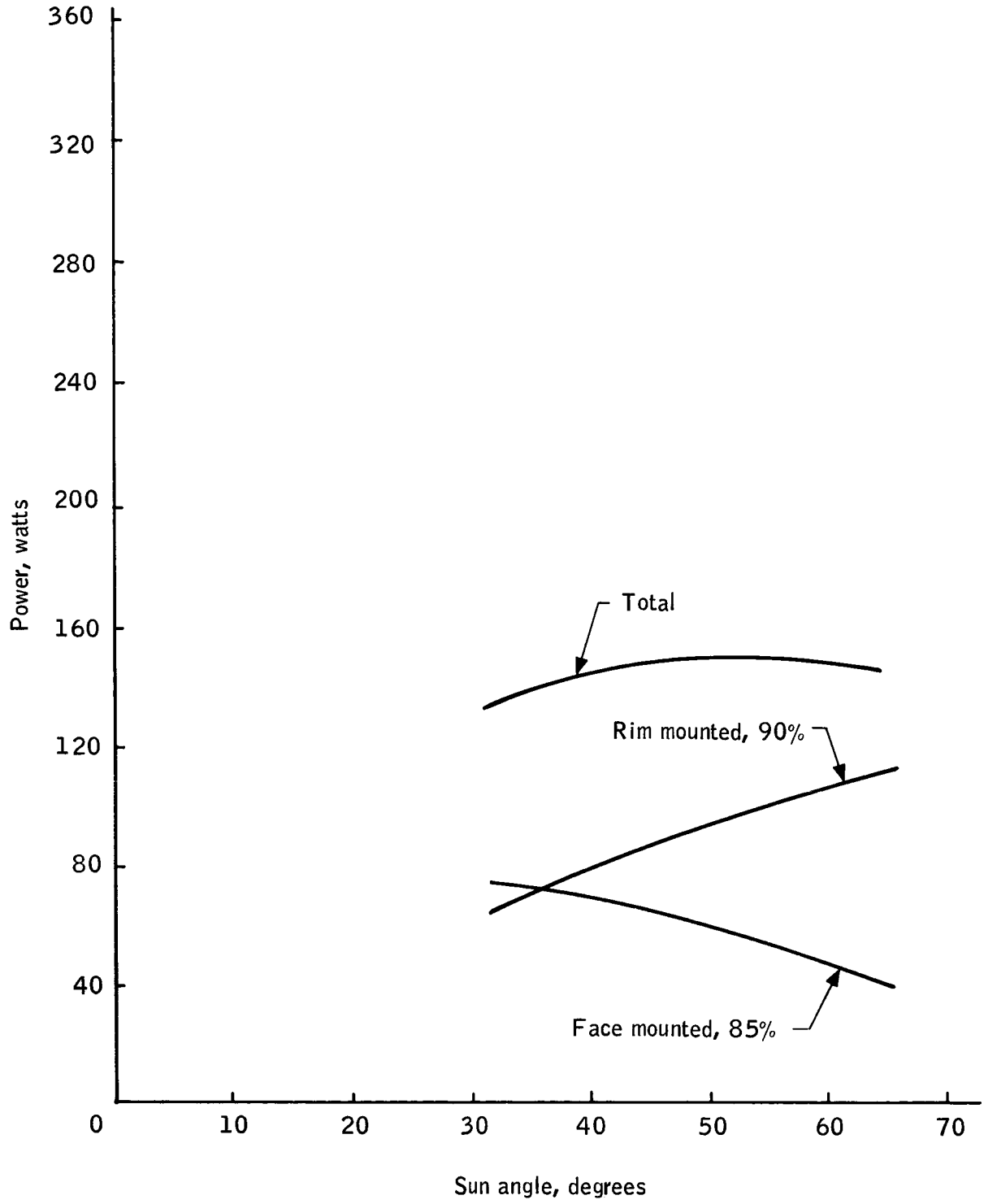

Figure 8. Unregulated Power Output as a Function of Sun Angle, Body-Mounted Cells - 44" Spacecraft

Several possible configurations have been examined, including large panels which would be mounted against the front surface and rotated or folded out as in the Lunar Orbiter Vehicle. It has been tentatively concluded that the best approach would be to use panels folded back along the side surfaces during launch. Two hexagonal configurations (one with cells on the front face, and one with cells only on the panels) and one octagonal configuration (cells on the front face) were investigated. Total volume would be slightly reduced when compared to the circular cylinder; however, the flat mounting faces would be easier to fabricate and could be more easily employed as mounting surfaces for internal hardware. The panels could also be readily separable from the main body to minimize handling damage.

Although the panel arrangement is more complex than the body-mounted case, reliable hinge and erection mechanisms are available which allow a high confidence level in the deployment of the panels. Electrical reliability advantages in the ability to parallel cells and the simpler design would seem to outweigh mechanical disadvantages. Panels are also interchangeable; thus logistics problems are reduced.

Expansion capabilities are easily obtained on two configurations by adding more cells to the panels. In the case where no cells are used on the front face, the panel is filled. Expansion is possible by increasing the length of the panel or by adding cells to the front face.

The magnetic moment from the cell currents can be minimized and, if necessary, virtually eliminated by careful cell layouts. Normal good practice in laying out circuits so that loops are as small as possible and opposing currents are adjacent will usually suffice. If more reduction is necessary and the added weight and expense can be tolerated, magnetic effects can be virtually eliminated by returning the current through a conductor the width of the circuit mounted directly below the cells. It should be noted that, unlike the body mounted case where some of the cells were always shadowed, this array is symmetrical about the axis of the spacecraft, and the effects of currents in the array should be virtually negligible. Although no absolute value was given for the magnetic moment, it is felt that normal good practice will be sufficient.

Hexagonal with cells on panels and front face: The first, illustrated in Figure 9, utilizes a hexagonal body with six deployable paddles with cells on the front face. For the minimum case, dimensions of these paddles are tentatively 24.13-inches wide by 30-inches long. On each paddle would be placed six rows of cell groups. Each row consists of 36 series-connected submodules, each with five 2x2 cm cells in parallel. Three of these rows would make one string of 108 cells. Specific layouts were made on the front face utilizing 1920 cells divided into two circuits of 8 in parallel by 120 in series. The maximum power output would be 57 watts at 31° incidence at 40.2 volts, 49 watts at 45° incidence at 42.7 volts, and 32 watts at 64° incidence at 50.3 volts.

The power levels from the six deployable units at equilibrium temperature at the three incidence angles would be approximately 244 watts, 212 watts, and

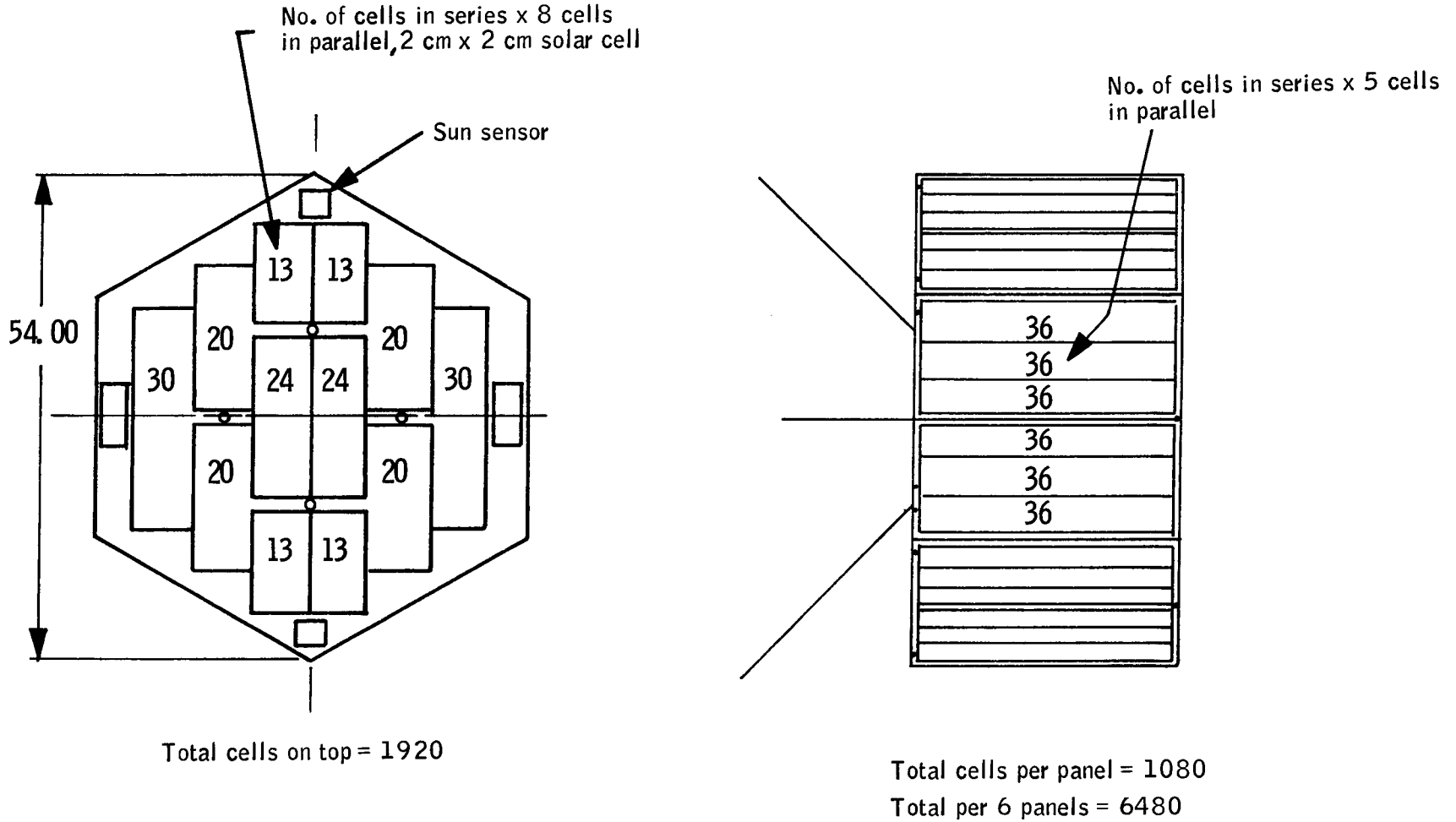

Figure 9. Solar Cell Configuration, Hexagonal Body

137 watts, respectively. Adding these outputs to the 1920 body-mounted cells for this design, the total system outputs would be 301 watts, 261 watts, and 169 watts at sun angles of 31°, 45°, and 64°, respectively.

The configuration selected uses panels 25.62-inches wide by 44.23-inches long with two circuits of 8 in parallel and 108 cells in series which provides 10 368 cells in the array on the panels. In the minimum case, at 64° incidence, these six panels provide 208 watts, at 45° incidence 324 watts, and at 31° incidence 367 watts. Growth can be provided by mounting cells on the front face or by using longer panels. Figure 10 shows variation of the power output for the hexagonal cases as array illumination and temperature changes with sun angle.

Octagonal with cells on panels and front face: Figure 11 shows an alternate octagonal design which, from the point of view of the uhf antenna requirements, would appear to be preferable. For the specific preliminary design selected here, the eight panels would be 19.34 inches by 30 inches. On each panel there would be two circuits of 108 series-connected 4-cell submodules. These 108 units would be divided into three rows making six rows per panel. The total cell complement here would be 6912 cells, which would generate 260 watts, 226 watts, and 146 watts at the three solar incidence angles of 31°, 45°, and 64°, respectively. With the output of the 1920 cells on the front face, the total outputs for this eight-panel design would be 317 watts, 275 watts, and 178 watts, respectively, for the three sun angles. This design meets the power requirements for all sun-angle orientations. Expansion could also be accomplished by increasing the panels to a length of 44.23 inches. The number of cells would be the same for this eight-panel design as for the extended six panel design, resulting in power levels of 457, 394, and 238 watts for the three solar incidence angles.

Battery

The three major secondary electrochemical storage systems that have been developed for space are nickel-cadmium, silver-cadmium, and silver-zinc cells.

The prime decision criteria is cycle life for the one-year design mission. As nearly 5600 charge-discharge cycles would be required in a 94.6 minute orbit, the silver-zinc system may be immediately rejected as it has not yet demonstrated 1000 cycles with reliability. This analysis will therefore compare the reliability of nickel-cadmium and silver-cadmium batteries as a function of the number of cells within the batteries. The analysis will be based on a depth of discharge of 25 percent in a near-earth orbit of 1.5 hours and on an equal level of confidence. It will be assumed that the mode of failure will be random in nature, and the distribution of life is best described by the exponential. The effect of wear-out failures has been eliminated since it is not a contributing factor in the nickel-cadmium system for one year of life at a depth of discharge of 25 percent. Insufficient information is available on silver-cadmium systems to make any meaningful statements about a wear-out failure mode. The first phase of the analysis was to ascertain a failure rate parameter λ for both the nickel-cadmium cell and the silver-cadmium cell. Crane Naval Ammunition Depot, TRW Systems', and flight data were utilized

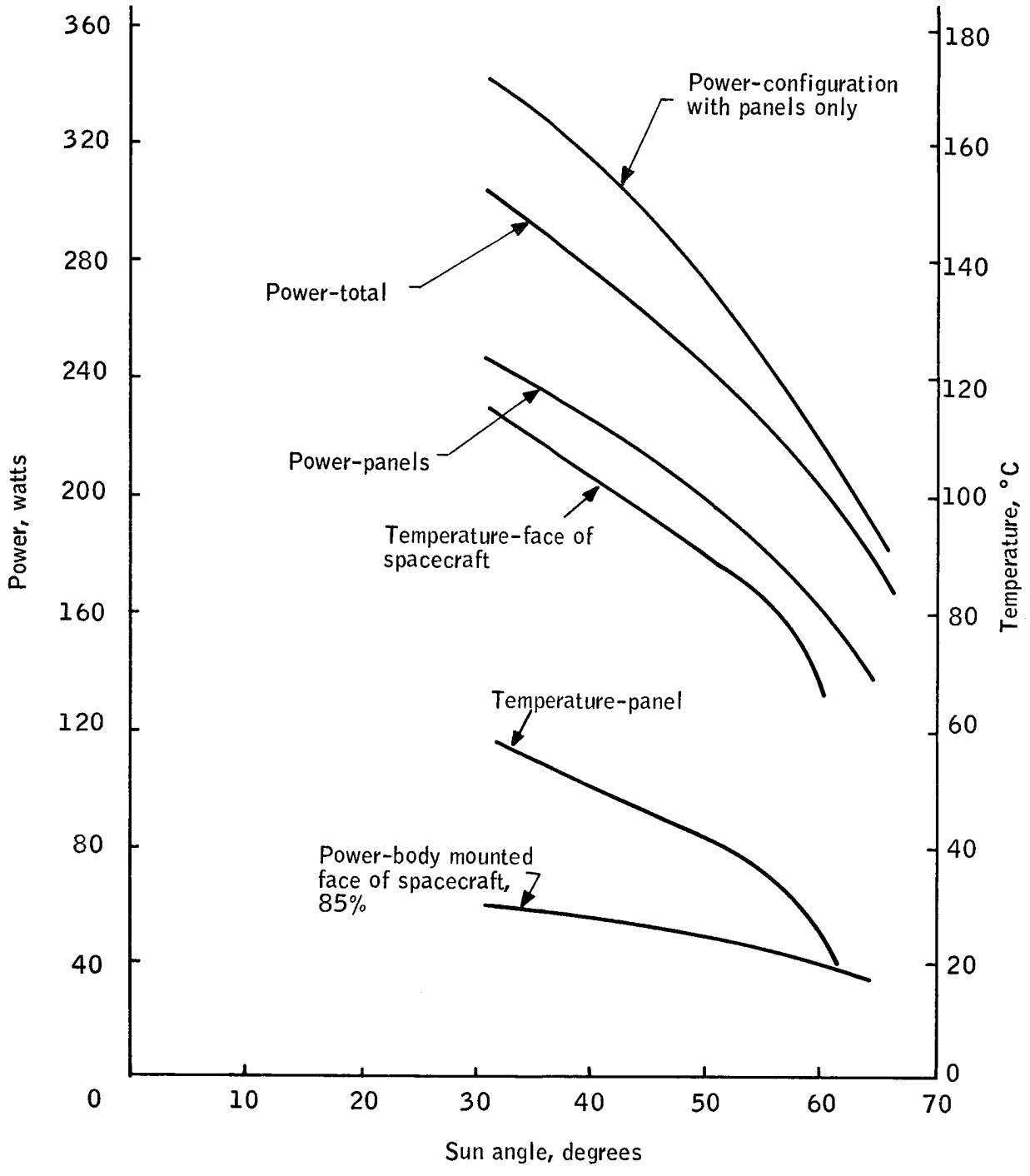

Figure 10. Unregulated Power Output as a Function of Sun Angle, Basic Configuration with Fold-Out Panels

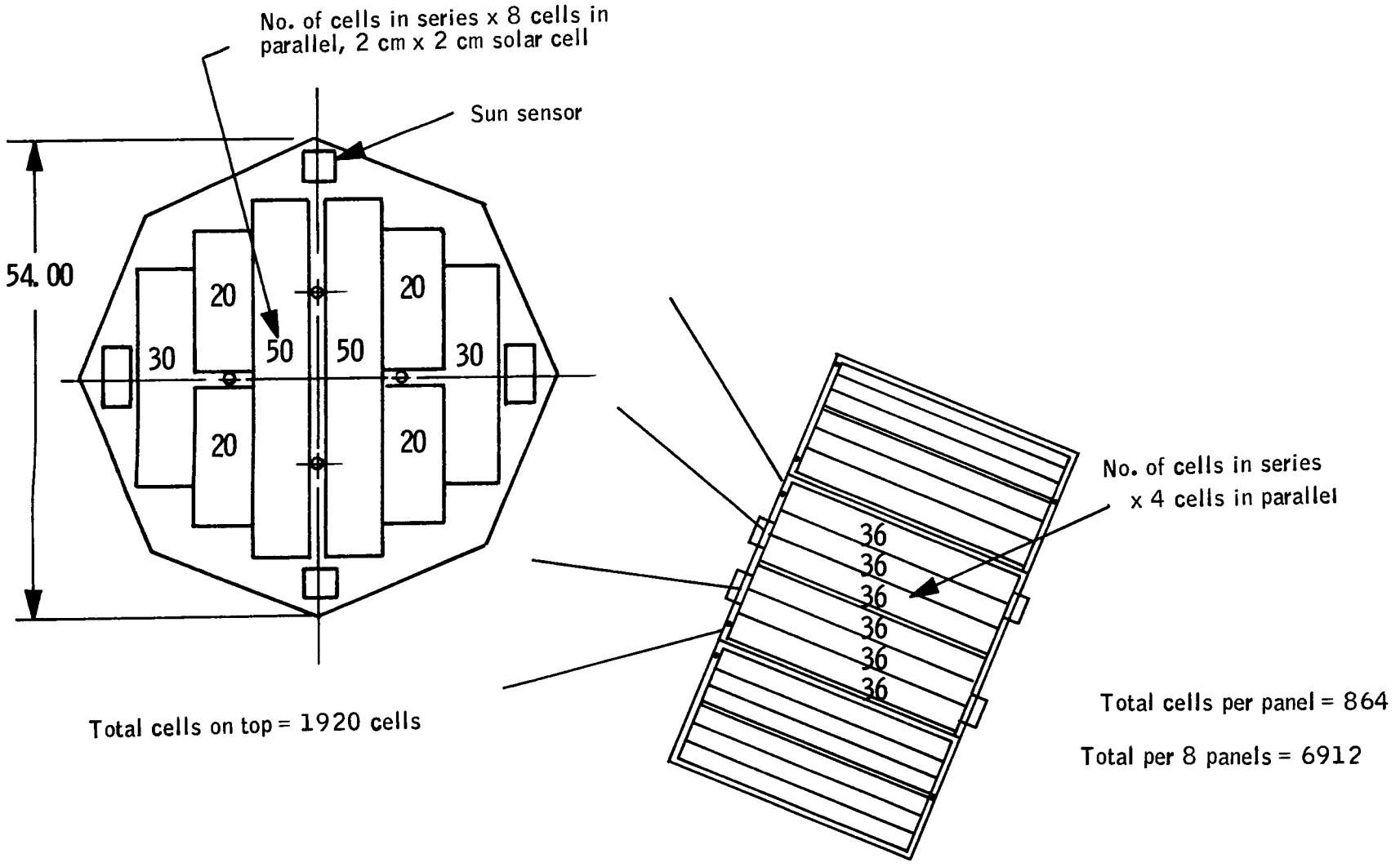

Figure 11. Solar Cell Configuration, Octagonal Body

to determine the failure rate (refs. 1, 2, and 3). From more than 2 800 000 cell hours for nickel-cadmium and nearly 150 000 cell hours for silver cadmium, failure rates have been determined.

Utilizing the failure rate of 1.39×10^{-5} for the silver-cadmium cell, a probability of 0.8984 at an 80-percent confidence level for survival exceeding 8000 operational hours resulted. The nickel-cadmium failure rate of 6.95×10^{-7} yielded a probability of survival exceeding 8000 operational hours to be 0.9944 at an 80-percent confidence level.

Reliability estimates of series-connected cells results in the multiplication of individual cell reliabilities to ascertain total string reliability. Figure 12 shows the battery reliability of both nickel-cadmium and silver-cadmium batteries as a function of the number of cells in series. It can be seen that the nickel-cadmium battery reliability varies from 0.9348 for 12 cells in series to 0.8544 for 28 cells in series. Based on an equal confidence level of 80 percent, reliabilities for the silver-cadmium battery vary from 0.2764 for 12 cells in series to 0.0498 for 28 series-connected cells.

If it is desired to equate reliabilities for the silver-cadmium battery equal to the nickel-cadmium battery, the confidence estimate for these reliabilities in the silver-cadmium system will degenerate to a level of 10 percent.

Figure 13 shows the comparison of battery reliabilities at an equal confidence level of 50 percent. It can be seen that the nickel-cadmium battery reliability varies from 0.9771 for 12 series-connected cells to 0.9469 for 28 series-connected cells. The reliabilities for the silver-cadmium battery vary from 0.6390 to 0.3500 for 12 and 28 series-connected cells, respectively.

The above reliability and confidence estimates have been established utilizing the following mathematical expression.

$$\chi^2_{\alpha;\, 2\, r+2} = \frac{2T\ \ell n\ 1/P}{nt} \tag{8}$$

where:

T	=	total unit demonstrated hours
t	=	desirable life = 8760 hours
P	=	probability of survival
α	=	confidence level
r	=	number of failures for the above

It is necessary to state at this point that the confidence estimates are based on reliability statements rather than on the mean-time-between-failure parameter. If it is desired to calculate reliability numbers based on confidence estimate of $\hat{m}$ $(1/\lambda)$, the above equation must be modified. The probability of survival function for the exponential distribution for n series-connected components is:

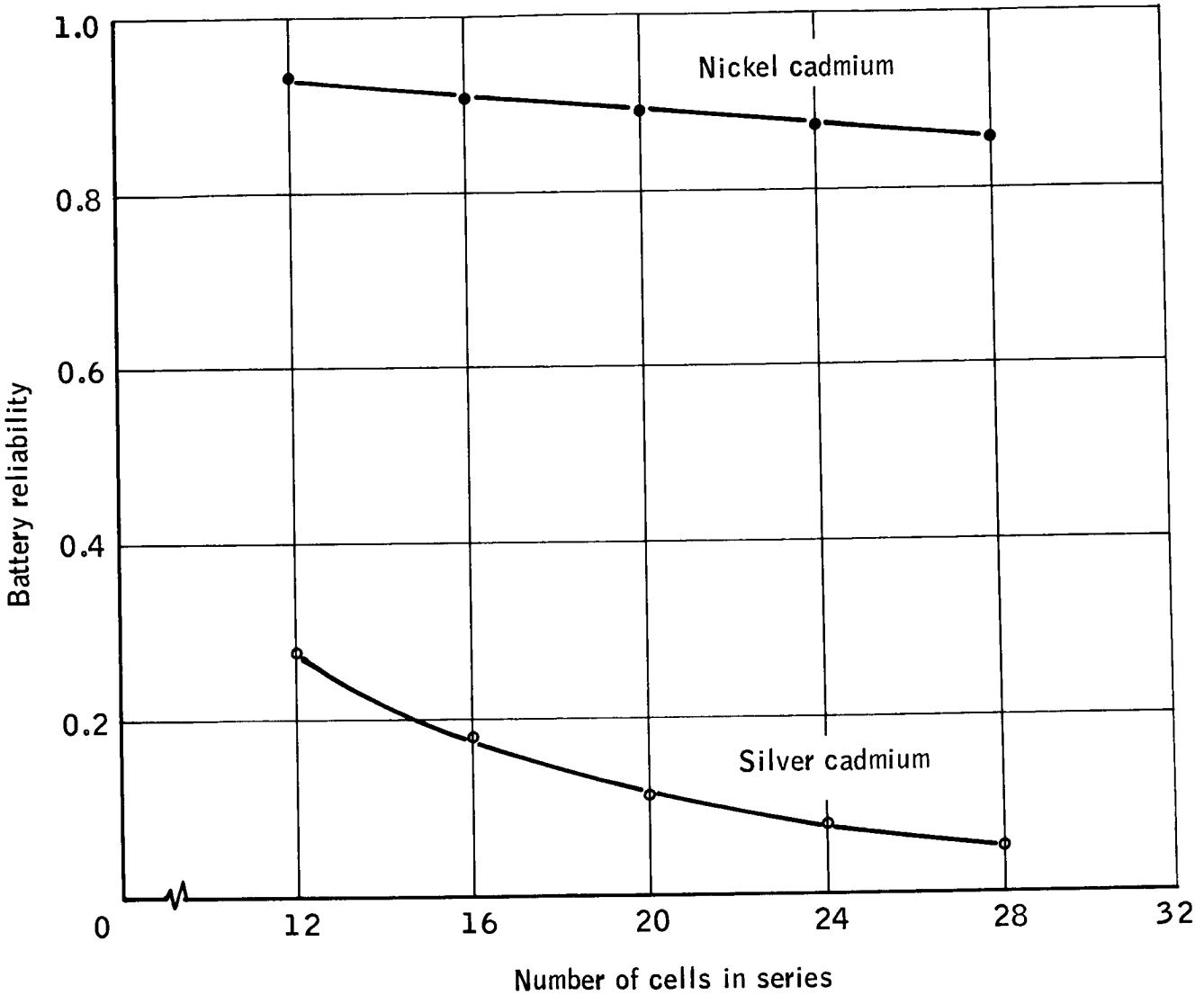

Figure 12. Battery Reliability Comparison Based on 25 Percent Depth of Discharge and an Equal Confidence Level of 80 Percent

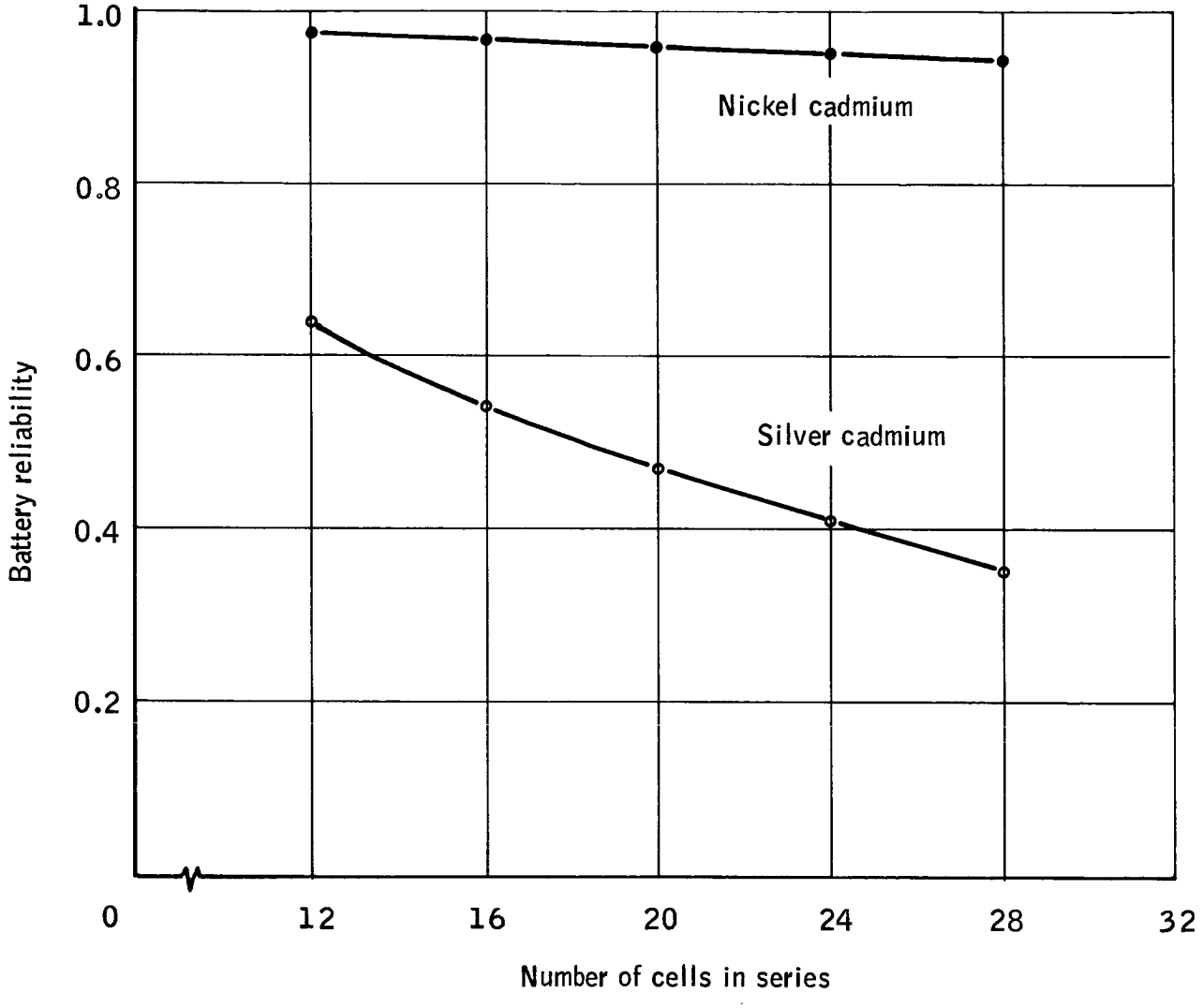

Figure 13. Battery Reliability Comparison Based on 25 Percent Depth of Discharge and an Equal Confidence Level of 50 Percent

$$R(t) = P = e^{-nt/\hat{m}} \tag{9}$$

where n = number of cells.

Solving equation (9) for $\hat{m}$ and substituting into equation (8) we get:

$$\hat{m} = \frac{2T}{\chi^2_{\alpha;\, 2r+2}} = \frac{1}{\lambda} \tag{10}$$

Based on the total number of test hours (T = 2 876 242) and the number of failures (r=2), there is 50 percent confidence that $\hat{m} \geq 1\ 077\ 244$.

Substituting this number in equation (9), a reliability can be calculated for a 28-cell battery having a reliable life of 8760 hours. The calculated reliability is 0.795 based on a 50 percent confidence of the mean-time-between failures. This calculation is not to be confused with the earlier calculation which gives a confidence estimate of reliability number.

Based on the above analysis, the nickel-cadmium system has the higher reliability, and the reliability increases as the number of series-connected cells decreases.

The prime use found for silver-cadmium batteries in space applications has been in satellites where the nonmagnetic construction of batteries is necessary. The majority of applications of silver-cadmium has been in satellites with orbital periods of 5 to 24 hours, which allows lower charge rates and fewer actual discharge cycles. The apparent watt-hour per pound advantage of silver-cadmium over nickel-cadmium is approximately 17 W-hr/lb considering cells only, and 12 W-hr/lb complete for batteries in the five to six ampere-hour capacity range.

One major difficulty with the silver-cadmium cell is its inability to be overcharged at rates above C/100. The more complex and less permeable separator system used in the silver-cadmium cell to control the migration of silver away from the silver electrode also restricts diffusion of oxygen to the cadmium electrode, causing a higher oxygen equilibrium pressure in the cell for a given overcharge rate. However, the charge efficiency of the silver electrode is high, on the order of 97 percent, and virtually no oxygen is produced until the electrode is about 90 percent charged. The silver-cadmium cell shows a sharp voltage rise near end of charge and provides a method of charge control by voltage that appears quite attractive. Voltage limited charging of the cell can be used to reduce current to the safe overcharge level as full charge is reached. While this method is effective for single-cell charging, a problem is encountered in charging series strings of cells. As the end-of-charge voltage rise is relatively rapid and overcharge capabilities limited, minor differences in charge efficiency can cause severe imbalance in cell end-of-charge voltages. Individual cell voltages rising above 1.65 volts thus generate internal gas pressures that do not readily recombine and limit the attainment of full charge on other cells in the string.

Extensive cell-selection procedures must be used to reduce this imbalance to an acceptable level.

A charge technique has been developed to minimize unbalance problems. By reducing the charge voltage limit as current decreases to a particular value (indicating the approach of end of charge), the current is further reduced to a value well within overcharge ability without forcing voltage higher. The technique has been used on IMP III successfully; however, maximum charge rate was approximately C/10, indicating longer orbits than 100 minutes (ref. 4).

The charge characteristic of nickel-cadmium cells and batteries has no sharp voltage transition at full charge. It is important when charging at high rates to terminate or reduce the charge current before the cell potential rises to a level high enough to permit the evolution of hydrogen. This limiting voltage is a function of temperature and is depicted by Figure 14. The nickel-cadmium system does permit overcharging, and the rates of acceptable maximum overcharge are defined in Figure 15. The current rates are acceptable for continuous overcharge, but much lower rates may be used to maintain full charge if desired.

The nickel-cadmium cell is less efficient during charge than the silver-cadmium cell, and the efficiency is a function of charge rate and temperature. At C/2 rates, the watt-hour efficiency would vary from 80 percent at -4°C to about 65 percent at 40°C. Comparable ampere-hour efficiency to silver-cadmium's 95-percent efficiency would be 85 percent for nickel-cadmium at 26°C.

A development that has added greatly to the simplification of recharging nickel-cadmium batteries is the Adhydrode adsorbed, hydrogen third electrode. This third electrode is sensitive to oxygen and produces a signal which is proportional to its partial pressure within the cell. Within the nickel-cadmium cell, oxygen is evolved from the positive (Ni) electrode as the cell approaches a state of full charge. When connected to the negative electrode through external circuitry, oxygen within the cell is combined with adsorbed hydrogen on the third electrode. The combination requires electron flow between the third electrode and the negative electrode. It is this current flow or the voltage drop across an external resistance that can readily be used to indicate a full state of charge.

The advantage of being able to determine end of charge can best be demonstrated by comparison with alternate charge techniques. Initially, satellite batteries were sized to allow the energy discharged during eclipse to be replaced at the battery safe overcharge rate. For example, if 1.5 ampere hours were discharged during eclipse, and 60 minutes were available for recharge and required overcharge, a two-ampere rate would be required. A battery capacity of 20 A-h would be used to allow recharge at the safe rate of C/10. As satellite power demand increased, battery size could become extremely large when limited to less than 10-percent usage. The next step uzilized the high rate recharge capability of nickel-cadmium when partially discharged. A stepped, taper charge system, with initial rates of

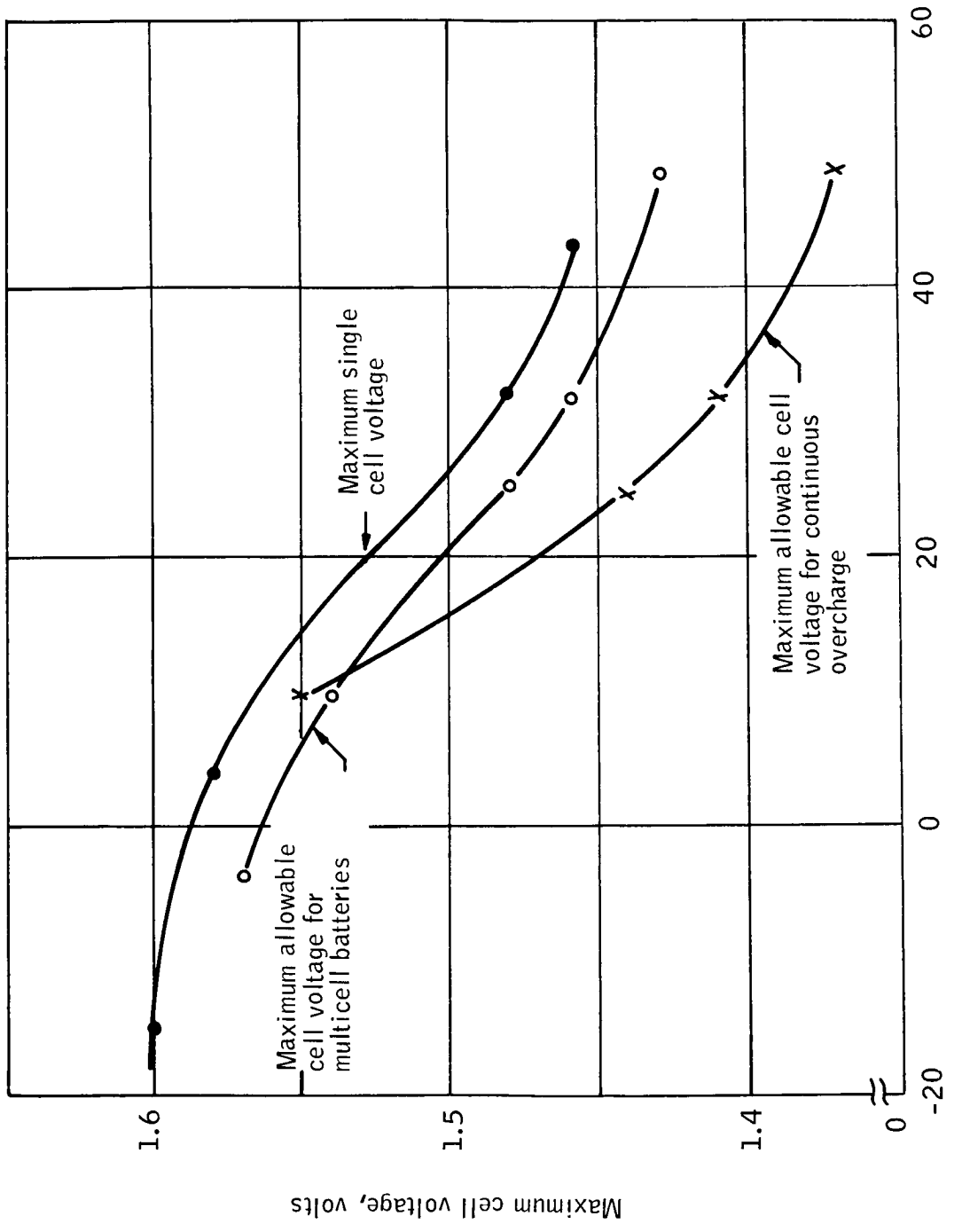

Figure 14. Maximum Limiting Voltage for Charge Control of Hermetically Sealed Nickel-Cadmium Cells

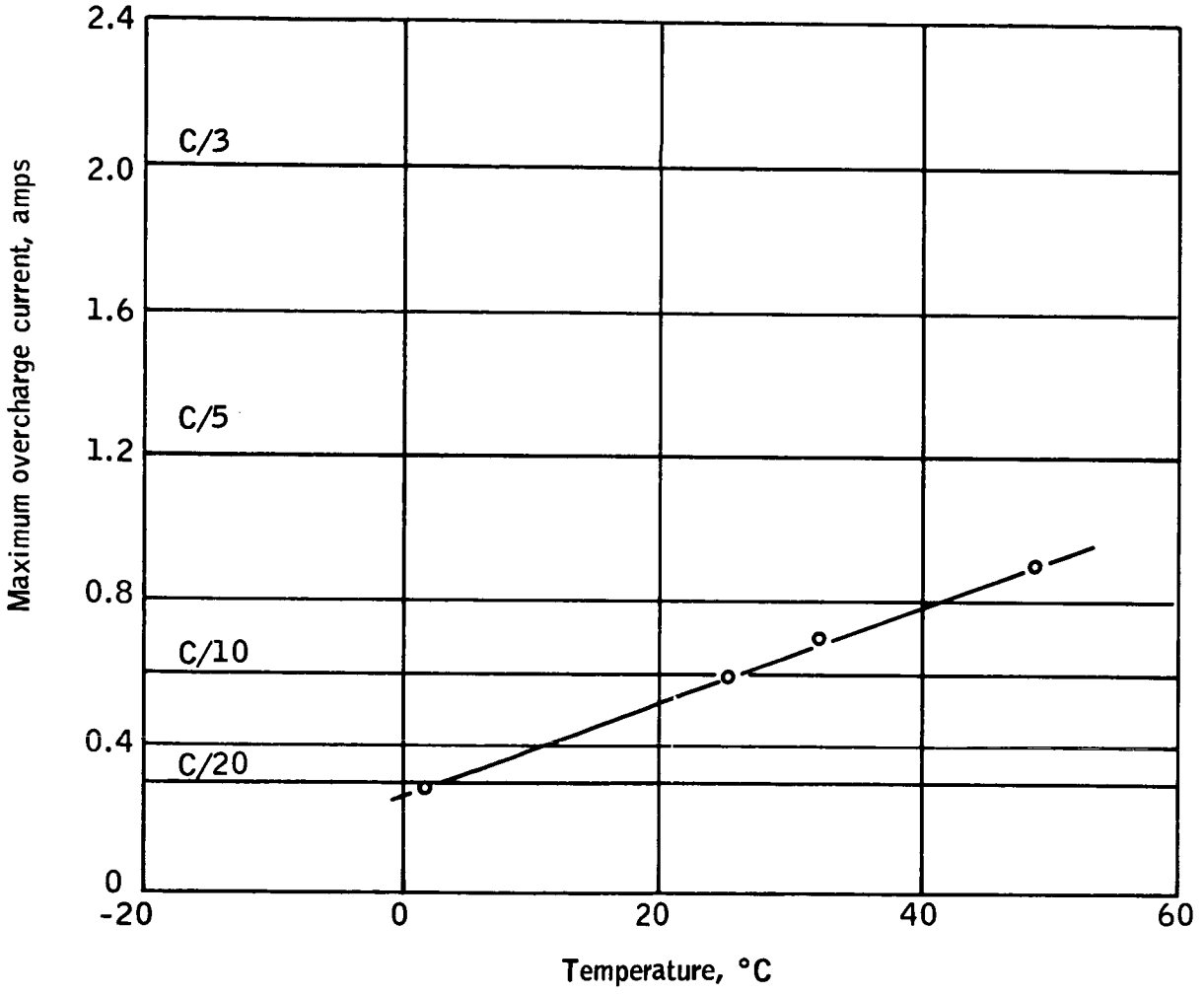

Figure 15. Maximum Recommended Overcharge Current for VO-6HS Hermetically Sealed Nickel-Cadmium Cells

approximately C/2 and final rates within overcharge capability, has been developed. Switching to lower current steps was accomplished by sensing battery voltage. The charge cycle for a 20 A-h battery might be: charge at 10 amperes to voltage limit, switch to seven amperes to voltage limit, switch to five amperes to voltage limit, trickle charge at one ampere for remainder of charge period. This complex system, using temperature dependent voltage limits, would be established based on empirical testing to verify completion of charge. Straight constant potential charging cannot be practically accomplished because thermal runaway problems and associated temperature limiting methods are not compatible with long life in nickel-cadmium batteries.

There are two modes of charge-discharge cycling to which the HDS spacecraft battery can be subjected. The first mode is the more commonly used and consists of a constant-current charge to a limiting voltage, which is compensated by temperature, followed by trickle charge. Based on the accuracy of injection into orbit, the charge-discharge cycle can vary between the extremes of 70 min charge/24 min discharge, and 58 min charge/36 min discharge. If a two-ampere charge to a voltage limit, which is dependent on temperature, followed by a trickle charge of 0.45 ampere is used, Table 5 will show the capacity removed as a function of temperature as well as the t total capacity returned. Recharge requirements for 2 ℃(35°F), 24℃(75°F), and 38℃(100°F) were assumed to be 108 percent, 115 percent and 125 percent, respectively. The voltage limits associated with the temperature were 1.56V, 1.50V, and 1.46V. Reviewing Table 5 shows that the cells are fully charged, and an excess amount of capacity is available. Some additional work must be done to determine more accurately the charge efficiencies and voltage limits since these are temperature dependent and hence are dependent upon vehicle thermal balance conditions.

Table 6 is similar to Table 5 except that it details the capacity removed and returned for the 58 min charge/36 min discharge mode of operation. It may be seen that, in either mode of operation, sufficient energy is available to charge fully the battery when utilizing the two-step, constant-current charge routine.

The second mode of operation, utilizes the Adhydrode charge control technique. Use of the Adhydrode enables maximum use of the energy available and minimizes the heat dissipation within the battery. As the satellite enters the sunrise portion of the orbit, the solar array is cold and, hence, able to deliver higher magnitudes of current. Since the battery is in a low state of charge when entering the sunrise portion, the charge efficiency is extremely high and capable of accepting high charge currents. As the solar array increases in temperature, the current delivery capability decreases. The state of charge of the battery is increasing during the charge mode and, hence, its charge efficiency is decreasing. The two effects are compensating each other, resulting in a maximum and efficient energy utilization.

In the previous mode of operation, the charge rate was reduced to a trickle charge when limiting voltage was reached. With the use of the Adhydrode, it is not necessary to reduce the current to a trickle charge at this point. One can continue charging at the maximum voltage limit until the Adhydrode

TABLE 5. - BATTERY CHARGE CHARACTERISTICS VERSUS TEMPERATURE

	Discharge at 2.25 amps, 24 minutes	Charge at 2.00 amperes to voltage limit and trickle charge at 0.45 amperes for remainder of 70 minutes total time						
Temp., °C	Capacity removed	Recharge require-ments	Total capacity required	Cap. ret. at 2.0 amps	Cap. ret. at 0.45 amps	Total capacity returned	Excess capacity	Voltage limits
2	54 A-min	108%	59 A-min	48 A-min	21 A-min	69 A-min	10 A-min	1.56V
24	54 A-min	115%	62 A-min	69 A-min	16 A-min	85 A-min	23 A-min	1.50V
38	54 A-min	125%	68 A-min	68 A-min	17 A-min	85 A-min	17 A-min	1.46V

TABLE 6. - BATTERY CHARGE CHARACTERISTICS VERSUS TEMPERATURE

	Discharge at 2.25 amps, 36 minutes	Charge at 2.00 amperes to voltage limit and trickle charge at 0.45 amperes for remainder of 58 minutes total time						
Temp., °C	Capacity removed	Recharge requirements	Total capacity required	Cap. ret. at 2.0 amps	Cap. ret. at 0.45 amps	Total capacity returned	Excess capacity	Voltage limits
2	81 A-min	108%	87 A-min	78 A-min	9 A-min	87 A-min	0	1.56V
24	81 A-min	115%	93 A-min	103 A-min	3 A-min	106 A-min	13 A-min	1.50V
38	81 A-min	125%	101 A-min	100 A-min	3 A-min	103 A-min	2 A-min	1.46V

signals the end of charge, atwhich time the charge can be completely terminated or the current may be reduced to some minimal value of about 0.1 ampere.

If maximum energy utilization and minimum heat evolution are required, the Adhydrode charge control is recommended. If heat dissipation is not a limiting factor, a two-step, constant current charge control is recommended. Both techniques have demonstrated successful operation in excess of one year; however, the Adhydrode system has not been flown in a satellite to date.

Heat dissipation characteristics of a battery system is an important criteria in the design and selection of the battery. The objective here is to determine the magnitude of energy which is being dissipated as waste heat in a 28-cell, six-ampere-hour battery using the third electrode charge control compared to a standard 28-cell, six-ampere-hour battery.

The amount of energy that will be dissipated when using the Adhydrode mode of charge control will be the difference between the total capacity required column and the total capacity removed column (Tables 5 and 6). If the Adhydrode charge control mode is not used, the amount of energy that is being dissipated as heat will be the difference between the total capacity returned column and the total capacity removed column.

This information is summarized in Table 7. The associated power rejection per orbit is tabulated with respect to the corresponding rejected capacity. Table 7 shows that the available power rejection of a 28-cell Adhydrode battery is approximately five watts per orbit. The average power rejection for a standard 28-cell battery is approximately 10 watts per orbit. Thus, the power rejection for a standard battery is twice that of the Adhydrode battery system, but the difference is of minor importance relative to the total electrical loss dissipated within the vehicle.

TABLE 7. - BATTERY ENERGY REJECTION VERSUS TEMPERATURE

	Adhydrode 28V06HSAD Battery				Conventional 28V06HSB Battery			
	70/24 Orbit		58/36 Orbit		70/24 Orbit		58/36 Orbit	
Temp., °C	A-min rejected	Power rej., watts	A-min rejected	Power rej., watts	A-min rejected	Power rej., watts	A-min rejected	Power rej., watts
2	5 A-min	2.08	6 A-min	2.5	15 A-min	6.28	5 A-min	2.50
24	8 A-min	3.34	12 A-min	5.0	31 A-min	12.80	25 A-min	10.90
38	14 A-min	5.85	20 A-min	8.35	31 A-min	12.80	22 A min	9.08

POWER SYSTEM CONCEPT

Electrical Power System

Philosophy of design. -- In accordance with the basic philosophy of the study to achieve a reliable system design and not merely a high reliability number, certain fundamental requirements must be met as listed below:

- The system must make minimum use of newly developed components and must concentrate instead on the application of proven concepts and components.
- The power system design must be coordinated with the requirements of other systems to minimize the possibility of difficulties associated with ground loops and other sources of interaction and error.
- System operation should be independent of continual supervision and control from the ground.
- System requirements must be examined for worst case operating conditions to avoid potentially marginal operation or over design.
- Fault protection is required so that failure of any given subsystem will not result in loss of the power system. In this way, there is the maximum probability that any failure, even one which results in loss of primary data, will not fail the power supply and prohibit transmission to the ground of evidence about the nature of the failure.

The fundamental requirements can immediately be translated into effects on the tradeoff areas and design requirements and restrictions as follows:

- The recommended battery is a proven type nickel-cadmium battery.
- Power conditioning and all other subsystems must filter out noise generated on their power and signal leads. They must also be designed for tolerance of line noise in accordance with uniform standards.
- Size of the solar array must be adequate to supply the required power without possibility of a bistable operating point.

Design limitations. -- It is possible to translate the orbital performance of the vehicle into a curve showing power availability, since this is a function of the relationship of the spin axis to the sun line. It is also possible to calculate an approximate value of power demand as a function of vehicle time

after launch, since the increased shadow fraction which occurs during certain portions of the year influences battery drain and, hence, the required power to achieve recharge. It is to be expected that maximum power demand will occur at precisely that time when minimum power is available, in view of the fact that maximum shadow fraction is correlated with least favorable sun angle. At the least favorable sun angle, the solar-array power capability is drastically reduced from its maximum value. Therefore, at the time when the shadow fraction is highest, the battery will be required to supply greater energy, and the solar array will then be required to return this greater amount of energy in less time than for smaller shadow fractions. These factors are plotted in Figures 16, 17, and 18 and clearly show that for the worst-case sun angle and shadow fraction associated with 3-sigma slow precession for an October 28 launch the point in time at which the power system has the least available margin is at approximately 260 days after launch. At this time, the factors of increased battery drain and decreased power availability are at their worst with respect to system margin. Examination of the predicted performance for 3 sigma slow precession shows that for the nominal launch date, October 28, there are approximately 90 days centered about day number 260 during which this orbit requires the power system to operate with minimum margin. A study of the predicted sun-line angle shows that the nominal orbit is by far the worst of all those studied from the viewpoint of maintaining a high performance margin by the power system. Other orbits studied for alternate launch times show that at no time before day number 300 do any of the alternates reach 62-degrees inclination. For a September 1 launch, there is a period of approximately 50 days centered about day number 325 during which the maximum excursion is only 63 degrees. For a July 1 launch, there is a period of approximately 15 days following day number 350 during which the sun angle is greater than 62 degrees.

Refinement and finalizing of the performance requirements for the worst-case limitations result in the following requirements for the solar array:

- Array area is determined by the need for load power and battery charging, plus adequate margin at the 64-degree sun angle where least power is available and drain requirements are highest.

- Since array size is directly related to power demand, not energy required, battery charging must be arranged, insofar as possible, to take place over the longest feasible time so as to minimize total power demand.

- Peak power demands are not used to size the array because there is little load energy demanded, and the loss in battery charge energy is negligible even if the array is loaded to the high current side of the maximum power point.

- Required margin of array minimum power (at 64-degree sun angle) over actual average power demand is determined by expected current fluctuations above average value.

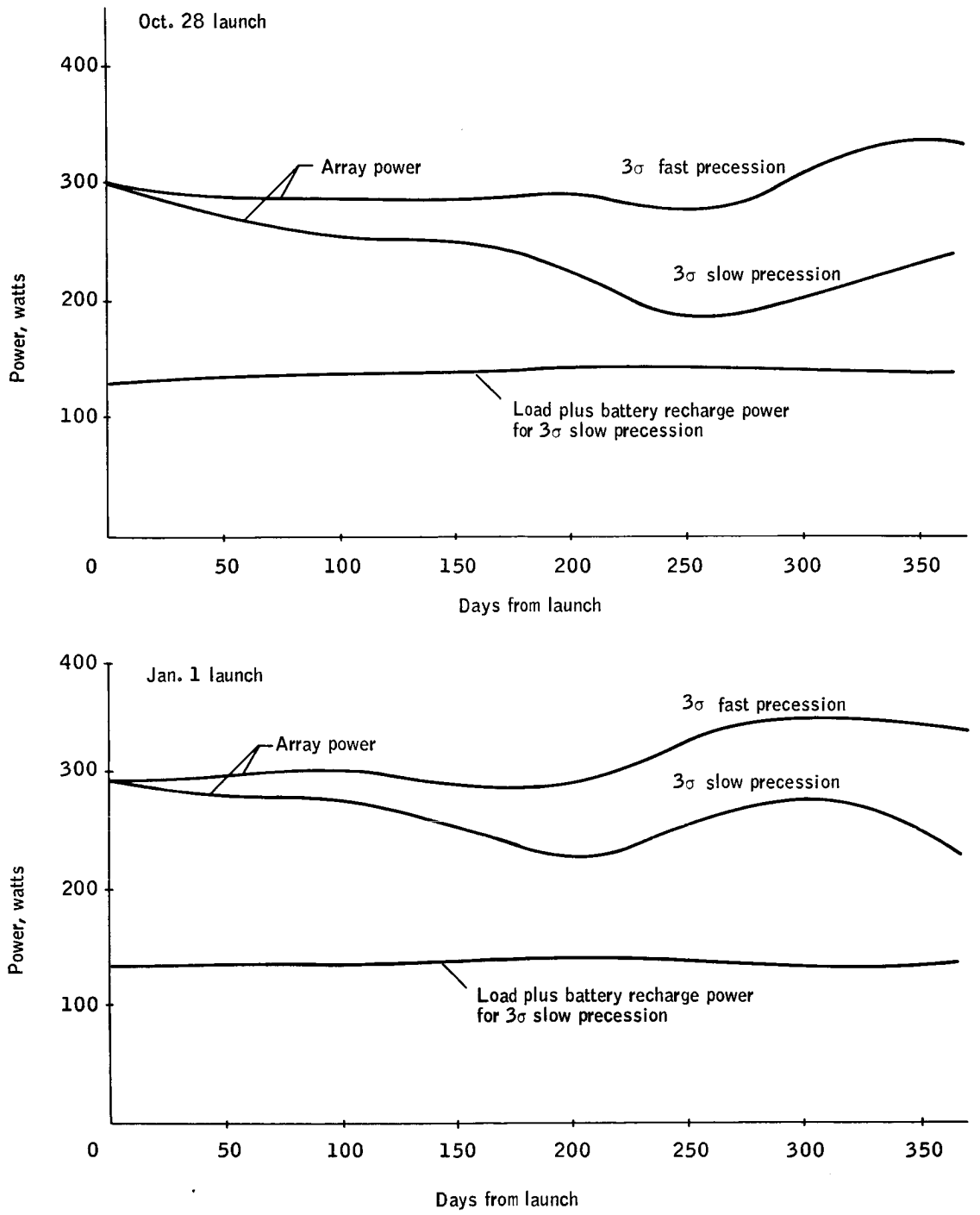

Figure 16. Effect of Orbital Variations on Power System, October 28 and January 1 Launches

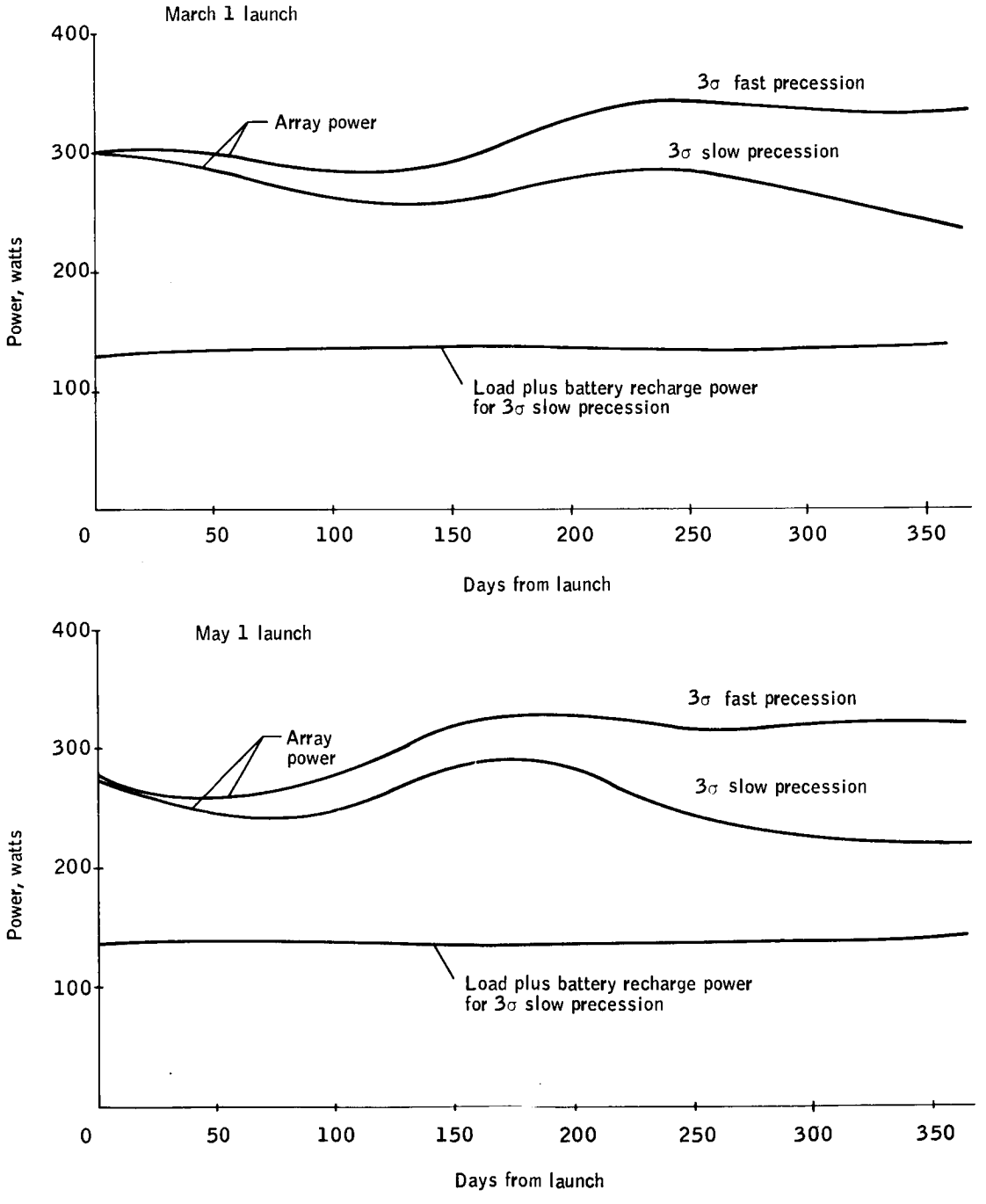

Figure 17. Effect of Orbital Variations on Power System, March 1 and May 1 Launches

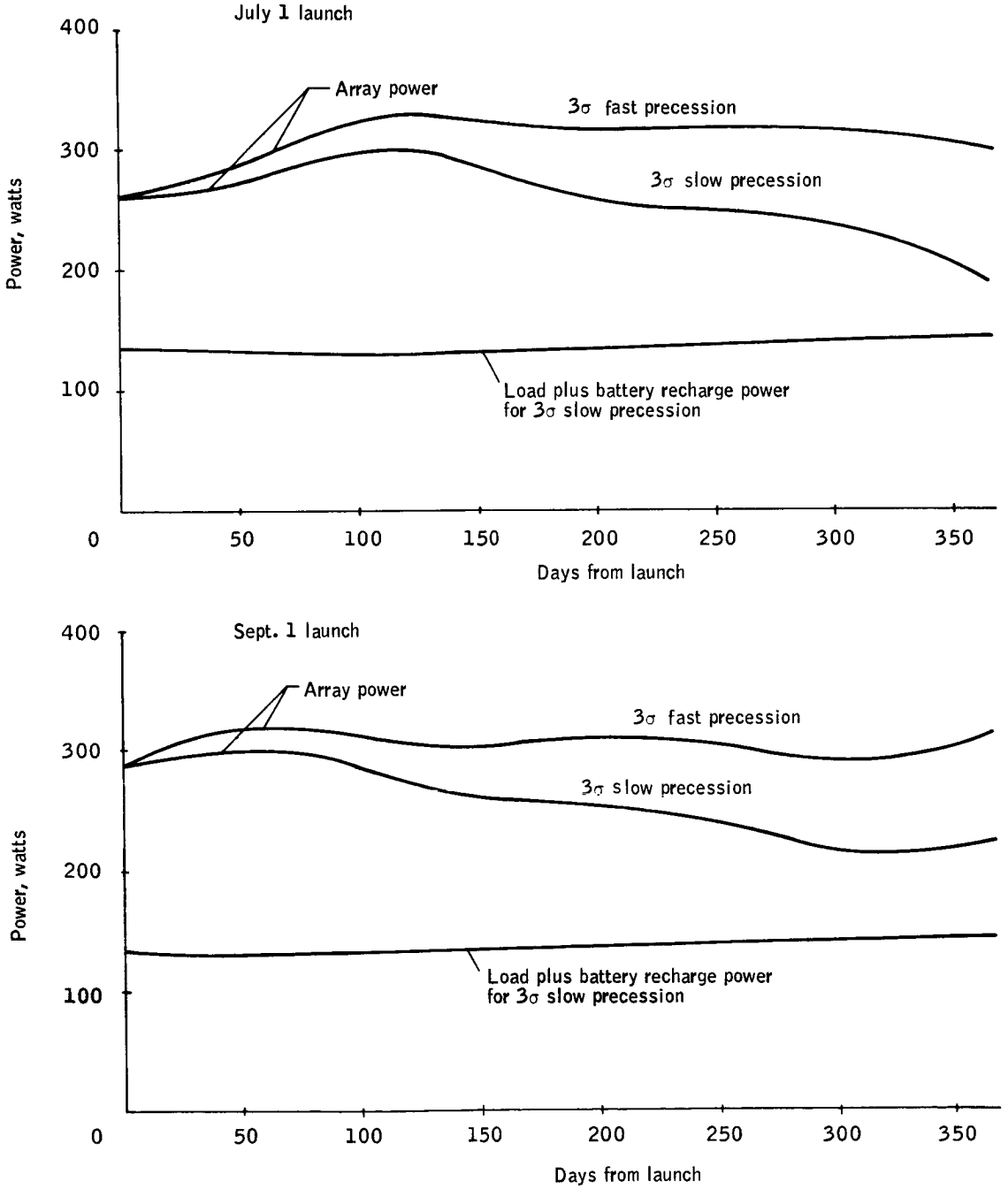

Figure 18. Effect of Orbital Variations on Power System, July 1 and September 1 Launches

- For the power conditioning equipment, the optimum number of series solar cells is that which produces at the 31-degree sun angle (where output voltage is lowest) sufficient voltage to permit operation of the charge regulators into the highest battery voltage. Since it is unlikely that the exact desired voltage corresponds to a feasible panel layout, the optimum is that nearest to the minimum allowable. Parallel cell requirements are those needed to produce the necessary current plus margin at the 64-degree sun angle. Final solar array panel layout and voltage may be influenced by other factors.

- Worst power demand occurs for simultaneous conditions of 35 minutes shadow at 64-degree sun angle.

- Power system limitations in regard to vehicle magnetic moment must be observed.

- Battery requirements of temperature and charging for the actual installed conditions of thermal transfer must be strictly observed to assure against destructive gassing.

Block diagram description. -- The power subsystem concept incorporates the most applicable components studied into a subsystem capable of providing the required power. Operation is described with reference to Figure 19. Power users will be provided with dc buses of +28 and +5 volts with respect to common. Design value of the power usage is 20 watts at 5 volts and 50 watts at 28 volts, with a 26-watt periodic load on the 28-volt line. Regulated outputs are supplied by switching regulators which operate from the unregulated power bus.

The unregulated bus derives its power from the solar array during satellite day and from the battery during satellite night. The battery is diode coupled to the unregulated bus so that load power is automatically taken from the array when it is available and from the battery when array power is not available. The standby battery and charger are available for use if the working set fails.

A switching type charge regulator is used to obtain constant-current control capability, which is the desired mode of charging for the battery.

If either of the regulated bus voltages are pulled significantly below their regulated value, a large fault current is supplied by means of a rectifier which couples the lower cells of the battery directly to the line. Thus, large currents are available for actuating protection devices or clearing faults.

Subsystem operating characteristics. -- The power subsystem operating characteristics are represented by the Figures 20, 21 and 22. These figures depict the approximate volt-amp characteristics for the solar array for the nominal and the two 3-sigma conditions of 31-degree and 64-degree sun angle. These plots represent the array characteristics expected after one year of operation in the expected environment, that is, all deteriorations expected

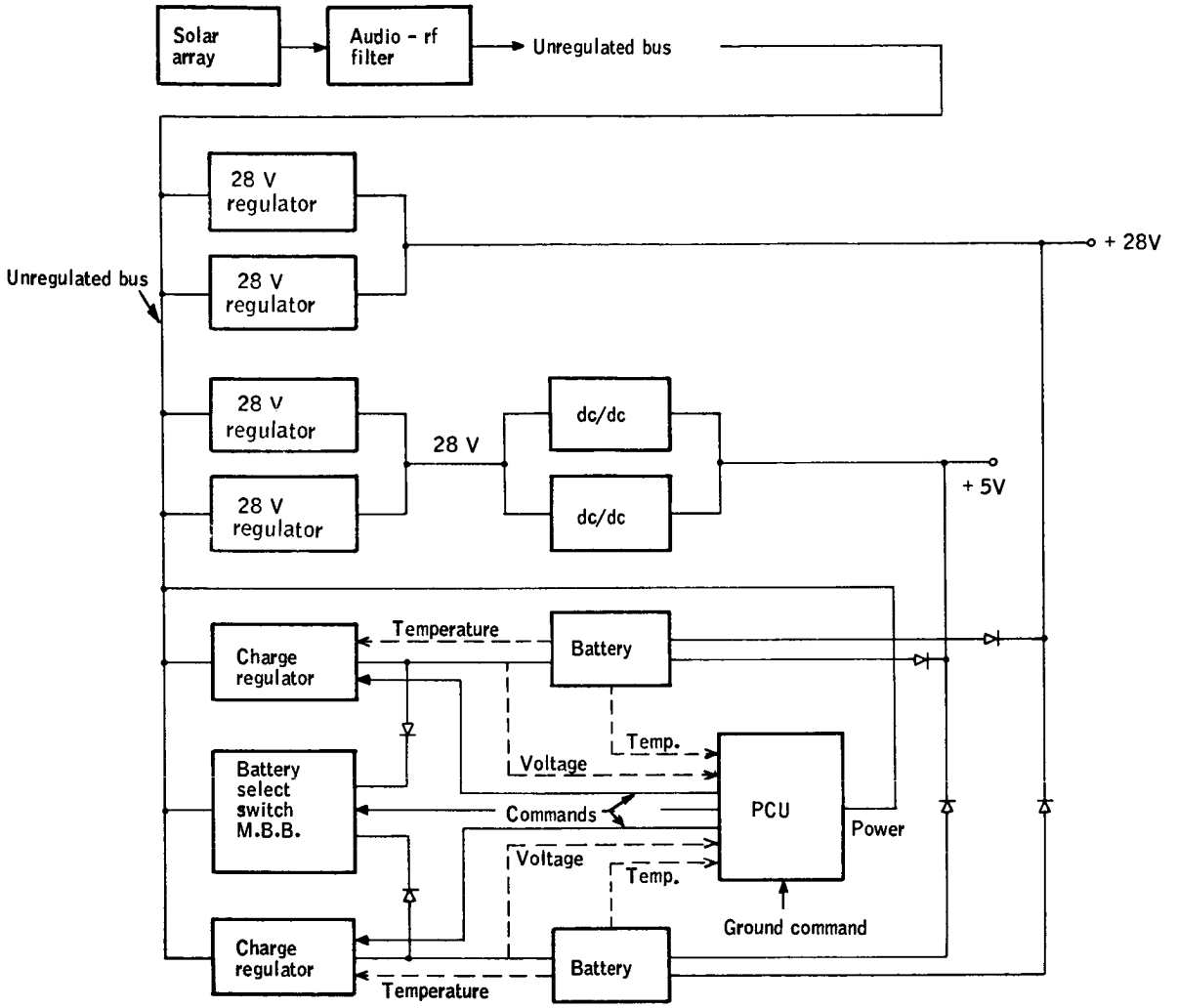

Figure 19. System Block Diagram

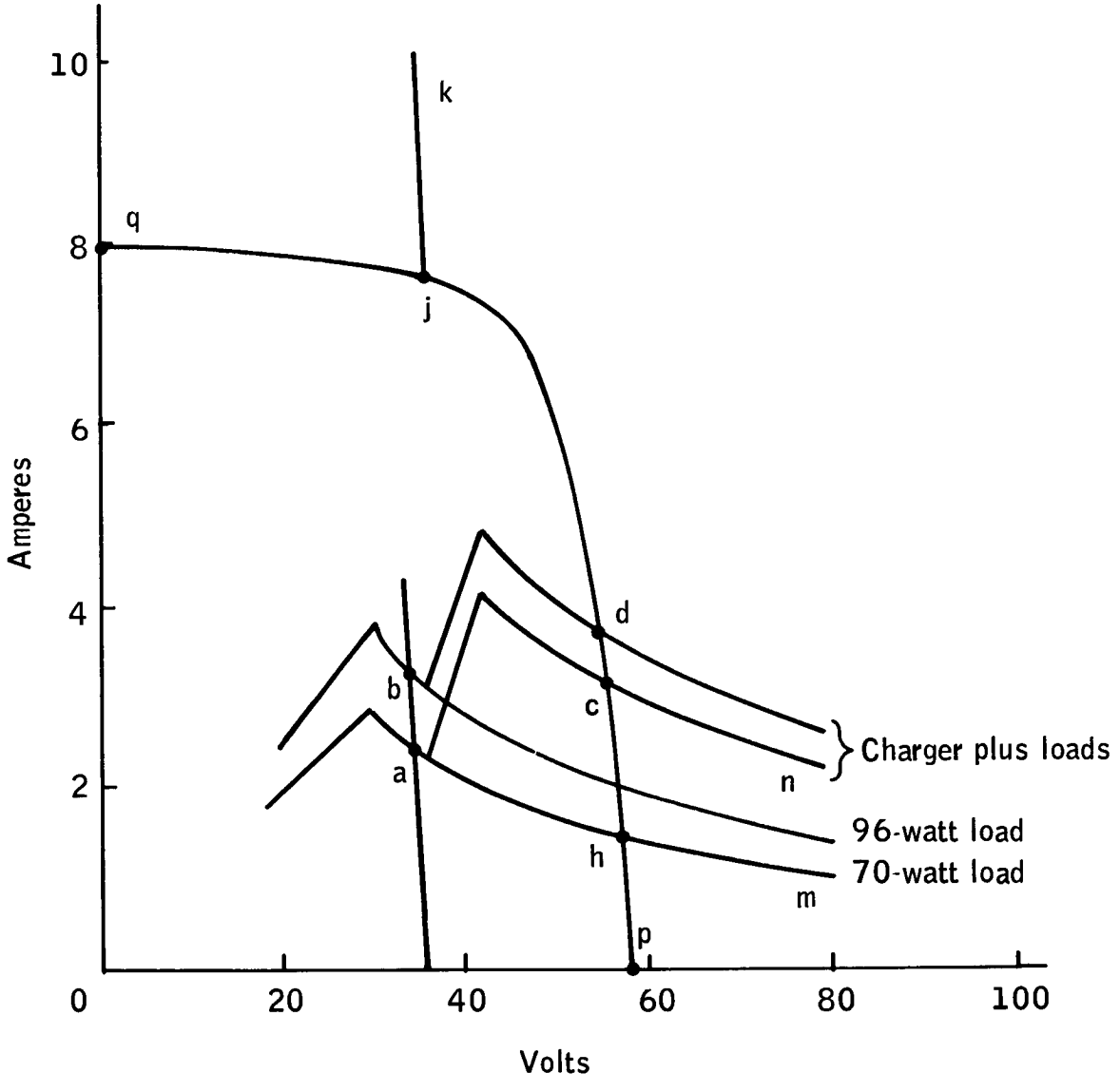

Figure 20. System Operating Characteristics, 45° Sun Angle

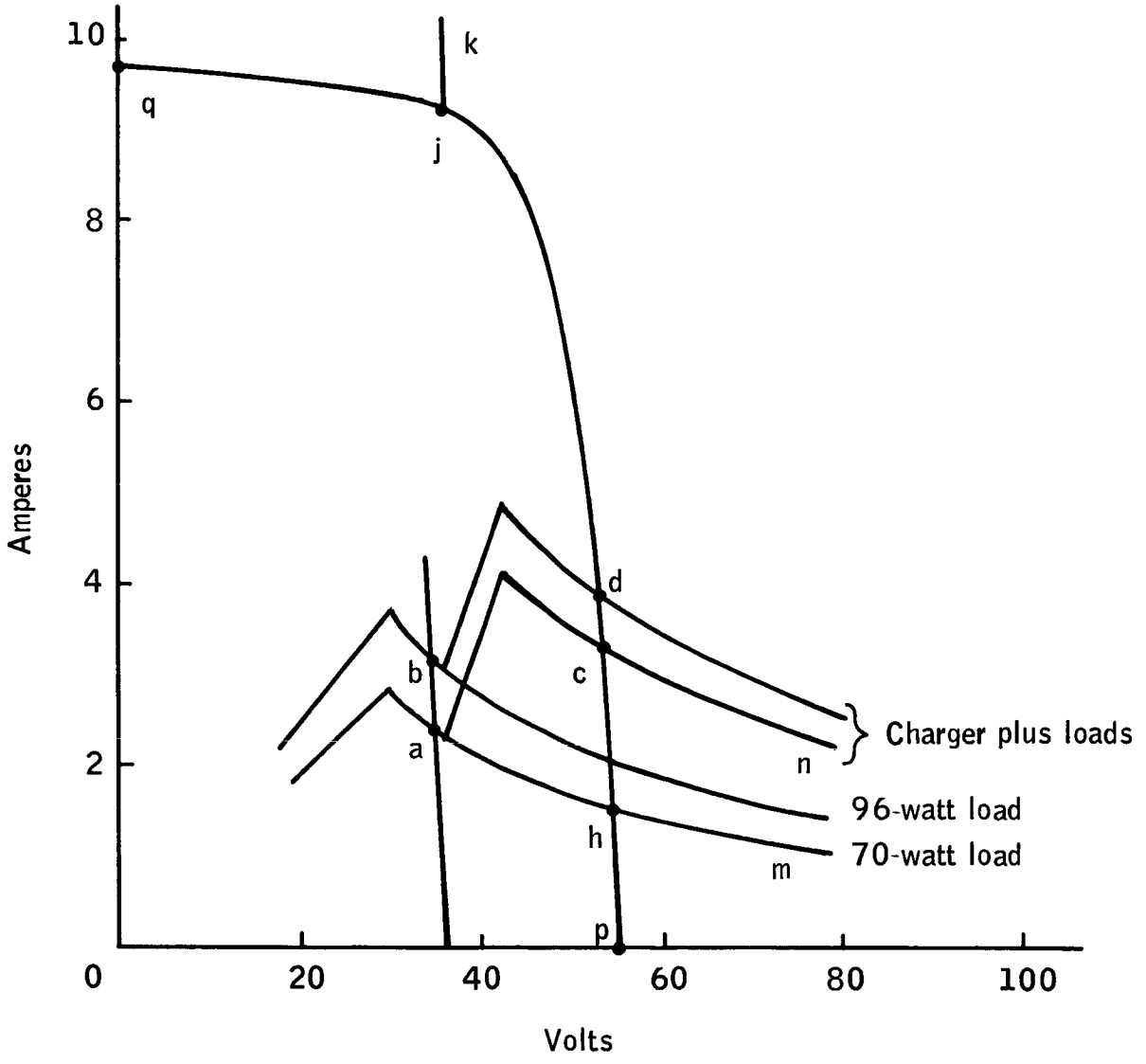

Figure 21. System Operating Characteristics, 31° Sun Angle

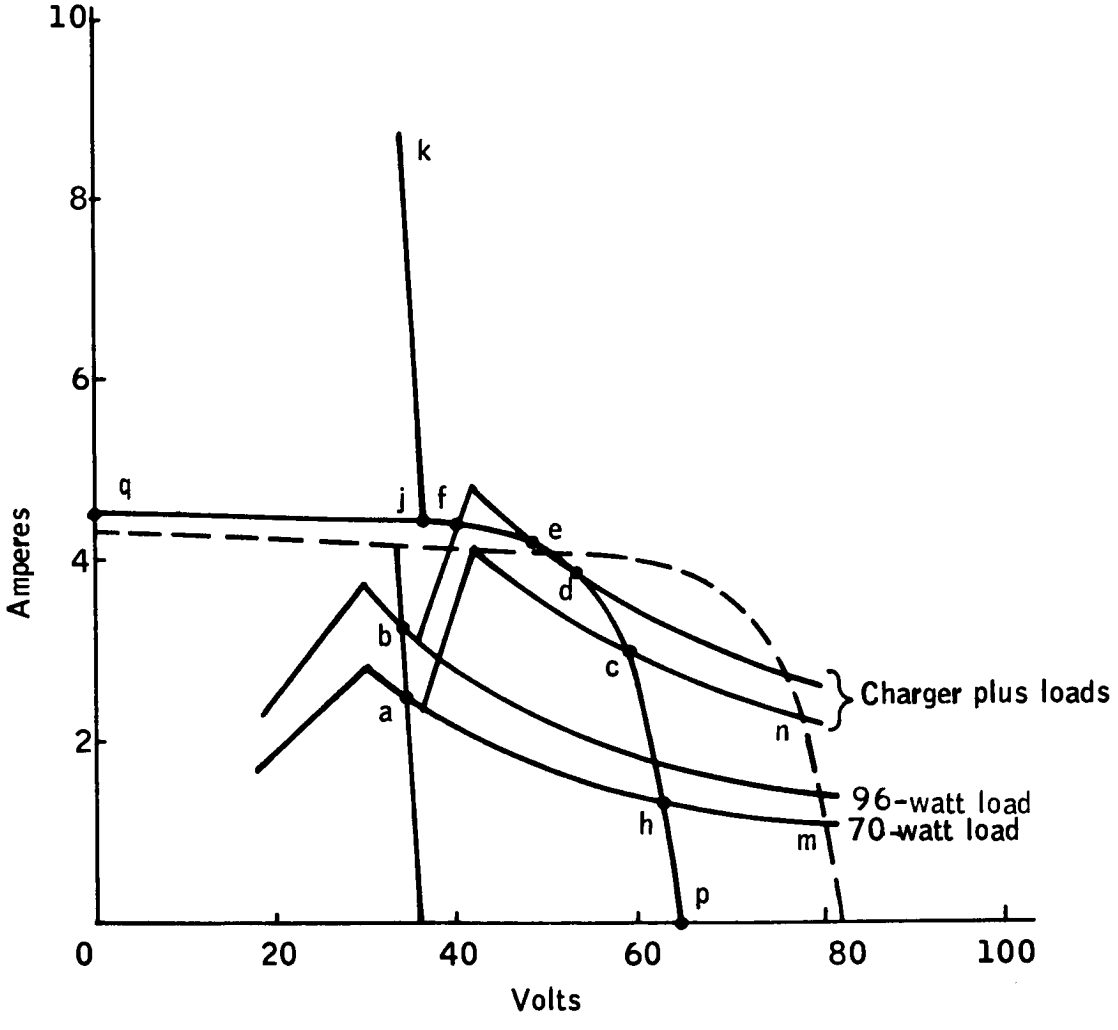

Figure 22. System Operating Characteristics, 64° Sun Angle

during the one-year operating period have already been included. The open-circuit voltages and short-circuit currents to be expected are indicated by points p and q, respectively. Volt-amp characteristics (Figure 20) for the regulators at normal load and the charger as reflected to the array are given by the curve through points a - m and c - n, respectively. During peak loads, the curves pass through b and d instead of a and c. With increase in voltage, the load plus charger current is shown to fall off, as would be expected from the nearly constant efficiency of the power conditioning. For decreasing voltage, the constant-power mode of operation terminates at the voltage where the switching regulators have insufficient differential voltage across them. Where the differential is not adequate, operation is typified by cessation of regulator switching and approximately one-to-one transfer of current from input to output.

The line through b and a, extended back to the zero-current line, represents the volt-amp curve of the battery and, hence, the unregulated bus during satellite night. During satellite day, unregulated bus characteristics are represented by the curve p-c-d-j-k. Intersection of the load and the supply curves at a represents the operating point during satellite night and average load. Addition of peak-load conditions moves the operation to b.

Assuming vehicle operation at the nominal 45-degree sun angle and that the charger does not immediately draw current from the array, emergence of the vehicle from earth's shadow would result in shift of operating point from a to h. Addition of the charger load would result in a change in operating point from h to c. At this time there is a surplus current of about 3.8 amperes array current. The above statement neglects the fact that, when the array first supplies current after earth's shadow, the volt-amp curve is somewhat different from that shown. It is clear that normal operation is represented by one of the four points a, b, c, or d.

If the vehicle moves to a 31-degree sun angle, all of the above statements hold except that there is a surplus of array current of about 5.3 amperes (Figure 21).

The limiting case, however, is the 64-degree sun angle represented on Figure 22. For this condition, there is an intersection of two additional points on the load curve with that of the array curve, namely e and f. For those voltages between about 41 and 49, the load requires more power than the array is capable of delivering. Because of this, point e is not a stable operating point, and any transient operation at this point would immediately be followed by degeneration to point f, where decrease in voltage is accompanied by decreased load requirement and increased power capability. Point d is also a stable operating point, for the same reason, although marginally so.

The significance of the above discussion is that if, for any reason, load requirements should exceed that represented by point d, there would follow an immediate degeneration to the operating point f. Change of operating point from d to f could result from a load transient or a peak of ripple current.

Gradual availability of current from the array, such as that which occurs following earth's shadow during each orbit, could latch operation at this point. All of this discussion has been with respect to operation during peaks of power drain, and is not a power system limitation since the peak power drain exists for only a short period of time. For "normal" load conditions, operation is at point c until the batteries are charged. For this point, stable operation is unconditional and essential to a satisfactory system design.

The ultimate system limitation on maximum sun angle is associated with the fact that in normal operation the current fluctuates about the average operating point c. This fluctuation is the result of peak currents required by switching regulators, warm-up transients associated with the attitude control system, and other as yet undefined current surges due to switching. Peak currents drawn by all sources must be maintained at a value less than that which would pass the peak power point for the solar array. Filtering for the regulators in question will hold the ac current reflected into the array to less than 0.250 amp peak to peak. If the peaks due to three regulators occur simultaneously, unlikely since switching is entirely noncoherent for the three regulators, the current peak would be drawn only occasionally. Normal operating current is 3.0 amps, and current peak would be under 3.3 amps for simultaneous load peaks, assuming worst-case distortion. Array current at maximum power is 4.2 amps, a margin of 27 percent over the 3.3 amp value. Added protection against the effects of a one-time current peak is provided by the circuit monitor described below.

Operation at point f represents a "power limited" condition, that is the power required for "normal" system operation in the constant power region (through points e and d) is not available from the array at this value of voltage. This results in the battery charge current being reduced to a value lower than programmed. Since this condition can exist only for the short duration of the high-value peak load and for a very short time immediately following satellite night, there are no adverse consequences (see later discussion). Over a longer period of time, the "latch up", corresponding to an operating point such as f, would cause battery failure through inadequate recharge. Reference to Figure 10 shows that for increasing sun angle above 64 degrees, there is only a degree or two of margin until this limitation is encountered. Increase in the sun angle, at which the system fails for lack of array power, can be achieved by delaying application of the charger load following availability of array power at satellite sunrise. If this is done, operating point a will be followed by operation at point h and, immediately after application of the charger load, by operation at point c, which is the desired stable operating point. Alternatively, a circuit which would detect "switching" in the charge regulator could be used in the absence of switching, but with the flow of array current, the charger would then be switched off for a short period of time to allow the array to achieve higher voltage. Immediately following earth's shadow, the array has reached very low temperatures and hence has a different volt-amp characteristic. This is shown by the dotted array curve in Figure 22. As the array warms, the characteristic gradually changes back to that through c and h, the characteristic assumed for the previous discussion.

Battery charging. -- Battery charging is accomplished with a constant-current charge for the duration necessary to reach the maximum limiting voltage, followed by a moderate rate trickle charge. This charge regimen is adequate for maintaining battery operation over the entire, expected temperature range. For the worst-case orbit, the battery charge will continue at the initially established high rate for nearly the complete orbit. For the least severe case, the duration of the high rate battery charge will be considerably shorter. During this period, the standby battery will be charged at a constant-current rate about half that for the working battery, which should maintain the standby battery in essentially new, unused condition. A drop in battery voltage below a predetermined value will show that the working battery is unable to supply the required load. Continuous monitoring of the battery voltage permits the system to switch to the standby battery whenever an abnormal, low-voltage condition exists so as to maintain continuous, uninterrupted power to the spacecraft control and data handling subsystems. After switchover, the standby battery becomes the working battery and experiences the same charge program as the original working battery.

The charge regulators provide one of two charge programs to each of the batteries:

1. Working battery - charge at 2.0 amp until "limiting voltage" is reached. Charge thereafter at 0.45 amp.

2. Standby battery - charge at 0.1 amp until "working" battery reaches "limiting voltage". Charge at 1.65 amp until "standby" battery reaches "limiting voltage". Charge thereafter at 0.1 amp.

The life and reliability considerations of this study are based on complete switch-out and abandonment of the failed battery since this results in a system of minimum complexity. Further optimization of the charge control system may be possible in the early design period since redundant battery chargers are provided. Options, other than complete switch-out of the failed battery, would include application of a trickle charge, application of all available excess array power, or an attempt to recondition the failed battery by remedial discharge and recharge measures. Use of any of these alternate control modes is dependent on the ability to determine the type of battery failure from available status monitoring data, the effect of possible release of battery gases on the spacecraft, and circuit complexity.

Ground command. -- Ground command provisions allow ground control or selection of any mode of system operation in the event of revisions in operational requirements or problems in system operation after spacecraft launch. Ground command requirements are also established by automatic control versus ground control complexity tradeoffs and by requirements for automatic control override. The specific identification of each ground command is established in the preliminary design stage as system interfaces are determined. The following command requirements have been established:

- Power system override - five commands
- Power reclosure - seven commands
- Emergency and mission termination - four commands

Status monitoring. -- Electrical power system status monitoring will indicate ground command requirements, will monitor protective system status and will provide a system history for failure analysis. Status monitoring also monitors redundant equipment to indicate the need for launch of a back-up spacecraft. A monitoring points budget has been established to ensure adequate provisions for power system monitoring:

- Battery status - six points
- Array status - six points
- Load status - eleven points
- Redundancy status - three points

Subsystem Operation

For the purpose of this discussion, the orbital flight will be separated into three distinct phases during each of which the mode of operation differs from that of the others. These conditions are prelaunch, launch, and steady-state orbit.

During the prelaunch period, the power system will be in an essentially steady-state operation, and all power will be applied from an external power source. External power will be coupled to the system at the unregulated bus. Presence or absence of power on this external lead will then simulate presence or absence of illumination of the solar array. If in addition to this the external supply has a volt-amp characteristic similar to that of the solar array, a very good degree of simulation of orbital conditions can be accomplished. During this mode, the charge regulators will be effective in maintaining the batteries at full charge, and removal of the external power supply will result in assumption of the load by the battery. By means of the ground override, it will be possible to test the capability of either battery to supply the load, and also by means of monitor points it will be possible to ascertain that both batteries are fully charged before deciding whether launch should proceed. It is necessary, in addition, that switching be provided so the batteries can be totally disconnected from the load to avoid undesired discharge.

The launch phase of the flight commences when connections to external power are broken permanently and ends when the vehicle is in orbit at the proper angle with respect to the sun and deriving power through the deployed solar array.

If all goes well, the length of time between assumption of the load by the batteries and the flow of power from the deployed array will be approximately 11 minutes. If array deployment proceeds on schedule, the battery will have supplied approximately 15 watt-hours of output during the interim, or about eight percent of the capacity of one battery. If there are 20 minutes of remaining sunlight following deployment of the array, the working battery will be fully charged before the commencement of the first earth shadow. For this sequence of events, the vehicle has then achieved the equivalent of the steady-state orbital conditions in approximately 30 minutes.

In the event of a failure which prevents acquisition of the sun in the length of time required, there are approximately five-hours operation available from both batteries operating at full load. This figure is extremely pessimistic because it assumes absolutely no power available from the solar array. The five-hour period can be extended considerably if portions of the load are removed during early phases of the flight.

The steady-state orbital operation of the power system is determined largely by the orbital condition of sun angle and shadow fraction. Effects of these variations on the power system are discussed in the previous section. During normal operation, represented on the operating characteristics diagram for the nominal 45° sun angle (Figure 20), operation is represented at either point a or b during satellite night, depending upon whether or not communications equipment is in operation.

During satellite day, operation is at point c or d, once again depending upon operation of the communications equipment. Normal variation through sun angles to 31° shows that points c and d are slightly changed in their location, as shown in Figure 21, due to the change in the volt-amp characteristic of the array. The limiting condition at 64° sun angle is also shown (Figure 22) with the multiple crossover of the supply and demand characteristics represented as points d, e, and f. Potential difficulties associated with this fact are dealt with as discussed in the power system description.

During the period of a year, there may be failures within the power system and other subsystems. These possibilities are dealt with by either disconnecting the subsystem in which the failure occurs, or in the case of the power system, by redundant components designed into the system.

All parts involved are in active redundancy, except in the case of the battery where one of the batteries is held in standby redundancy simply being maintained near or at full charge by means of the charge regimen described. Switchover in this case is automatic. Switchover is based on either excessive battery temperature or low end-of-discharge voltage. If a condition arises in which there is instability in the battery resulting in undesired switching between batteries, this can be overridden by ground commands and the battery selection made permanent.

Solar cell and cover glass. -- Because of possible large temperature excursions due to the various sun-angle orientations to which the spacecraft may be subjected and because of the desire to use a relatively high voltage (44 V) from the array for better power system efficiency, it would be desirable to use a low resistance cell. The main disadvantage to the use of such a cell is its lower resistance to radiation degradation.

Temperature coefficients of the voltage at maximum power are typically 2.35 mV/°C for a Heliotek 10-ohm-cm cell as compared to 2.15 mV/°C for a Heliotek 2-ohm-cm cell. Figure 23 shows typical temperature characteristics for a 2 x 2 cm, 2-ohm-cm N-on-P solar cell.

Similarly, the filter characteristic was chosen to reflect the shorter blues and ultraviolet portions of the spectrum where the solar cell conversion efficiency is low, thus reducing the solar cell temperature at the low angles of incidence.

The radiation environment that will have an appreciable influence on solar cell performance will be comprised of high-energy protons and electrons trapped in the earth's radiation belts, high-energy solar protons from solar flare activity, and ultraviolet solar radiation. The high-energy proton and electron radiation causes damage to the silicon crystal lattice which results in a degradation in the voltage-current characteristics of the solar cell in both the voltage and current axes. These high-energy particles also cause darkening in glass or silica cover shields and the adhesive used to bond them. Ultraviolet radiation does not damage the solar cell; however, it does cause darkening of the cover shield materials and the adhesive used to bond them. Darkening of these materials decreases light transmission, thus degrading the current output of the solar-cell voltage-current characteristic.

The radiation analysis was divided into two basic types: 1) the resulting solar cell output degradation due to high energy particles on the crystal lattice, and 2) the darkening effects of the cover slide and adhesives.

Trapped particle radiation environment was determined from reference 5. Solar proton prediction and probabilities were determined from references 6 and 7. Solar protons were projected such that there is a 0.99 probability that the actual protons encountered in a year will be less than the estimate used.

As can be seen from Figure 24, by using a cover slip of six-mil thick (0.035 g /cm^2) fused silica, complete shielding of low-energy protons (below 4 MeV) results. Using this choice of cover material the remainder of the radiation analysis was made.

Using a Heliotek nominal 2-ohm-cm solar cell with a six-mil, fused silica cover slide, a radiation analysis for the prescribed orbit including an estimate of solar protons was made (Appendix D). This analysis indicated that at end of life the loss from hard-particle damage would amount to eight mV

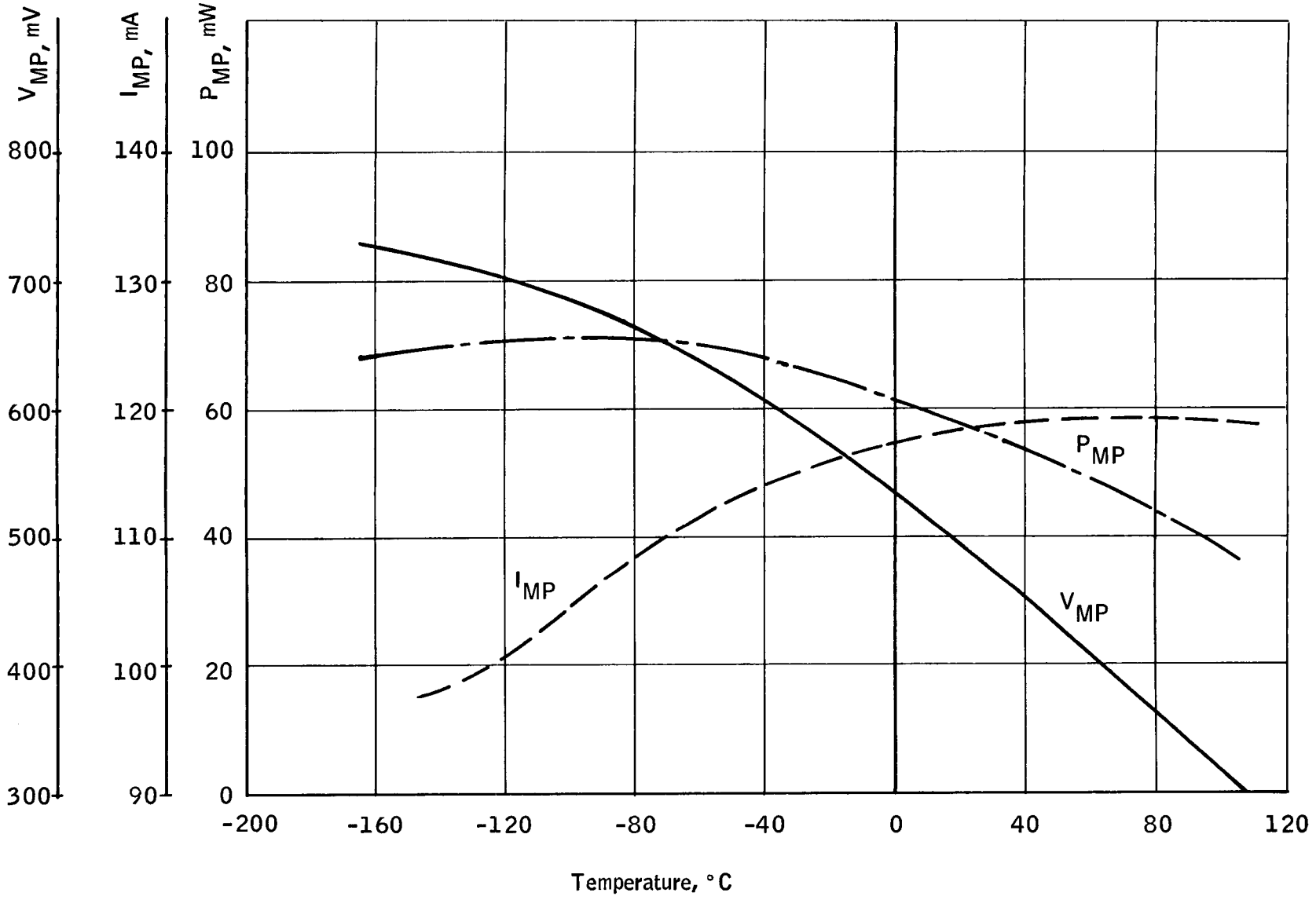

Figure 23. Temperature Characteristics of Typical Heliotek 2-Ohm-cm N/P Type A T-2020 Solar Cell Mounted on Panel Including all Assembly and Filter Losses But Without Diode Losses, Under AMO sunlight, 140 mW/cm^2, Std. 119

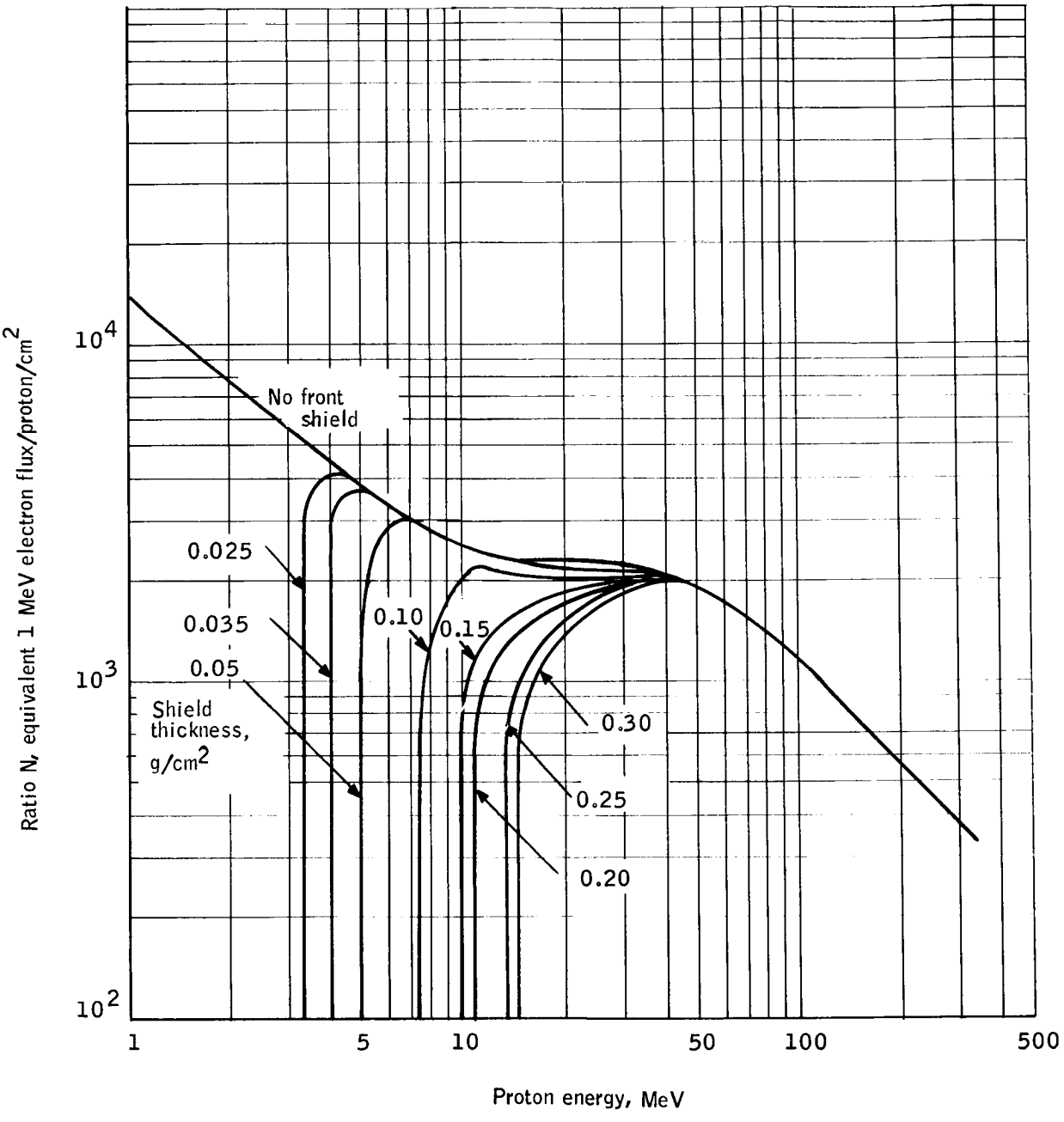

Figure 24. Solar Cell Damage Equivalent to 1 MeV Electrons as Functions of Proton Energy Infinite Back Shielding [From ref. 8]

per cell in voltage at maximum power and 3.5 percent in the corresponding current.

It has been assumed that the satellite will be located in a position in space that would receive all the protons anticipated. In fact, this is not the case because the HDS orbit is at a low altitude, and in most cases the protons from the sun must pass through the earth's magnetic field before reaching the satellite. The protons are not likely to pass through the earth's magnetic field without being trapped. Therefore, the only solar protons which are likely to bombard directly the satellite are the ones coming in from the polar regions, which comprise a small percentage of the total flux. Use of the solar proton flux without the magnetosphere shielding thus incorporates into the design some safety factor.

Cover glass particle radiation damage will have a darkening effect on the cover slip, thus decreasing the current from the solar cell. In addition, ultraviolet radiation can cause darkening of some cover glass and adhesive materials (refs. 9, 10, and 11).

Heliotek has also done extensive ultraviolet radiation testing on fused silica adhesive covers and these have shown a 0.7 percent degradation in I_{sc} after exposure to 170 hours to an ultraviolet source which was equivalent to 25 suns. This would correspond to about one-half year exposure. It is assumed that a 1.5 percent degradation in short-circuit will cover the darkening effects anticipated from fused silica, bonded either with RTV 602 or Sylgard 182.

Solar array performance calculations. -- The HDS orbit has been tentatively defined as: sun synchronous, 97.38° inclination, 500 km altitude, with a 3:00 p.m. launch in late October 1969. The angle of incidence relative to the vehicle spin axis will vary through the year on either side of the nominal 45° initial value. Taking into account the anticipated three-sigma limits for launch error, the angle of incidence from the sun line to the spin axis can vary from a minimum of 31° to a maximum of 64°.

The maximum spacecraft envelope is generally described as a cylinder 54 inches in diameter and 44-inches high. Cylinder diameter is limited by the Thor-Delta shroud while cylinder length is somewhat flexible. The spacecraft will rotate about its axis at approximately 3 rpm. The axis itself will be maintained in close orientation perpendicular both to an earth radius and to the plane defined by the orbit plane. In this oriented mode, the top face (opposite to the booster interface) will be illuminated in accordance with the sun-line angle variation from 31° to 64° as discussed above. The rim of the cylinder will be rotating about the spin axis, and the incidence angle of the element in the plane defined by the sun line and spin axis will range from 59° to 25° to the sun line. The rear end-face of the spacecraft would not be illuminated after orientation.

The actual spacecraft surface will require several openings which cannot be obstructed or have any objects within given field angles. On the cylindrical surface of the spacecraft there will be a radiometer port 16 inches in diameter

and a sun shade which shades the rear 18 inches of one side. On each face adjoining to the radiometer port will be a seven-inch diameter starmapper viewport. In addition, near and parallel to the center cross-sectional plane are eight (8) uhf antenna slots spaced at 45° intervals. On the rim just below the front face (opposite the booster) are two areas 3-1/2 inches wide by 7 inches long reserved for horizon sensors which are 180° apart. There are also 3 inch by 3 inch areas reserved for sun attitude sensors, which will be located near the baseplate on the rim. There are also four (4) vhf antennas on the surface constructed of 1/8 inch diameter rod, 21-1/2 inches long, each end extending at an angle of 45° from the face outwards from the spin axis. The mount points of these antennas are one-inch diameter and are 90° apart around the spin axis, forming a square with 21 - 1/2 inch diagonals.

Based upon the above constraints, the most satisfactory approach was concluded to be that, upon deployment, the array would be planar at the front face of the spacecraft with cells mounted on panels only or on panels and on the front face. Further temperature considerations of the spacecraft precluded use of the latter.

With the choice of a tentative configuration of six panels only, the next step is a satisfactory electrical and mechanical cell layout. The basic criteria to meet were:

- Power under worst conditions: 189 watts
- Angle of incidence from sun line to spin axis: 45° nominal varying from 31° to 64°
- Temperature on face of panels: 45° angle: 43°C
31° angle: 56°C
64° angle: 17°C
- Minimum unregulated maximum power voltage from array: 44 volts (189 watts)

The minimum maximum-power voltage could be met under the worst conditions at the 31° angle utilizing 108 nominal 2-ohm-cm Heliotek N-on-P cells. Figure 25 shows the output of such a cell mounted on a panel including all assembly losses, but not including diode drops or radiation damage. Figure 23 is a plot of the temperature characteristics of this cell.

With the above as a starting point, a power analysis was made to determine the number of series strings required to meet the power requirement at the 64° angle of incidence, the worst case.

The radiation analysis indicated that at end-of-life the loss from hard-particle damage to nominal 2-ohm-cm Heliotek N-on-P cells would amount to eight mV per cell in voltage and 3.5 percent in current. An additional 1-1/2 percent loss in current can be anticipated from ultraviolet damage to the cover glass and adhesive system. Another 2.6 percent was allowed in the design to account for various rms instrument and radiometry measurement

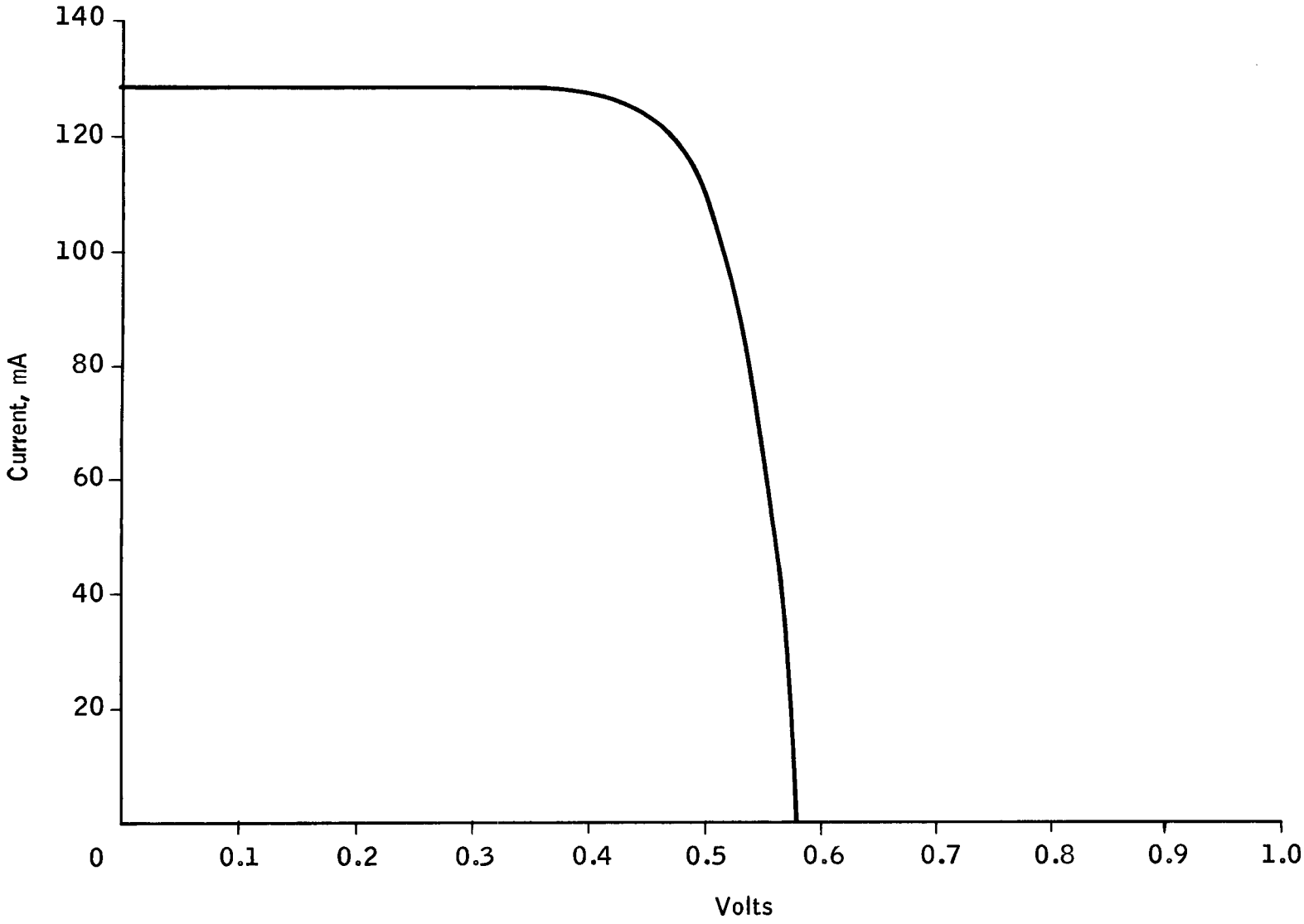

Figure 25. Electrical Output of Typical Heliotek 2-Ohm-cm N/P 2x2 cm Type AT-2020 Silicon Solar Cell Mounted on Panel Including all Assembly and Filter Losses, Spectrolab Solakote B or OCLI 207, at 28°C at AMO Solar Intensity, 140 mW/cm^2, Std. 119, at Start of Life Without Radiation Damage

uncertainties, and an additional 3.5 percent to reflect the minimum anticipated solar constant. Specific allowances were further made for the fall-off of both voltage and current with angle of incidence as well as the thermal characteristics of solar cells. Figure 10 indicates the anticipated fall-off due to sun angle.

This analysis indicates that this power requirement of 189 watts could be met with 96 strings at the 64° angle.

Solar cell array construction. -- The solar cell array would be made up of six identical hinged panels of half-inch aluminum honeycomb construction. Mounted on each panel are two circuits of eight cells in parallel by 108 cells in series. Each circuit would be isolated by redundant diodes to add reliability in the event of a circuit short. The circuits are laid out symmetrically so that the magnetic effect of each circuit is cancelled by the circuit immediately adjacent to it. Figure 26 shows such a layout.

The resultant assembly consists of a 0.002- to 0.005-inch-thick insulation sheet of epoxy impregnated glass cloth bonded to the aluminum substrate. The solar cell circuits are bonded to this insulating layer by means of a one- to two-mil layer of adhesive. This latter adhesive is of resilient silicone rubber such as RTV 41 or RTV 511. The cover slides are mounted on the cells by means of an elastic adhesive such as RTV 602 or Sylgard 182.

The problem of interconnections in the solar cell arrays, though apparently simple, is a critical area and merits careful consideration. There are various aspects of this problem, ranging from inter cell connections to interpanel connections. This discussion particularly relates to intercell connections within groups of cells in an unbroken, interconnected, series-parallel arrangement. It is understood that such groups are series connected to other such groups to form the complete circuits; such connections should always be completed with redundance to maintain high reliability. Such redundancy is particularly important where complex circuits with numerous circuit reversals are involved. The problems arising from the thermal and mechanical stresses within rigid assemblies led to the parallel submodule system of interconnection. The "Solaflex"* technique is based upon the use of a tab strip system. In this arrangement cells are connected into small parallel groups, using a "tab strip" soldered along the bottom of the cells. Upon mounting, each cell is independently suspended on its own resilient adhesive pad, isolated from the other cells except for electrical contact through flexible, stress-relieved tabs. Thus, virtually no stresses are transmitted from cell to cell. As a result, thermal stresses are minimized and, since the array is relatively flexible, it is less likely to fail due to vibration or shock.

---

*The arrangements described above, and developed by Spectrolab, are covered by U. S. Patent No. 3094439, now reissued as Patent No. Re 25,647, assigned to Spectrolab, Division of Textron Electronics, Inc., and by additional pending patents.

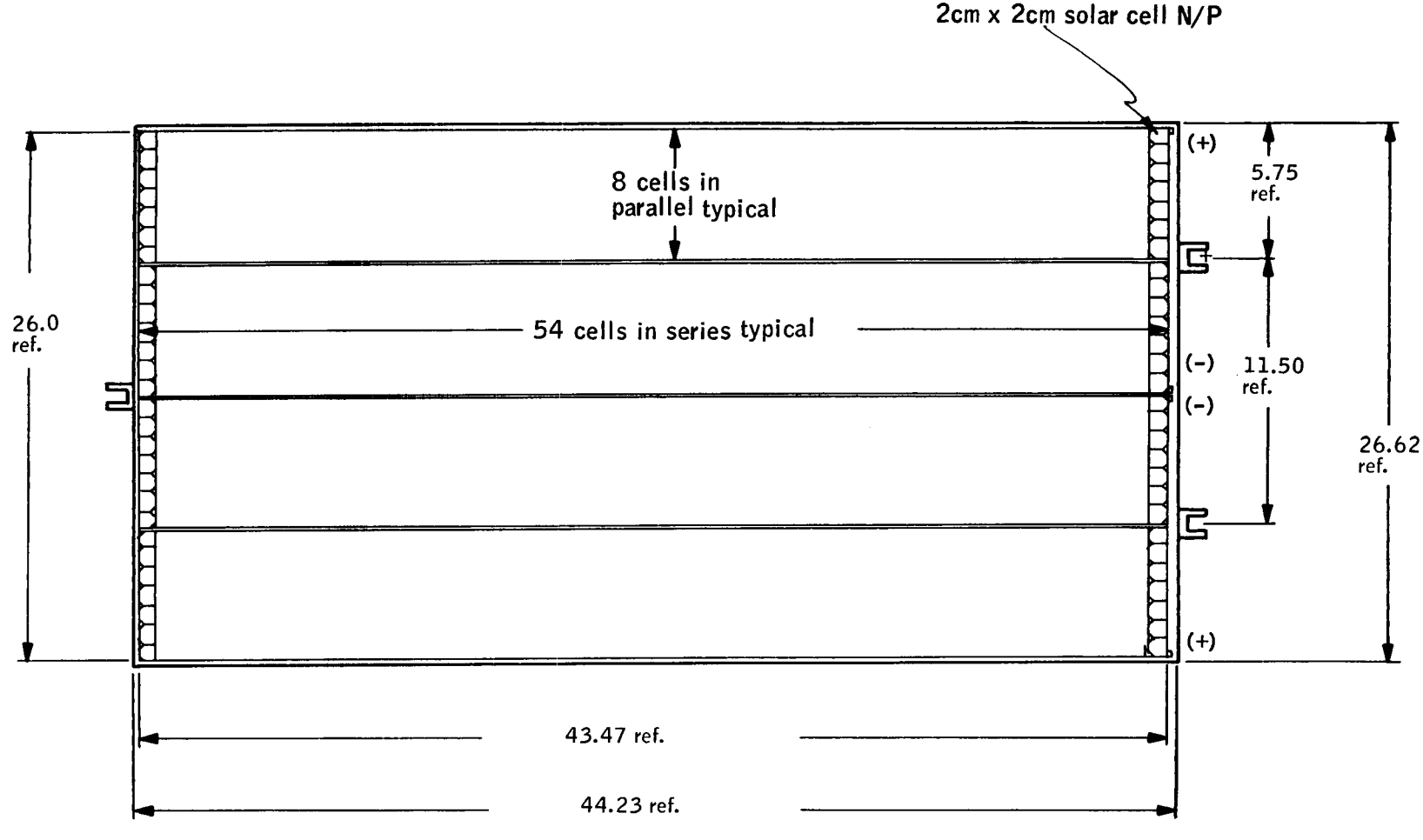

Figure 26. Typical Panel Layout of 6-Panel Array

The series interconnecting tabs extend out and up from the edge of the bus and are stress relieved before connection with the next succeeding series group, as shown in Figure 27. Redundancy is achieved by use of these multiple tabs and connections. Another feature of this cell interconnection system is that parallel current loops are effectively eliminated; that is, in a circuit using matched cells, current flow is in the series direction only, and flow in the parallel direction is eliminated. In the case of mismatch or cell degradation, only the differential current is distributed in the parallel direction.

In the case of individual cell failure or degradation, this interconnection system substantially increases reliability. The same parallel contact strip connects all juxtaposed series units with at least two connections (in some cases four) per cell.

Parallel interconnections made across both the N and P sides of parallel adjacent cells provide redundancy in both parallel and series directions. Spacing between the cells in series is a nominal 17 mils with 10 mils in parallel, giving excellent area utilization.

This tab interconnection configuration provides a substantial gain in solar cell array reliability (as much as a factor of 1000 for circuits involving as many as ten cells in parallel). The primary source for the increase in both system performance and reliability of the parallel-series "Solaflex" arrangement lies in the averaging of the currents from the various cells, thus tending to even out nonuniformities due to both initial cell properties and degradations from various sources. In the case of a cell open either from contact failure or from a fracture, the balance of the cells tends to pass the circuit current. However, in case of such a loss, the full circuit current cannot necessarily flow through the balance of the cells.

The interconnection system utilizes from two to four connections for each polarity of contact, substantially reducing the possibility of loss from an interconnection failure. Although cell stresses are considerably reduced and redundant connections are used on both positive and negative cell terminals, there still remains the possibility of cell fracture. An improvement in interconnection techniques has reduced circuit degradation due to cell fracture by an additional factor of at least two or three. The basic approach here is to use an extended tab interconnection strip so as to maintain continuity across that portion of the cell which is still connected in the circuit. In this way, a cell fracture will, on the average, remove only about one half of a cell, and the power loss is thus equivalent to less than one half the loss for a more conventional system.

Reliability. -- A reliability analysis for the six panel configurations is included as Appendix E. The reliability of the solar panel deployment mechanism is included in the spacecraft launch and injection reliability.

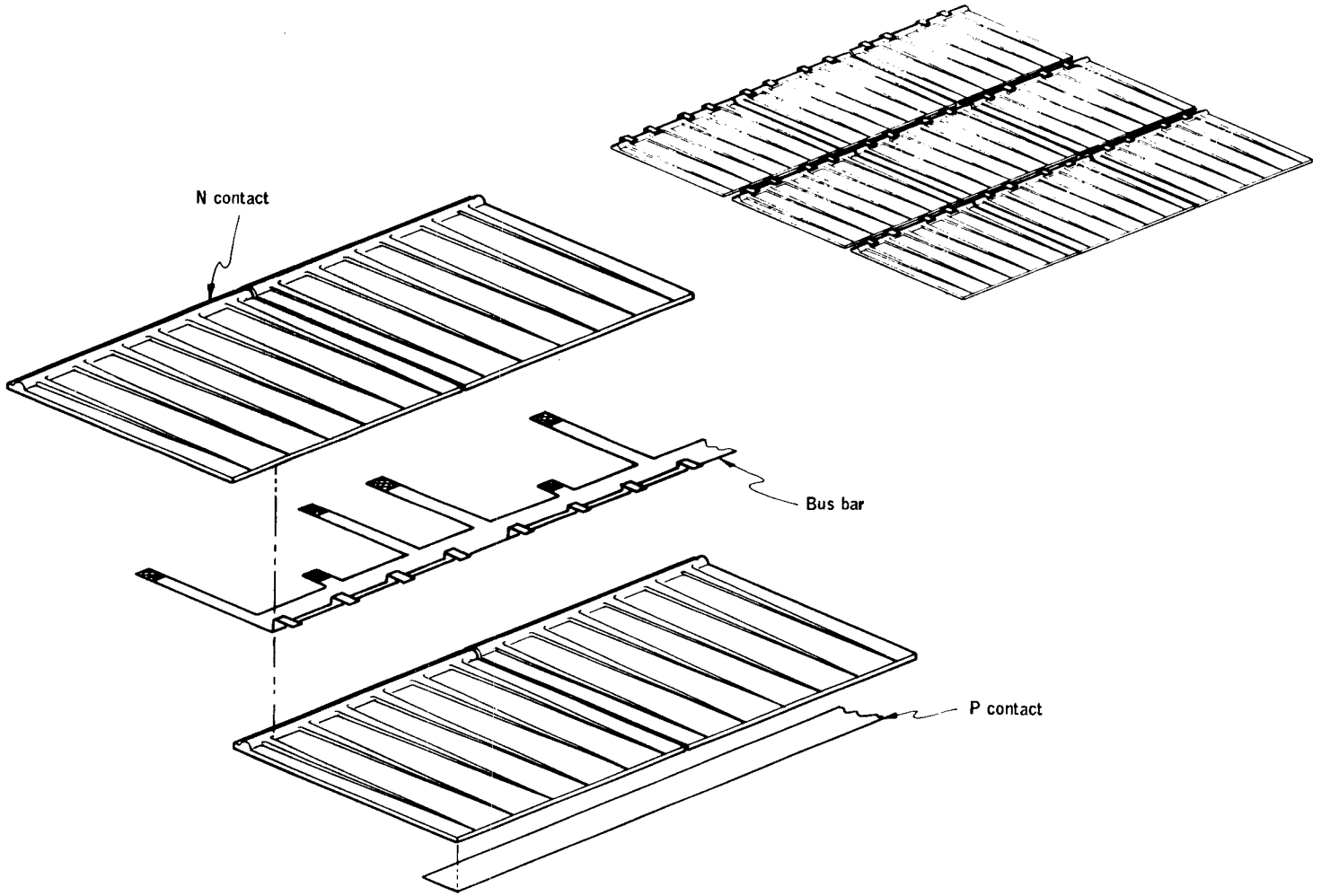

Figure 27. Solar Cell Interconnections

Reliability figures have been obtained from published data available for such items as diodes, solder connections, etc. In the absence of such numbers engineering judgment has been used. Testing of completed circuits to verify numbers of this magnitude is not feasible. Losses are most likely to come from temperature shock and collision damage.

The figures used for cell breakage in the analysis reflect some thought of these occurrences. The probabilities of encounters with micrometeoroids with an area of one square meter in one year are given in Table 8 for various kinetic-energy particles (ref. 12). The exact correlation with cell loss is open to interpretation and judgment.

In establishing the optimum circuit design, basic cell characteristics and the current-limiting effects of solar cells must be considered. In Figure 28 is shown the effect of loss of a single cell both by open circuiting, one cell at a time, and short circuiting across a given submodule of a module composed of 29 series-connected, five-cell parallel submodules. It is clear that in both cases the loss is substantially greater than the proportionate loss of the number of cells.

Consider for example the circuit which has 96 solar cells in series, five in parallel. If such a circuit has a single, open, total cell failure, there will be a total of 95 submodules, which have five cells in parallel, all in series with a single submodule,which has four cells in parallel. Since all submodules are in series, the current through each will be equal, but the current through each cell will not. The effect of the loss of a conducting path (an open-circuit cell) will be to produce a current-limiting effect on the affected circuit. Composite characteristic curves are formed for such a module in the following manner: composite characteristic curves are constructed for a "short string" of five parallel by 95 series cells. Also, a characteristic curve for a single submodule of four cells is constructed. The composite characteristic curve for one open-circuit failure is then formed by adding together the values of voltage for equal values of current. The effect in maximum power for such a circuit with various numbers of cells in parallel is presented as Figure 29. It should be pointed out that this curve is representative of what can be expected by paralleling solar cells in all configurations, although this particular curve is for 10-ohm-cm cells with 96 in series. The Reliability Analysis, Appendix E, utilizes the actual data for the HDS.

Battery

Selection of the HDS battery requires an analysis of battery life, battery cycle, power storage requirements, available charge time, discharge rate, voltage limits,and battery environment. As previously indicated, the HDS mission duration and cycle life requires a nickel-cadmium battery.

A primary factor necessary for the battery conception is the power required from the battery in each orbit. Given the design power/orbit demand of 70 watts in a 94.6 minute orbit of which the maximum expected occult is

TABLE 8. - PROBABILITY OF ENCOUNTERING MICROMETEOROIDS OF AREA OF ONE SQUARE METER IN ONE YEAR

[From ref. 12]

Kinetic energy, ergs	Mass, grams	Probable no. of encounters in one year	Aluminum penetration, mm
1×10^{13}	1.25	1.3×10^{-6}	109
1.6×10^{12}	0.198	8.4×10^{-6}	59
0.1×10^{12}	0.012	2.6×10^{-4}	23
16×10^{9}	2×10^{-3}	8.4×10^{-4}	13
6.3×10^{9}	0.79×10^{-3}	2.2×10^{-3}	9.3
2.5×10^{9}	0.31×10^{-3}	5.3×10^{-3}	6.9
1×10^{9}	0.12×10^{-3}	1.3×10^{-2}	5.1
4×10^{8}	50×10^{-6}	3.4×10^{-2}	3.7
1.6×10^{8}	20×10^{-6}	8.4×10^{-4}	2.7
6.3×10^{7}	7.9×10^{-6}	2.2×10^{-1}	2.0
2.5×10^{7}	3.1×10^{-6}	0.6	1.5
1×10^{7}	1.2×10^{-6}	1.3	1.1

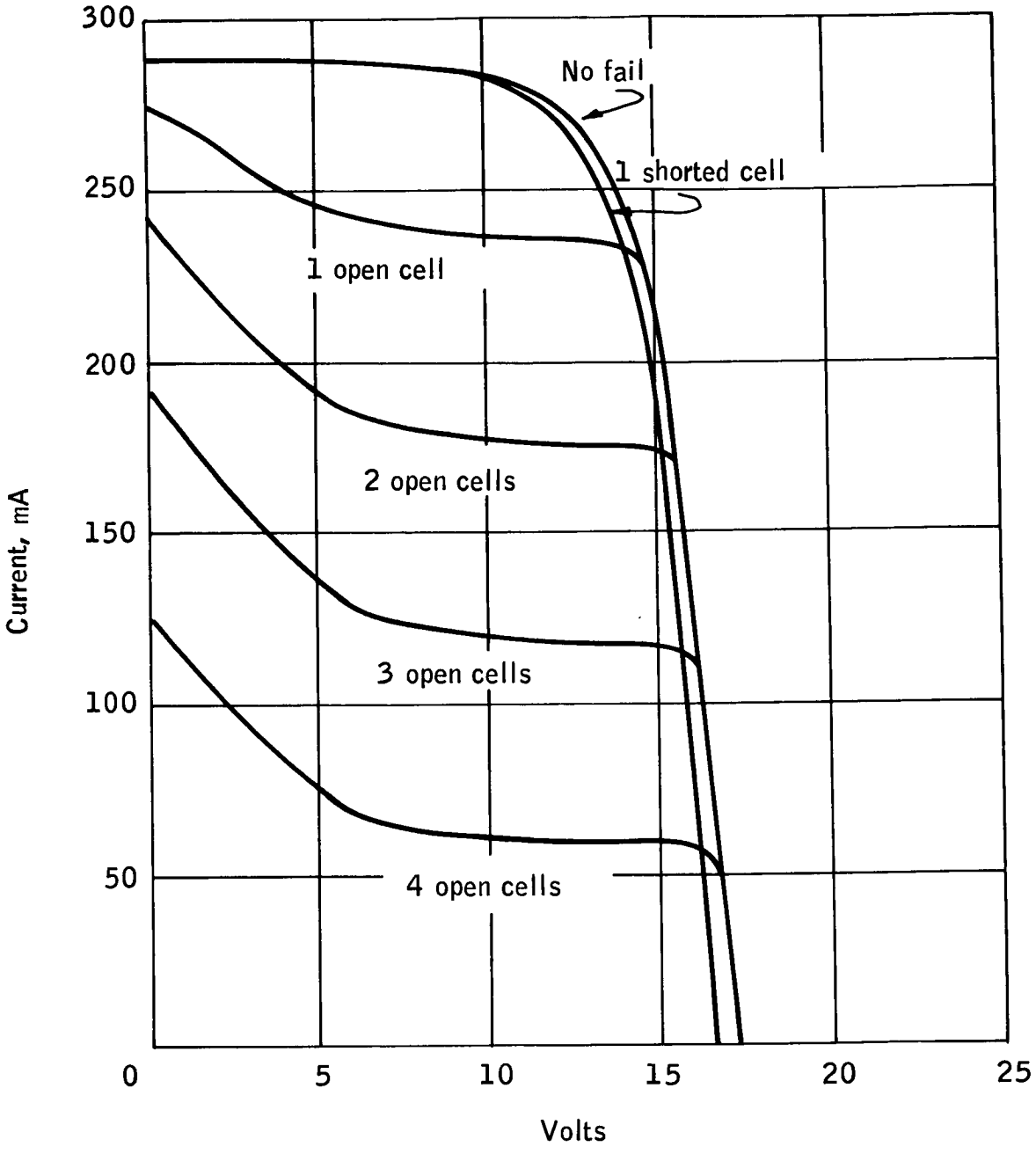

Figure 28. Effect of Cell Failures on Circuit Performance of Module with 29 Series-Connected, 5-Cell Parallel Submodules, Failures are Complete Opens or Complete Shorts

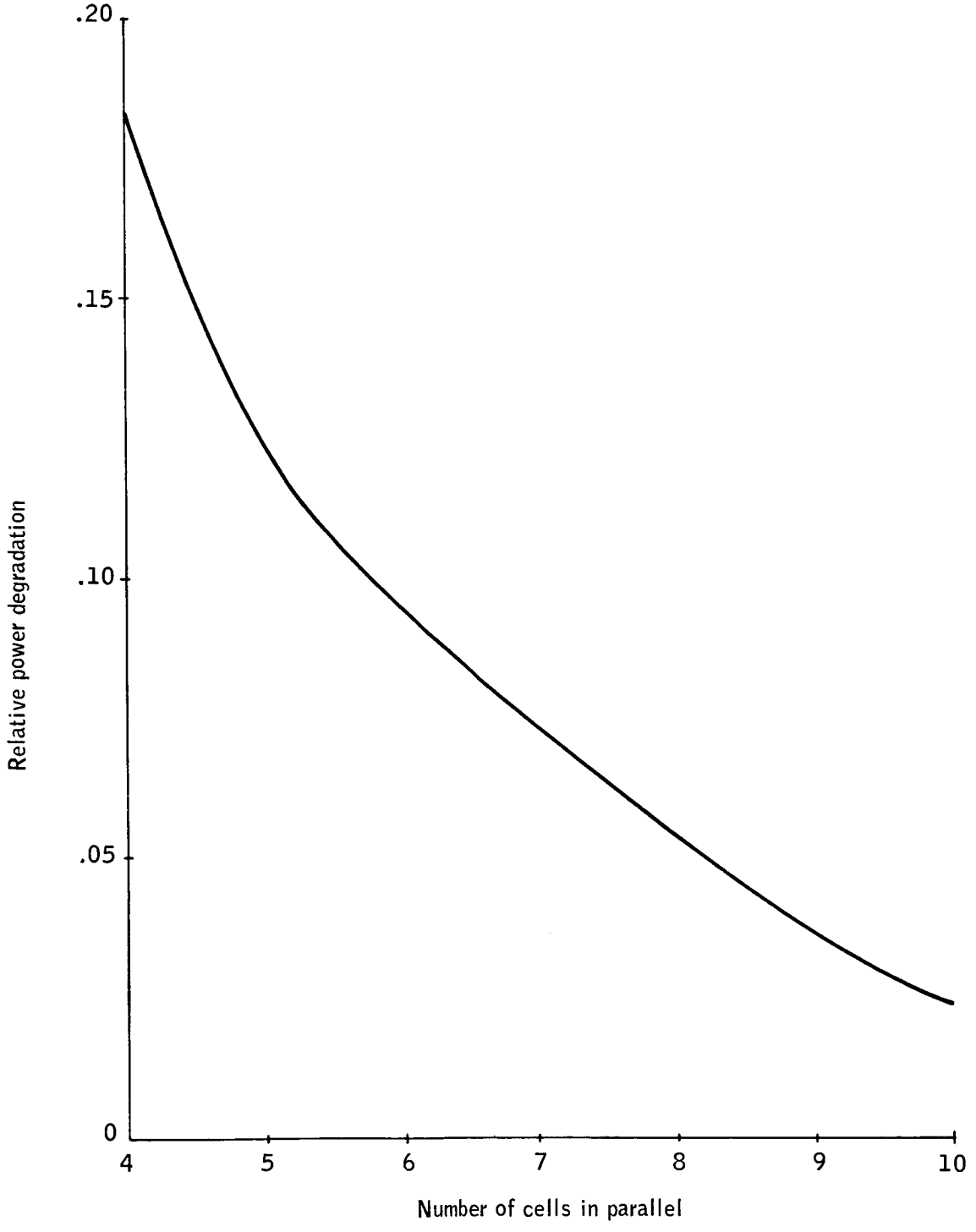

Figure 29. Power Degradation for Single, Open-Circuit Failures, N/P, 10 Ohm-cm Cells, 96 Cells in Series

36 minutes, and considering an 89.4 percent overall efficiency in regulation during battery operation, the gross battery demand/orbit is 47 watt-hours.

In order to consider a number of alternatives for the required power, four cells of standard size and capacity in five configurations were investigated. The largest configuration considered will yield over 30.8V at end of orbit discharge throughout the mission. This voltage level is above the satellite regulated bus voltage (28V) by a margin adequate to provide efficient regulation. The smallest configuration would provide a voltage level below which voltage conversion and regulation becomes exceedingly inefficient. From these extremes and the three intermediate configurations, any configuration between the extremes can be predicted. The four standard-size nickel - cadmium hermetically sealed cells considered are the 3, 6, 9, and 12 ampere-hour cells.

Table 9 provides a comparison of capacities, configurations, weight, and depth of discharge for the constant watt-hour demand of the satellite load in eclipse.

Figure 30 depicts two variables of Table 9, i.e., the number of cells in series to the percent depth of discharge. A decision band is established on depth of discharge covering the 25-percent to 40-percent range. This band is one of demonstrated reliability for the intended mission life. From these curves, a number of alternative configurations and capacities are considered acceptable. These are a 12 A-h battery of 12 or 13 cells, a 9 A-h battery of 12 to 17 cells, or a 6 A-h battery of 15 to 28 cells.

Figure 31, battery weight versus number of cells for the various capacities, shows that it is advantageous to consider only the 9 A-h battery from 12 to 15 cells and the 6 A-h battery for 16 cells or more.

Considering the effect of battery voltage on the charge regulator, load regulator, and solar array, the overall efficiency is optimized, without introducing other problems of higher voltages, by using the 28-cell battery. This system will provide efficient regulation of voltage from the array to the battery or load and from the battery to the load. Since the battery weight differential between a 16-cell and 28-cell system is only about 9 pounds, it is conceivable that using less than 28 cells would impose inefficiencies causing more weight gain in the solar array and regulators than is saved in the reduced battery weight. Therefore, the conceptual battery is a 28-cell, 6-ampere-hour configuration.

Figure 32 depicts the extreme operational voltages for cell series from 12 to 28 cells. A battery temperature range is assumed for operation from 0°C to 40°C. The highest allowable voltage for charging is at 0°C and is 1.55 volts/cell. Minimum voltage within the depth of discharge range is expected to be 1.10 volt/cell at 40°C. The discharge plateau is relatively constant and conservatively represented at 1.20 volt/cell.

TABLE 9. -NICKEL-CADMIUM BATTERY COMPARISONS

Battery		Battery capacity, ampere hours	Capacity removed, ampere hours	Depth of discharge, percent	Battery weight, pounds
12-cell battery		3	3.26	100	- -
Min. V	13.2	6	3.26	54.5	8.9
Max. V	18.6	9	3.26	36.3	13.5
Range, V	5.4	12	3.26	27.2	17.4
Discharge plateau	14.4				
16-cell battery		3	2.45	81.6	7.7
Min. V	17.6	6	2.45	40.8	11.9
Max. V	24.8	9	2.45	27.2	18.1
Range, V	7.2	12	2.45	20.4	23.2
Discharge plateau	19.2				
20-cell battery		3	1.96	65.3	9.6
Min. V	22.0	6	1.96	32.6	14.9
Max. V	31.0	9	1.96	21.8	22.6
Range, V	9.0	12	1.96	16.3	29.0
Discharge plateau	24.0				
24-cell battery		3	1.63	54.4	11.3
Min. V	26.4	6	1.63	27.2	11.9
Max. V	37.2	9	1.63	18.2	27.3
Range, V	11.8	12	1.63	13.6	34.8
Discharge plateau	28.8				
28-cell battery		3	1.40	46.7	13.4
Min. V	30.8	6	1.40	23.4	20.8
Max. V	43.4	9	1.40	15.6	31.6
Range, V	12.6	12	1.40	11.8	40.7
Discharge plateau	33.6				

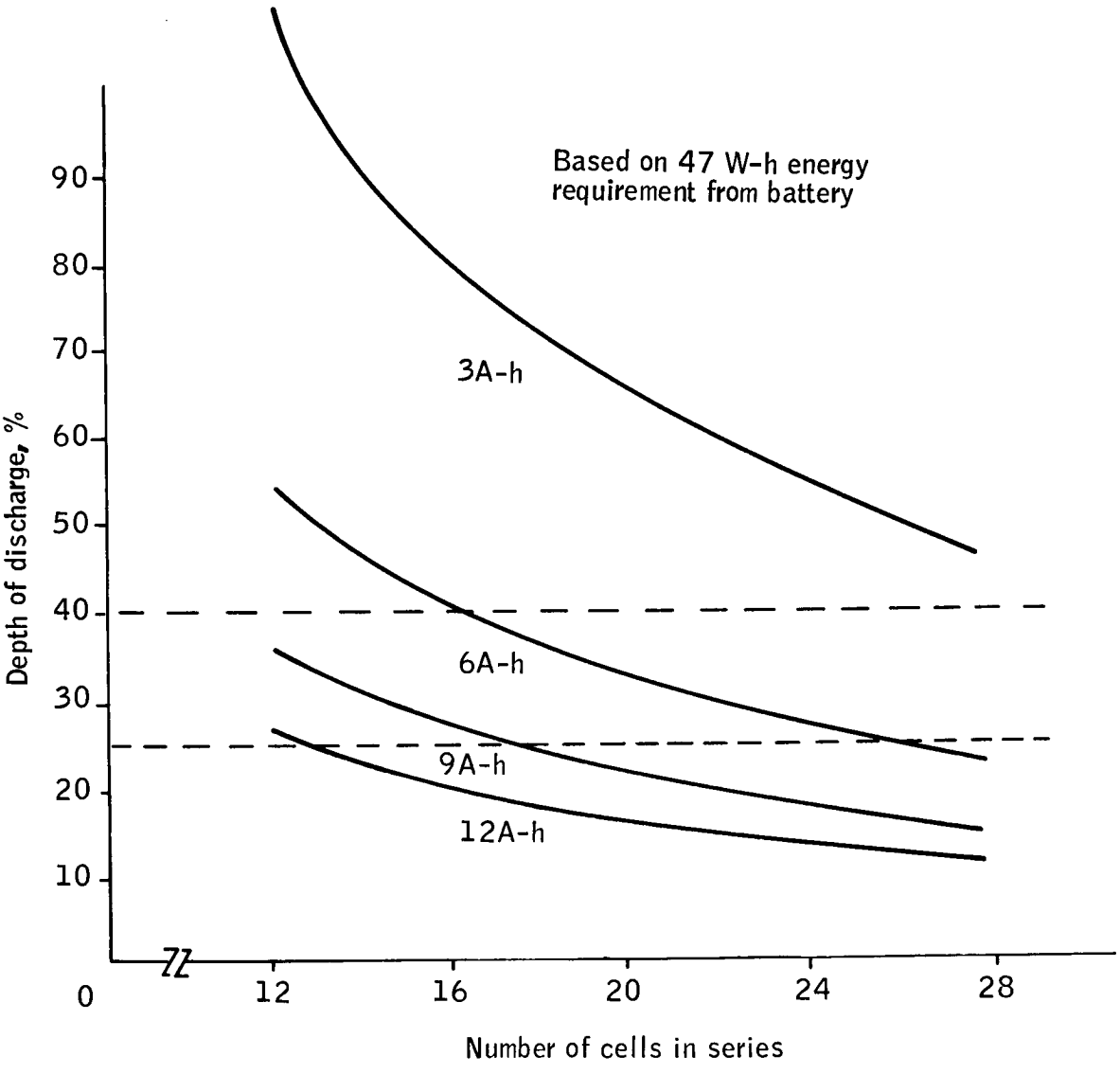

Figure 30. Batteries Capable of Meeting Depth of Discharge Requirements

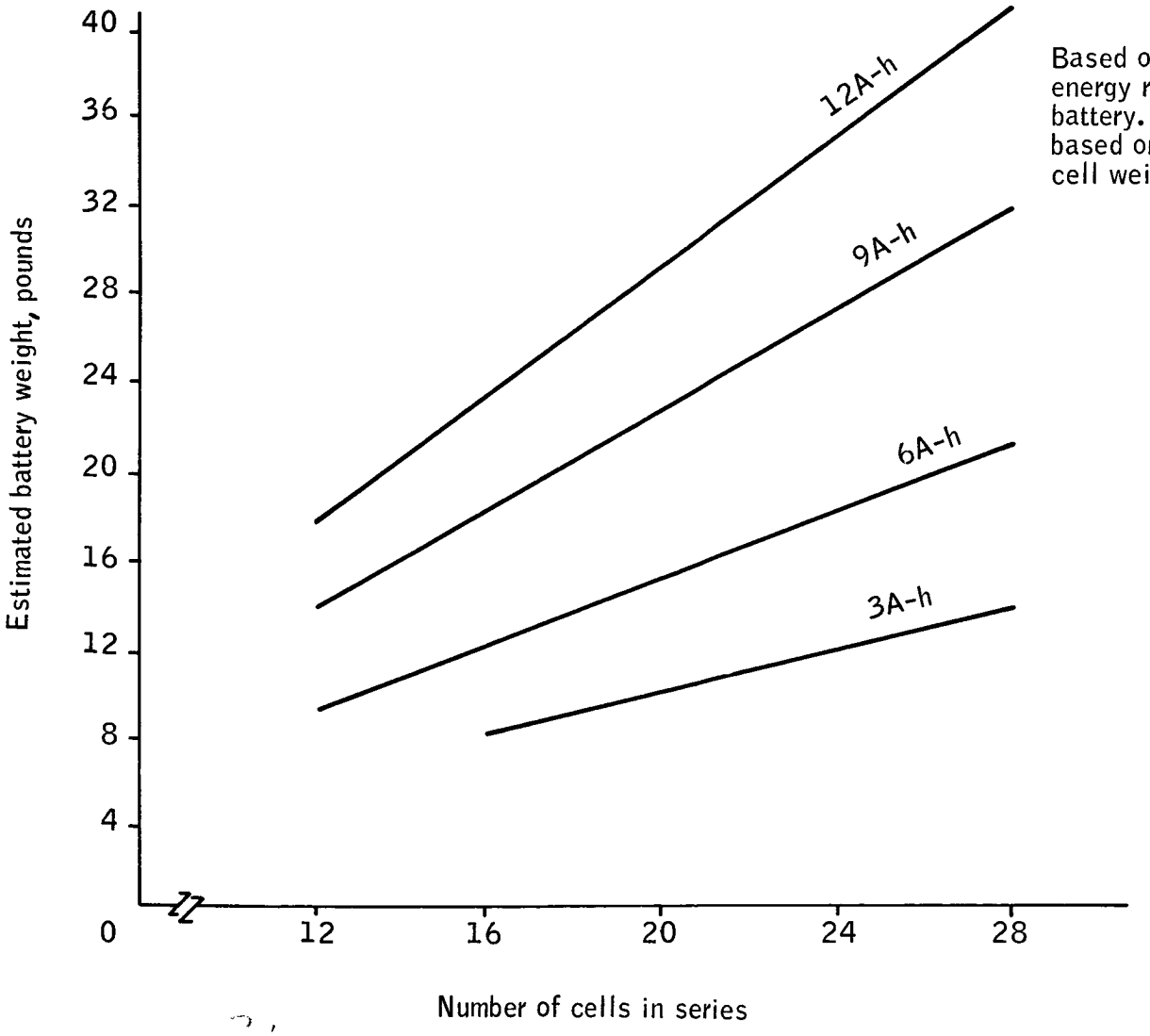

Based on 47 W-h energy requirement from battery. Battery weight based on 120% of total cell weight.

Figure 31. Battery Weight

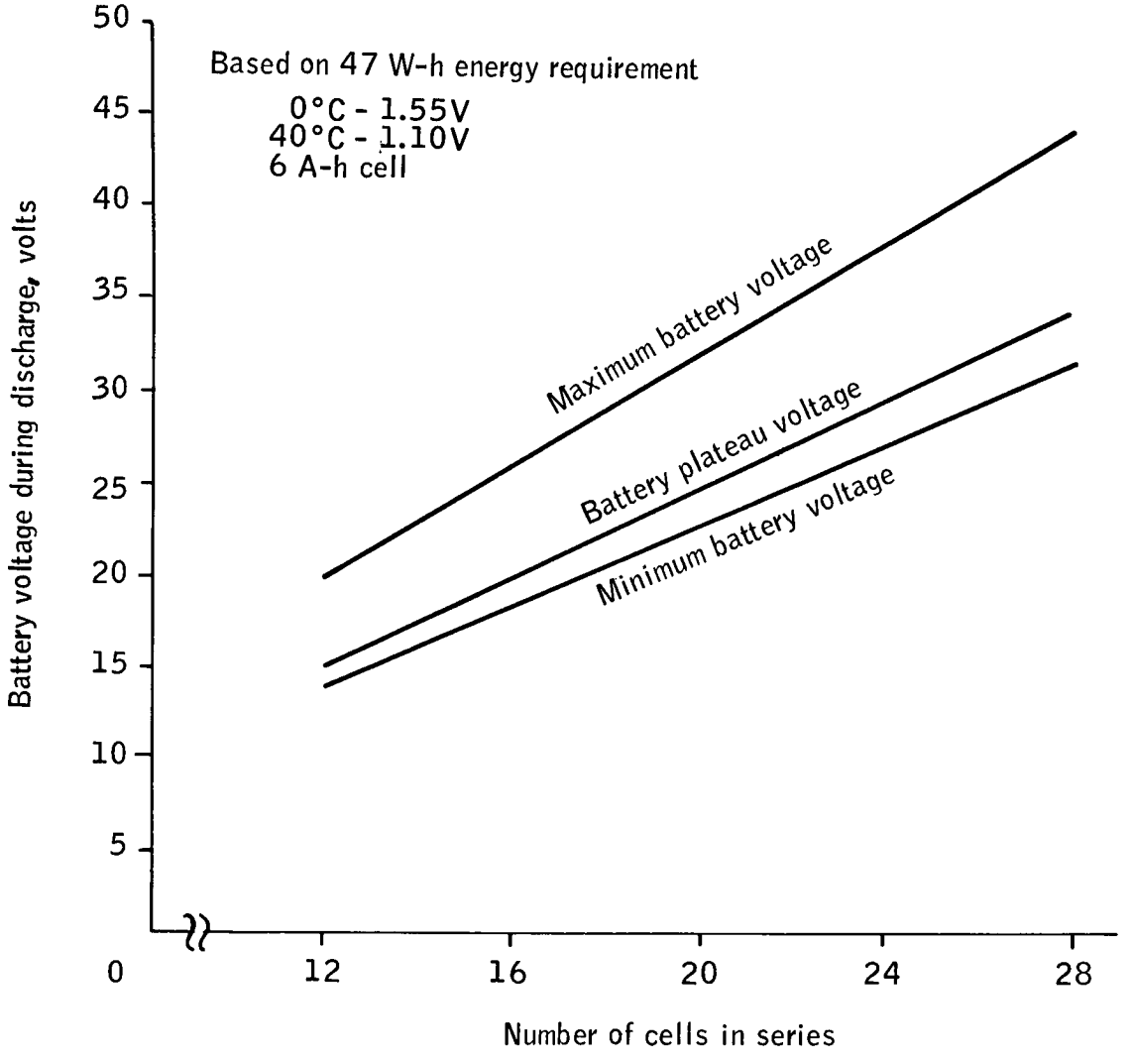

Figure 32. Allowable Battery Charge - Discharge Voltages

The energy input required for the design power demand in orbit is a function of the battery temperature and charge rates. Figure 33 depicts the percent overcharge required as a function of temperature for three charge rates. These data refer to ampere-hours of overcharge and must be converted to watt-hours for interface applications. Worst-case efficiency is estimated at 63.5 percent, occurs at 40°C (104°F), and yields an input at the battery of 74 watt hours. At temperatures below 32°C (90°F), watt-hour efficiency maintains a plateau of approximately 80 percent.

This would require an input energy of 59 watt hours throughout the remainder of the operating temperature range. Figure 34 demonstrates watt-hour efficiency as a function of temperature for 20-ampere-hour cells at four temperatures during simulated orbital operation over a span of 6000 cycles. The charge method used to develop these data was a stepped taper charge. The initial rate was 14 amperes and was reduced in three-ampere steps each time the predetermined voltage limit was reached. Final trickle current was 0.5 amperes.

This stepped-charge method would reasonably approximate the Adhydrode charge control method as a pessimistic estimate of efficiency. Use of voltage limit to control current and of the Adhydrode to signal actual end of charge should slightly improve efficiency to 5 percent.

Users of nickel-cadmium cells have reported in literature and discussion a phenomena described as "memory effect". Memory can be defined as that effect wherein a hermetically sealed nickel-cadmium cell, when subjected to a continuous, repetitive cycle routine of fixed depth and at a fixed temperature, appears to assume the capacity equal to the depth to which it is being discharged. For instance, a cell being discharged to a depth of 36 percent at 25°C will, after several hundred cycles, deliver little more than 36 percent of its capacity even if the discharge is continued to 1.0 volt. The effect is related to depth of discharge, temperature, and the value selected for low-voltage cutoff of the cell.

Many observers have reported this effect for all nickel-cadmium cells which suggests that it is a property of the active materials of the cell rather than the cell's construction or geometry. No satisfactory explanation has yet been accepted for the phenomenon, though several theories have been advanced.

It is interesting to note that the memory effect has primarily been observed in test programs where temperature is constant and where the cyclic electrical routine is monotonously repetitive. Battery failures, due to memory effect for depths of discharge as high as 50 percent have not been reported, but it has been observed that end-of-discharge voltage can fall to 0.9 to 1.0 volts. If a satellite power supply has been designed for an average individual cell voltage higher than 1.0, for example 1.15, the memory effect may indeed cause the battery to fail to perform. However, no satellite performance failures due to memory effect in the nickel-cadmium battery have ever been reported. There are several reasons for this; most discharge

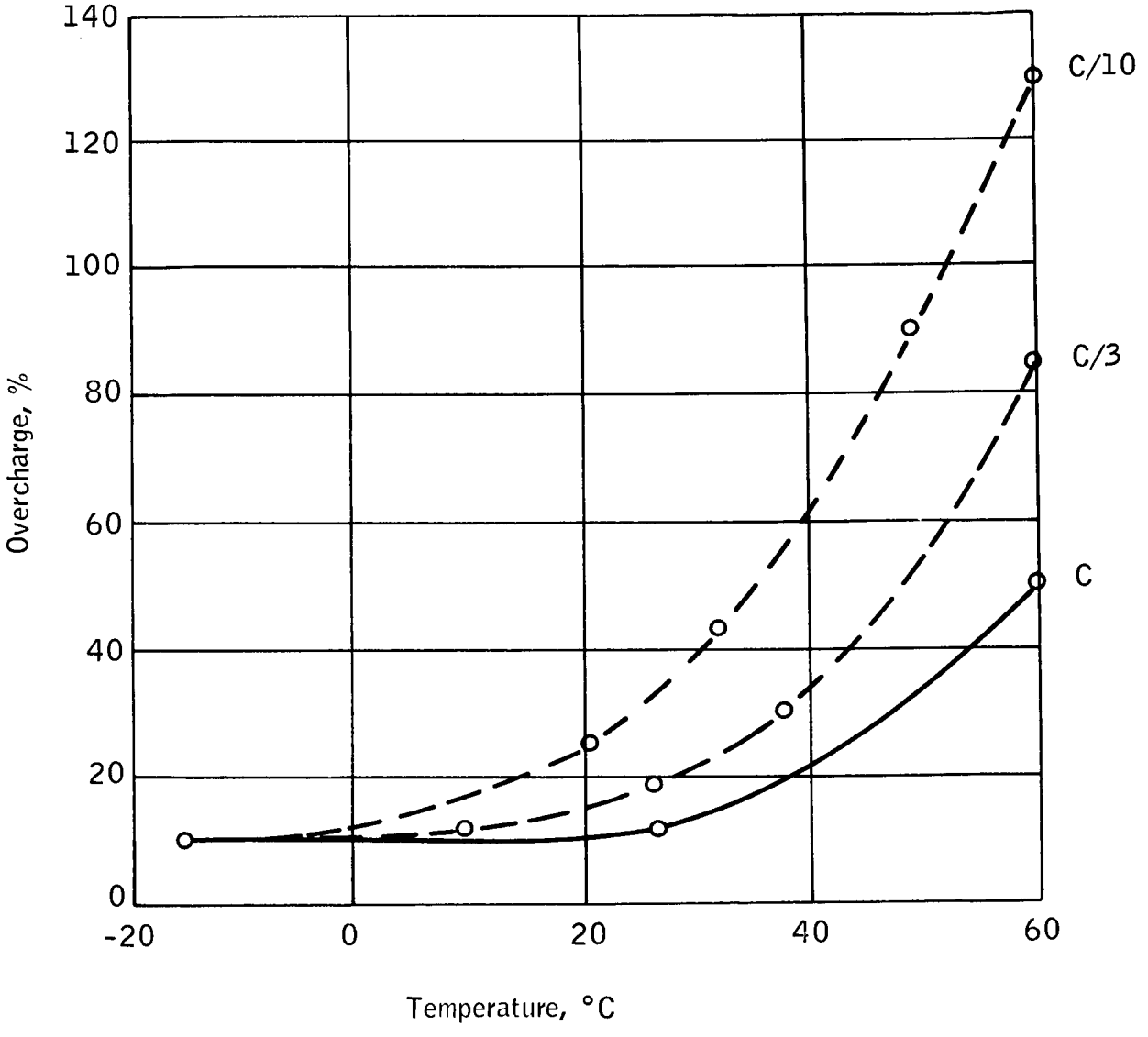

Figure 33. Recommended Percent Overcharge versus Cell Temperature for Hermetically Sealed Nickel-Cadmium Cells

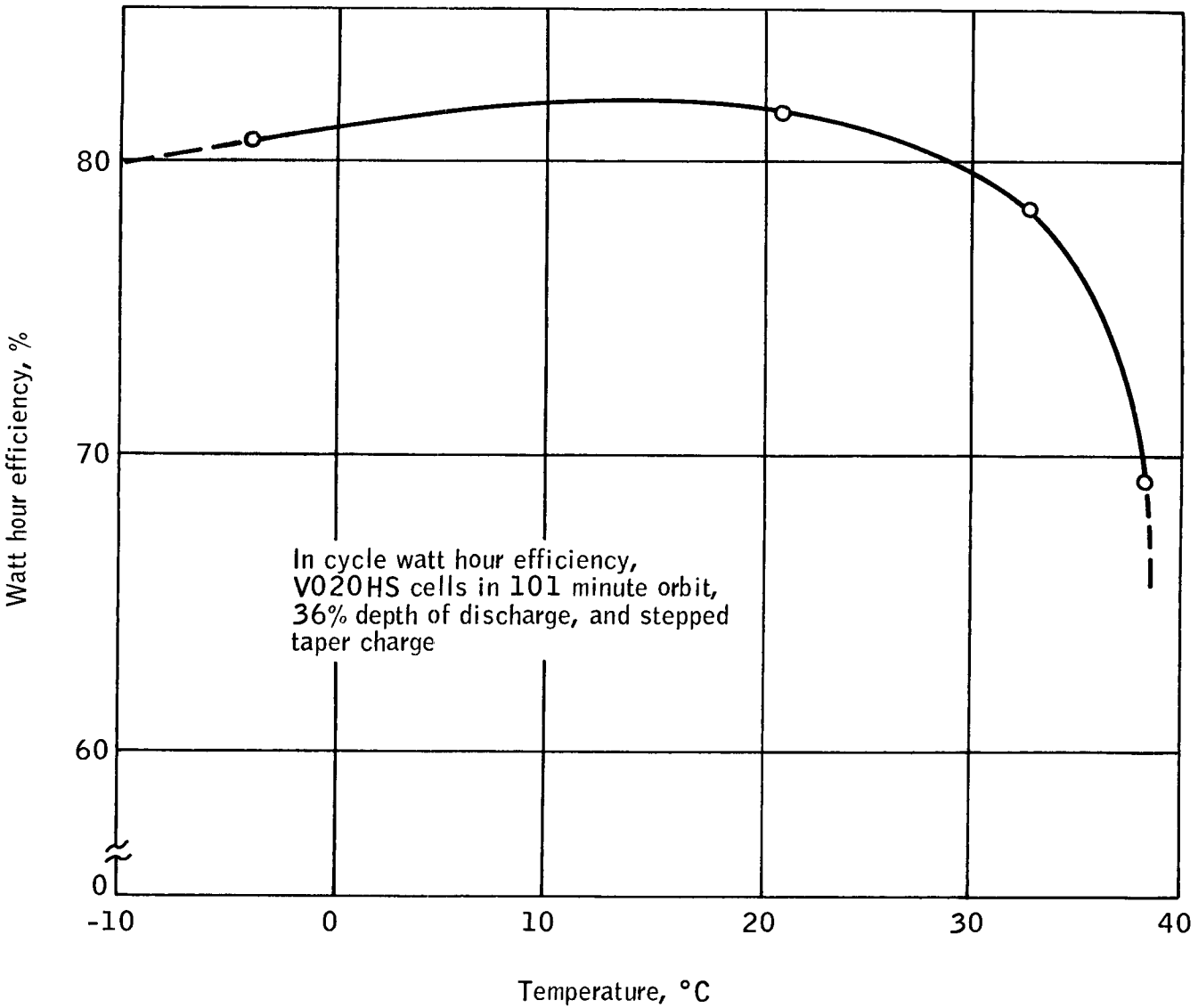

Figure 34. Temperature Effects on Battery Efficiency

routines have been 10 percent or less, most satellites do not have continuously repetitive cycle routines, and in most instances the battery temperature in orbit is not constant.

No known methodical program has ever been undertaken to study the memory effect, to develop and substantiate a sound explanation, or to observe what conditions would prevent it.

During the course of the battery development program for the OAO Satellite, cells were cycled in many different routines. It was observed that memory effect was not evident in cells cycled at 9°C but appeared at temperatures of 21, 32, and 43°C. Additionally, the effect was more pronounced at each higher step of temperature. The temperature dependency can also be observed in NAD Crane data end-of-discharge voltages at 0, 25, and 40°C (ref. 3).

Some life test data which is currently being accumulated by the Royal Aircraft Establishment in England on VO3HS cells for the UK III Satellite (ref. 13) indicates that for discharge depths of 10 percent there is no pronounced memory effect after six months of 90-minute orbits even at temperatures of 40°C and at 50°C. But for 50-percent depths of discharge, a significant deterioration of capacity is evident after six months or about 2500 cycles of operation at 40°C and at 50°C. However, after a complete discharge and a dead shorting of the cells followed by C/10 charge and overcharge for 24 hours, the total initial capacity is recovered.

It has been reported for Relay satellites that the memory effect was not observed because the operation of the satellite caused the batteries to sweep over a wide range of depths of discharge.

For Tiros, the memory effect was not observed because there were periods of 100-percent sun time during which the batteries were continuously overcharged at C/8 to C/10. Elimination or erasure of memory effect was attributed more to irregularity of the orbit than to continuous overcharge. In other words, it was concluded that the effect never developed rather than that it was erased by overcharge.

Before launch on OGO testing was done on repetitive cycling, and the memory effect showed up. This could be erased by completely discharging the cell, shorting it out, and then charging it, at which time nearly full nominal capacity was observed. This is, however, a difficult operation to perform in an orbiting satellite. It was also determined that if a cell was exhibiting memory, this effect could be temporarily allayed by raising the end-of-charge voltage from 1.45 to 1.48.

Reported data indicates that memory effect introduced by regular cycling at constant temperature can be almost completely erased by cycling the temperature of the batteries, e.g., from -18°C to 60°C.

It has been demonstrated that memory effect is more pronounced at high temperatures and deep depths of discharge. Cycling at 36 percent at 9°C does not allow the memory effect to develop.

As the HDS spacecraft orbit is one of repetitive nature, two criteria of the battery interfaces should be a low-voltage cutoff, as close to 1.0 volt per cell as is practical, and temperature control within a range of 0°C to 25°C. The use of an Adhydrode charge control system would aid in the control of temperature by allowing the charge current to be reduced to a value sufficiently low to prevent significant heating of the battery during overcharge. It has been shown that charge is endothermic, and battery temperature will remain close to the environmental temperature. Overcharge is exothermic, and the energy that cannot be used to charge the battery is rejected as heat. Through the knowledge of the actual completion of charge, heat of overcharge can be reduced. Discharge is also exothermic and is rate dependent; however, heating in the orbit shadow will aid in maintaining the battery in an operational temperature range.

A low-voltage cutoff of 1.10 volts per cell has been selected to be compatible with the expected cyclical routine and the power conditioning equipment. NAD Crane data, for Gulton 6 A-h Adhydrode cells, has indicated that end-of-discharge voltages at 40°C, 25-percent depth of discharge, do not drop to 1.10 volts average over more than 7 000 cycles. At 25°C and 0°C, voltages are approximately 1.15 and 1.20 respectively.

Therefore, the conceptual battery for the HDS satellite will be a 28 cell, nickel-cadmium, two-terminal, six-ampere-hour battery. Average discharge voltage throughout a temperature range of 0°C to 35°C will be 33.6 volts, and minimum discharge voltage will be 30.8 volts for the worst temperature condition near end of design life. Maximum charge voltage required by the battery will be 43.4 volts at 0°C and will be compensated at lower levels at higher temperatures.

Maximum energy removed during each orbit will be 47 watt hours for a nominal discharge depth of 23.4 percent. Minimum watt-hour efficiency in this cycle will be 63.5 percent at 40°C and will average approximately 80 percent from 0°C to 30°C. Battery temperature during operation can be monitored by placing thermistors between cells in the battery structure. The mechanical design of the battery shall consider the dynamic environment of launch and orbit injection and include a heat-sink surface for maintaining the necessary thermal balance. Estimated battery weight, based on similar space-qualified batteries of Gulton design, will be 20.8 pounds. While a temperature range of 0°C to 40°C is acceptable for the battery, the thermal interface between the spacecraft and the battery will be designed for a 0°C to 35°C range to maintain maximum watt-hour efficiency and reduce memory-effect considerations.

Audio and RF Filtering

A single audio and rf filter assembly (Figure 35) is used in the overall power system (Figure 19) to eliminate the need for similar individual input filters at each of the power conversion boxes in the system. The audio filter composed of L_1 and $C_{3\ A,\ B,\ C,\ D,\ etc.}$ is necessary to reduce the ac voltage ripple, reflected back into the solar array from approximately twice the peak load, and charging current to a maximum of 0.25 amp, peak to peak. Failure to provide for this type of array current ripple reduction could cause the

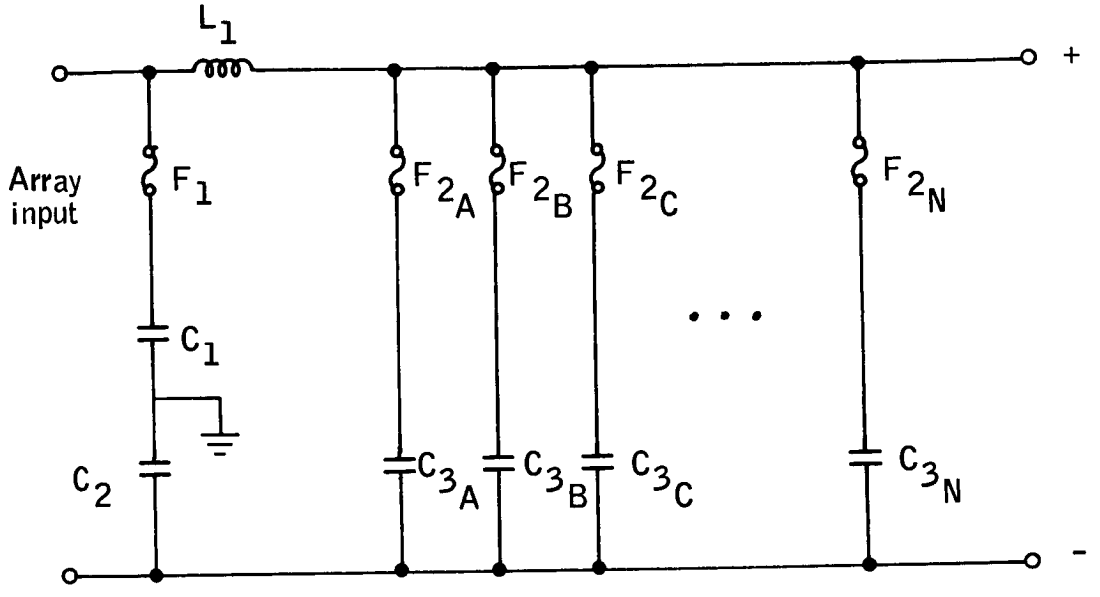

15 capacitors total
Est. weight 1.1 lb
Est. volume 22 $in.^3$

Figure 35. Audio - RF Filter

array to be pulled into a poor operating point and latch up. The tantalum foil capacitors are extremely reliable and experience has shown that this type rarely, if ever, exhibits a short failure mode; however, it was deemed prudent to fuse ($F_{2A, B, C, D, etc.}$) each capacitor with a short length of fine copper wire. This fine copper wire would clear any faulty capacitor by burning open with 20 amperes of current from either of the batteries.

The radio frequency filter portion of the assembly is made up of two one-μF ceramic capacitors placed physically as close to the input connector as possible. Fuse F_1 is all that is necessary since the negative side is at dc ground potential.

Battery Charge Control

Many approaches have been utilized in the satellite industry for optimum charging of nickel-cadmium batteries. The successful programs have one thing in common; they have treated the battery with special care by not considering it just a black box with an input and output. All successes have been achieved by developing the charge control around the specific battery in the system, i.e., ampere-hour rating, temperature environment, time for charge, depth of discharge, mechanical construction, etc.

In previous discussions (Control and Regulation), a fairly detailed comparison of the many methods of charging was made. Selection of a pulse-width, series control method was based on the many advantages over the shunt and straight series controllers.

The following discussion will consider the battery charge control a part of the complete power system and will describe in some detail the operation and specification of the proposed system.

The battery charge control system is based on the use of two identical charge control regulators each charging a separate battery.

At various times and under various conditions, the charging current must be either 0.1 amp, 0.45 amp, 1.65 amp, or 2.0 amp. The charge mode is arranged in such a way that only one of the two batteries can be charged at any one time (excluding continuous trickle charge).

The trickle charge control will consist of a series transistor biased for constant current or a resistor valued for 0.1-ampere trickle current. The 0.1 ampere is sufficient to keep the standby battery fully charged under the environmental conditions expected. The battery charge control, Figure 36, consists of a pulse-width regulator with output voltage sense, current sense, commutating diode voltage control, filter L and C, current switching regulation control, an overload bypass, and a three-volt bias supply.

Description of the operation of the basic pulse-width regulation technique can be found earlier in this report. Basically the input voltage is switched on and off so that average current after filtering, is equal to the desired battery charge current. This is accomplished by sensing the output current, comparing it with a constant reference, and then controlling the series switching transistors appropriately.

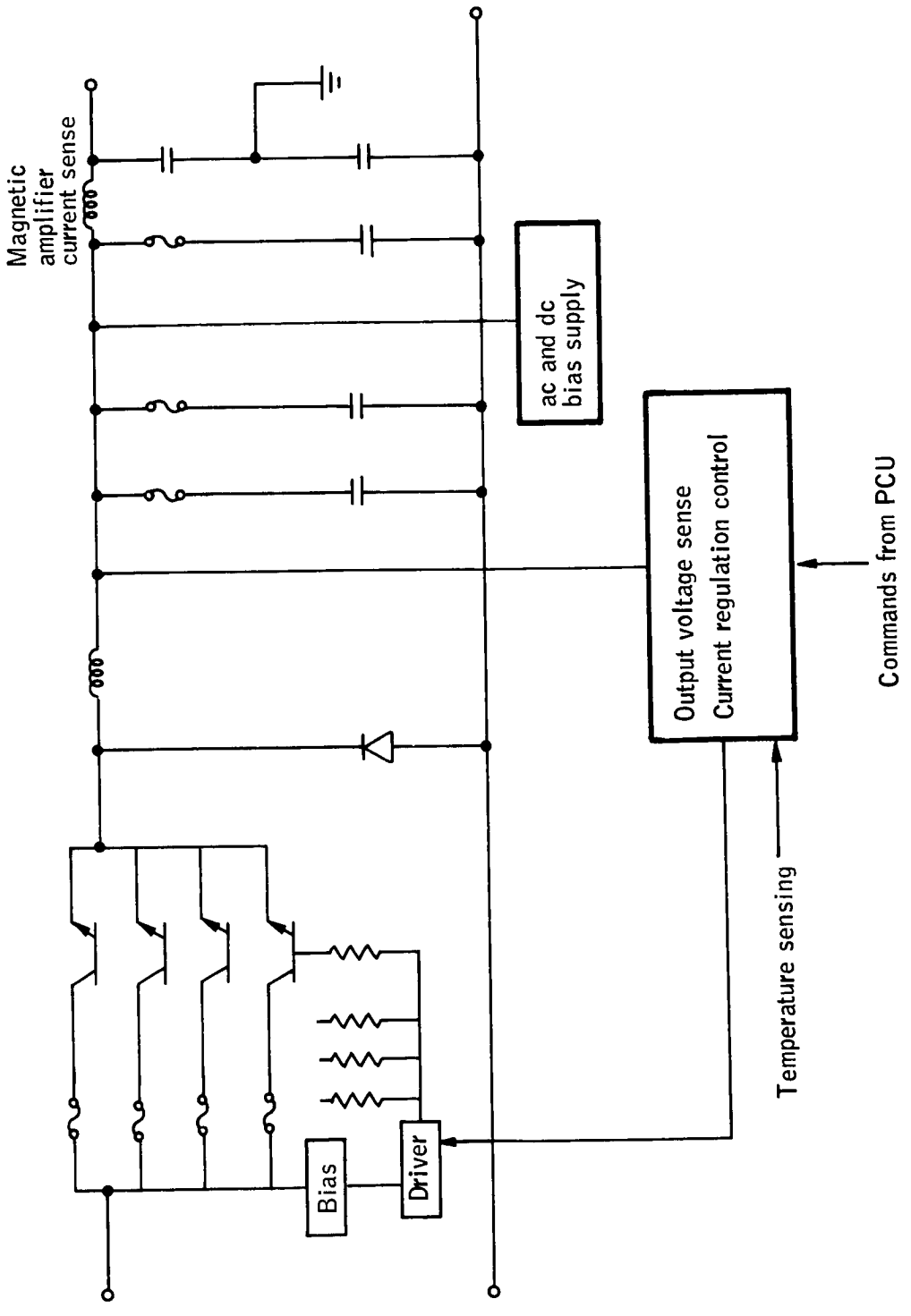

Figure 36. Battery Charge Regulator

An inverter/converter working from the charger output provides ac for a magnetic current sensor and dc voltage to forward bias the series switching power transistors, reducing the forward saturation voltage drop.

Each battery charge control regulator employs fuses to clear single component failures. An explanation of the fusing operation is as follows: the switching regulator was designed with four transistors in parallel each carrying approximately 1/2 ampere of current, thus supplying two amperes of charging current at the beginning of the charge mode. Each transistor has a semiconductor fuse in series with its collector lead. If a switching transistor shorts, all the current will pass through that transistor with a resultant increase in output voltage causing a large increase in battery current, thereby clearing the series fuse and shorted transistor.

Fault clearing of the filter and rf capacitors is accomplished with fine copper wire in a similar manner as shown in the input audio filter assembly, Figure 35.

Bus Voltage Regulation

Twenty-eight-volt bus. --The 28-volt bus regulator utilizes the filtered input voltage of 31 to 82 volts from the solar array or battery voltage and regulates the output to 28 volts ±2 percent at any instant of time, see Figure 37. The regulator is actually two regulators in redundancy operating into common output capacitors.

Operation of this regulator is substantially the same as that in the battery charge control regulator except that sensing holds the output voltage constant. Efficiency is maintained at the maximum by employing the regulators in a form of standby redundancy. The standby regulator is cut off since the working regulator operates at a slightly higher voltage. Each regulator operates completely independently of all portions of the other, except for the common output capacitors.

Since the load must be considered capable of faulty operation, a current limiting provision is utilized which provides approximately twice the maximum rated current into a fault yet limits the current of each regulator to maximum rated load current under all conditions, thus protecting the regulator from damage. Current limiting is obtained by sensing the input current with a small resistor. The voltage across this resistor is used to control switching of the series regulator transistors in such a way that the output current of that section cannot exceed 3.4 amperes. If neither section has failed, the current will be less than 6.8 amperes.

Internal fine wire fusing is used for fault clearance of the commutating diode and all filter capacitors. The P-200 Microlectron semiconductor fuses are in series with the switching transistors in the regulator and in series with the oscillator transistors in the bias converter.

Five-volt bus. -- Conversion to five volts can be directly through a switching regulator from the unregulated line, or through a dc/dc converter which can be used to derive the five-volt output directly from a 28-volt

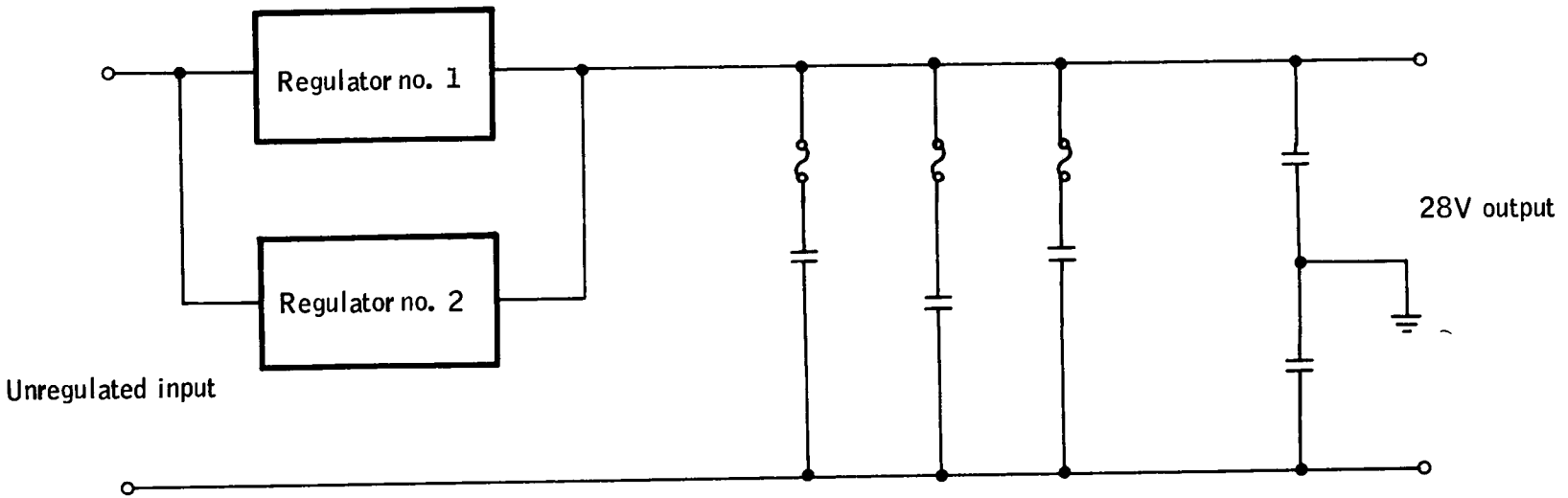

Figure 37. 28-Volt Regulator Block Diagram

regulator. In either case the efficiency is about the same since the commutating diode of the regulator approaches 100 percent conduction time. If a converter is powered from the output of the 28-volt regulator, interaction between the supplies due to load peaks or fault clearing would be encountered. By separating the functions completely with a separate 28-volt regulator for the five-volt converter, it is possible to isolate completely the supplies. The redundant input regulators are paralleled and contain the same internal fusing arrangements for fault protection as previously described (See Figure 38).

Regulation is performed at the higher voltage level where the ratio of voltage drop in the series switching transistors to the operating voltage is comparatively small. The resulting regulated 28 volts is then used in the dc to dc converters to obtain the five-volt load requirement and the three-volt bias supply.

Fail-safe precautions are taken in each converter by fusing each oscillator transistor so that a short circuit in any one would automatically cause its series fuse to open.

The output of the five-volt supply will be filtered to limit the peak-to-peak ripple to less than the 100 mV necessary for integrated circuits where digital information is stored.

External overload protection will be provided by current limiting of 10 amperes when both sections are working in parallel, or to five amperes with one section cleared off the line. External short-circuit protection will cause both sections to cut back to almost zero current, thereby isolating an external five-volt load short from the input power.

If necessary or desirable, separate output windings on the converter can be provided so that all subsystems can have isolated five-volt supplies.

Reliability and Weight

The reliability approach has been to assure that the basis for reliability calculations has been valid and based on test data of a common confidence level. In this way the resultant reliability numbers for the various system components reveal which of the components are the primary contributors to the power system unreliability. With this information, the appropriate steps may be taken to obtain the greatest feasible reliability. From the total mission reliability point of view, the power system is in the position of being a direct multiplier in determining total mission reliability. Because of this, the power system design should be such that no single-point failure could cause serious degradation in the power system. Accomplishment of this objective requires a prohibitive degree of redundancy. However, great improvement is possible if redundancy is employed in those places where components are most highly stressed relative to their rating. Failure rate prediction for highly stressed components is less accurate than for those at lower stress. A system weight comparison is also presented in this section since weight and reliability are correlated.

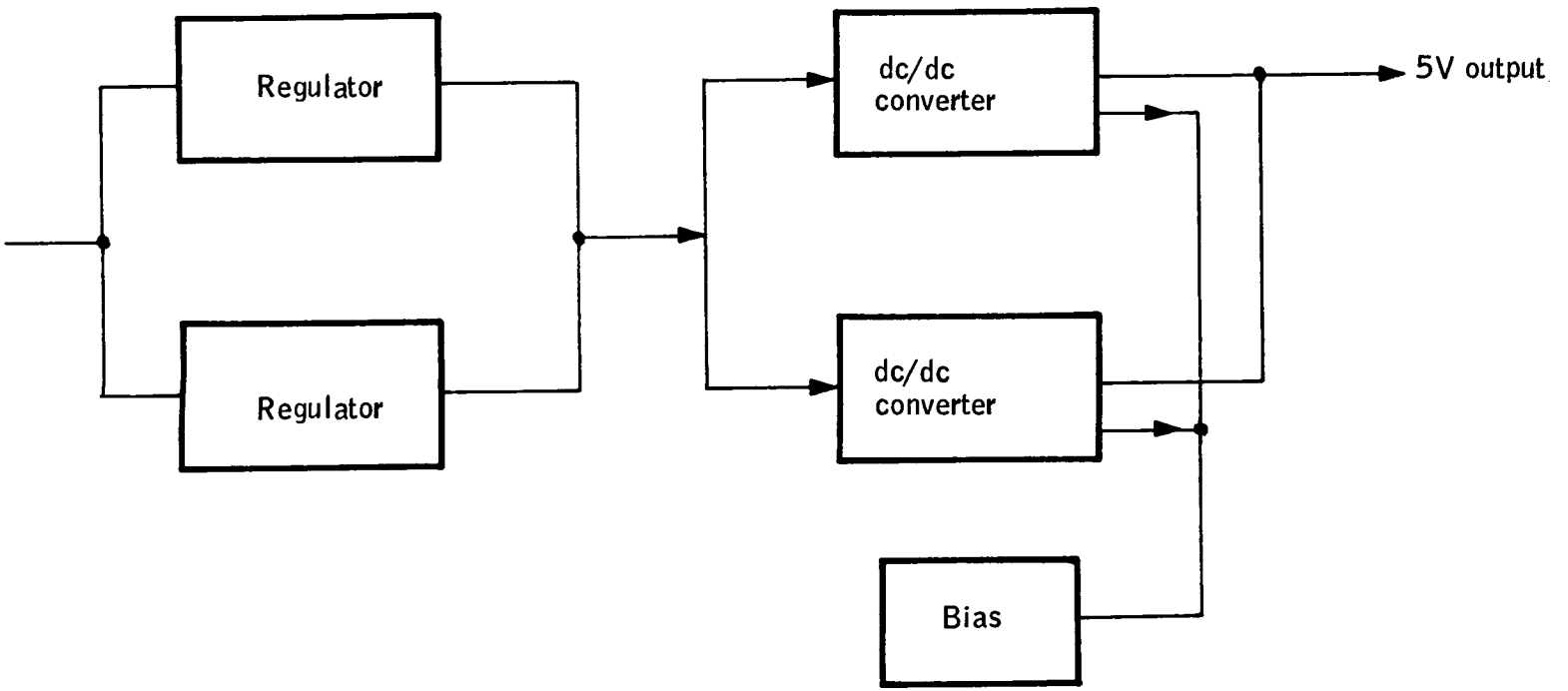

Figure 38. 5-Volt Regulator - Converter

Breakdown of the power system into its subcomponents shows that the reliability diagram has six series elements in cascade, that is, the system reliability is the product of the reliabilities of six subcomponents, and failure of any one of these constitutes failure of the system. A tabulation of the basic reliability and weight of each of these blocks is shown below. All figures are based on the use of failure rate data for which there is a demonstrated 50-percent confidence in the mean time to failure.

		λ	R	Weight, lbs
1.	Solar array	16×10^{-8}	.9986	36.4
2.	28-volt regulator	290	.971	2.1
3.	5-volt regulator	490	.951	2.5
4.	Battery	2610	.795	21.0
5.	Charge regulator	225	.975	1.8
6.	Power control unit	250	.970	4.5
		3881×10^{-8}	.68	68.3

These figures show conclusively that the probability of failure is largely that of the battery since its reliability figure is noticeably lower than the others. It is also significant to note that the solar array reliability is much higher than the others, the result of extensive redundancy within the array.

Based on the implementation of redundancy techniques, a new set of reliability figures is tabulated as follows:

		Equivalent λ	R	Weight, lbs
1.	Solar array	16×10^{-8}	.9986	36.4
2.	Filter	16	.9986	1.3
3.	28-volt regulator	19	.9983	3.0
4.	5-volt regulator	23	.9980	3.6
5.	Batteries and chargers	285	.975	44.4
6.	Power control unit	292	.974	5.0
		651×10^{-8}	.94	93.7

For this second tabulation, the reliability figure corresponds to the use of two batteries and two charge regulators and redundancy incorporated into the regulators. Dependence on the most likely single-point failures has been eliminated. This is the minimum acceptable degree of redundancy for the power system.

In the design of a redundant battery arrangement it is necessary to decide whether the redundancy should be active or standby. Comparison of reliabilities for the two cases shows that for active redundancy, that is both systems operating continuously and each supplying a portion of the total load, the reliability of the battery and charger combination is 0.950. If instead, the batteries are utilized in standby redundancy (one battery operates until it fails), then the other battery takes over; the reliability is 0.975. In view of the higher reliability for the standby redundancy, this mode of operation was chosen. This has a side advantage, namely that, since the working battery is being used at a greater depth of discharge and recharge, efficiency is somewhat higher and the battery recharge energy is less.

Comparison of reliability figures associated with the use of redundancy to that without redundancy shows a clear advantage for the redundancy used. Since the basis for the calculations is the same for all system components, the reduction in failure rate is the correct factor regardless of the confidence level of the data utilized.

Reliability success diagrams for the two arrangements are tabulated in Figure 39.

SPACECRAFT ELECTRICAL INTERFACES

This section contains a discussion of the interfaces of the electrical power system to the other subsystems of the spacecraft.

Electrical System Fault Protection

Fault protection of the electrical power system can be separated into two categories; those internal and those external to the power system. The overriding philosophy of electrical system protection is to isolate the fault to allow the remaining subsystems to continue operation.

Electrical power system internal protection is provided by a design in which no single failure will cause loss of the power system or degradation of the quality of the output. The means for accomplishing this are discussed in the section on regulation and control.

Failures which occur external to the power system can be isolated by disconnecting the particular load in which the failure has occurred. The isolation can be permanent, have provisions for automatic reclosing, or have provisions for reclosure by ground command. The type of isolation used is dependent on systems effectiveness analysis, type of fault expected for a particular subsystem(such as intermittent or permanent), and knowledge of spacecraft electrical design details.

The types of fault isolation devices which must be considered are as follows:

- Fuses
- Circuit breaker (aircraft type)

I "Non-redundant" configuration

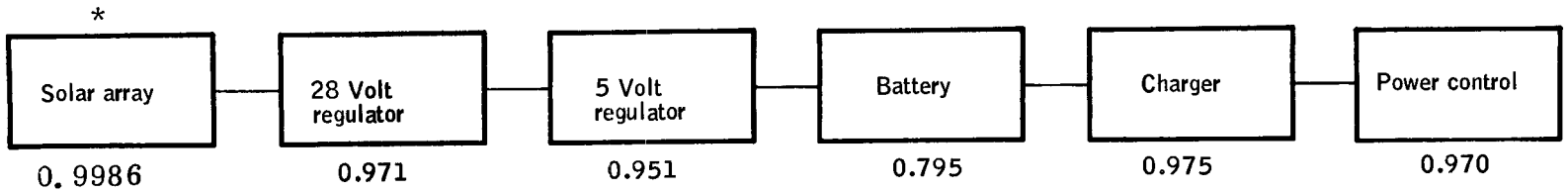

II "Redundant" configuration

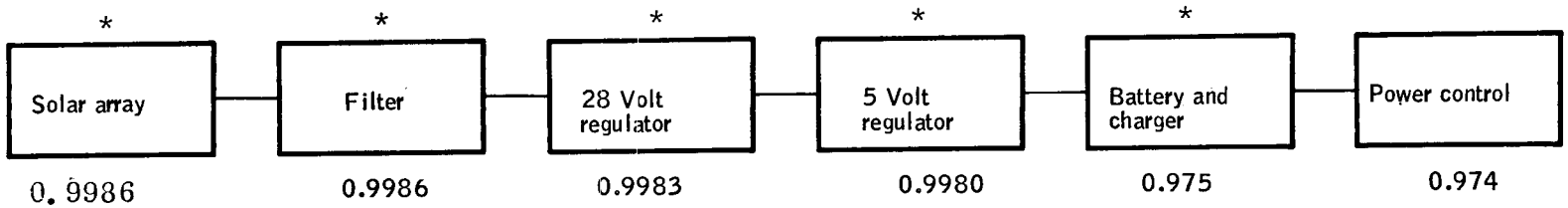

* Indicates presence of redundant connections or components

Figure 39. Reliability Success Diagrams

- Thermal heaters with automatic reclosing feature
- Solid-state interruption circuits designed for the specific application

The use of fuses as protective elements is straightforward and has seen application on existing spacecraft, such as Tiros (ref. 14). The characteristics of circuit breakers and thermal reclosing breakers have also been well established. The HDS electrical power system is capable of providing the required overload current to activate any of the above devices. Solid-state circuit breakers would be applicable in cases where very fast circuit interruption is required, such as arc removal, or where isolation at very small overcurrent is desired as in the case of component protection. This type of protection must be designed for each specific application.

The type of isolation provided for each subsystem must be determined in the early design stages. Present indications are that the HDS spacecraft will require fuses for permanent isolation plus overcurrent protection with provisions for ground command override for certain critical circuits.

Magnetic Moment Control

The magnetic moment of the spacecraft must be controlled to minimize experiment errors due to spacecraft attitude disturbances and spin-rate variations resulting from the interaction of the magnetic fields of the earth and the spacecraft. The magnetic moments should also be controlled to optimize the size of the magnetic torquing attitude control system.

Control of the spacecraft's magnetic moment will require knowledgeable design of the spacecraft structure and electrical system, careful selection of spacecraft materials and hardware, and testing as the spacecraft design progresses. A worst-case alignment of the magnetic moments described in the following analysis results in a moment of approximately 0.46 ampere-turn-meter^2. The feasibility analysis conducted in the attitude determination portion of this study indicates that a 1.0 ampere-turn-meter^2 moment can be accepted. Therefore, it is concluded that the present spacecraft concept is compatible with both experiment and attitude control system requirements.

Solar array stray field. -- The magnetic moment resulting from solar panel circulating current depends on the circuit configuration, differences between individual solar cells, and cell and circuit failures during one-year operation. The stray-field moment of an illuminated solar panel, with the present solar panel circuit concept and allowing for cell failures and one-year degradation, will be within the following limits:

$$|M_y| \leq 8 \times 10^{-4} \text{ ampere-turns-meter}^2$$

$$|M_x| \leq 8 \times 10^{-4} \text{ ampere-turns-meter}^2$$

$$|M_z| \leq 8 \times 10^{-4} \text{ ampere-turns-meter}^2$$

Moments are shown with respect to a single paddle only. The paddle is in the x-y plane coordinates as shown in Figure 40.

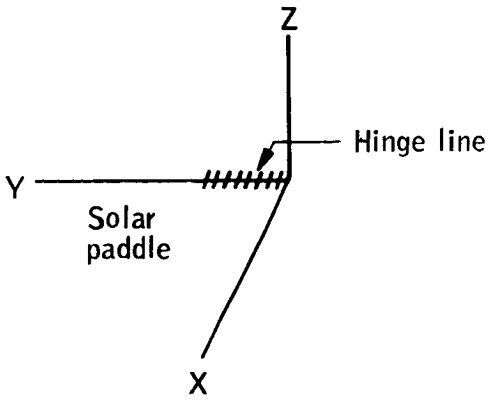

Figure 40. Paddle Coordinates

Consideration of various failure modes indicates that the maximum solar panel stray-field magnetic moment occurs with the loss of one series-parallel cell string. This loss can occur due to the failure of two diodes (probability of failure is 1.06×10^{-5} per year) or two end connections (probability of failure is 8.8×10^{-6} per year). The stray-field moment will be within the following limits, with the above double failure condition.

$$0.078 \text{ ampere-turns-meter}^2 \leq |M_y| \leq 0.08 \text{ ampere-turns-meter}^2$$

$$|M_x| \leq 8 \times 10^{-4} \text{ ampere-turns-meter}^2$$

$$|M_z| \leq 8 \times 10^{-4} \text{ ampere-turns-meter}^2$$

Battery magnetic moment. --

Stray-field magnetic moment: The stray field, due to battery current flow, can be held to a low level by using a battery construction in which the battery cells are mounted back-to-back so that the stray field on one cell opposes that of the other. The stray-field moment of a single battery, extrapolated from test information presented in reference 15, is expected to be of the following order of magnitude:

$$M_y, M_x, M_z \cong \pm 0.01 \text{ ampere-turn-meter}^2$$

A stray field moment of this magnitude should not present a problem; however, this moment could be reduced to a level in the order of 0.002 ampere-turns-meter^{-2} with current compensating loops if necessary.

Permanent magnetization moment: The spacecraft batteries have permanent magnet characteristics due to the presence of nickel material. Because of the nickel, the magnetic moment of the battery will vary with the magnitude of field to which it is exposed during an orbital revolution. Accurate determination of the battery moment will require tests to determine the magnetization curve. However, order of magnitude moments have been extrapolated from data presented in reference 15. The order of magnitude moments for a single HDS battery are as follows:

$$M_y, M_x, M_z \cong 5 \times 10^{-4} \text{ ampere-turn-meter}^2 \text{ post deperm}$$

$$M_y, M_x, M_z \cong 0.4 \times 10^{-2} \text{ ampere-turn-meter}^2 \text{ induced (0.26 gauss applied field)}$$

Spacecraft magnetic moment. --

Stray-field magnetic moment: Spacecraft area projected normal to any axis is approximately 1.5 meter^2. Maximum electrical current will not exceed four amperes. Evaluation of stray field data of existing spacecraft shows that wire twisting, wire routing, etc. will result in stray-field reduction and cancelation so that the resultant field will not be more than one percent of the total field. Therefore, the order of magnitude of the total HDS spacecraft, stray field is:

$$M_y, M_x, M_z \cong 4 \times 1.5 \times 0.01 = 0.06 \text{ ampere-turn-meter}^2$$

This does not include solar paddle stray field or eddy current field.

Spacecraft permanent magnetization moment: Reference 16 shows that the post deperm or post compensation magnetic moment of a typical spacecraft will be between 0.6 and 6.5 gauss - cm^3/lb. Therefore, it should be feasible to attain a design with a permanent magnetization moment of 0.03 to 0.4 ampere-turn-meter^2. Review of a considerable amount of test data contained in reference 16 also indicates that the induced magnetic moment (0.38 gauss) will be of the same order of magnitude.

Electromagnetic Compatibility

Nearly all electronic equipment generates "interference" components which are of potential significance to other electronic equipment. These "interference" components can exist at frequencies from zero to many megahertz. At dc and audio frequencies, these currents and voltages are commonly recognized and remedied as "common power supply" problems. At higher frequencies the circuit elements which suppress the lower frequencies may not perform in the same way. Military Standards such as MIL-I-6181,

MIL-I-26600, and MIL-STD-826A establish limit values for interference generation and interference susceptibility such that systems can be assured a high probability of noninterference among the using subsystems. For this program, a similar interference control document will be generated, tailored to the specific project objectives with realistic control levels.

Conformance of all subsystems to these requirements does not in itself guarantee freedom from all problems. Ground loops, the subject of later paragraphs of this report, can cause problems,even though there is conformance to the interference control requirements,and thus must be dealt with separately.

System grounding affects power system control, fault isolation, and signal transfer between subsystems. The following discussion concerns system grounding philosophy as it pertains to the HDS electrical system.

Common practice for modern systems dictates the use of a single-point grounding arrangement. This is based on the fact that since the structure is not designed to carry current it is not safe to design a system based on the use of structure as a current conductor, and this is because of the fact that bonding between adjacent structural elements is based on the need for structural integrity, not on the need for current-carrying capacity, and these interfaces can therefore be the source of large IR drop. Another factor is that if the structure is utilized to carry current there is a large area of potential difficulty associated with the generation of magnetic fields associated with the flow of current. With the use of a single-point ground, it is usual to carry three separate ground leads. These are 1) power ground, 2) signal ground, and 3) case ground. The power ground performs the obvious function of carrying power from the power system to theusing subsystem. The schematic diagram of the power grounding wires forms a tree with the branches all leaving from the power system. The signal ground provides for a signal transfer between subsystems and may or may not be isolated from the power ground. The case-ground connection serves as a means for guaranteeing electrical connection between the case of each subsystem and the system single-point ground and can be thought of as being electrically in parallel with the structure.

For the simplest circuit design of a given subsystem, the power ground and the signal ground are common within the box. In the case of interconnection of the output of one such subsystem to the input of another, a ground loop is unavoidable. This will not adversely affect the power system, but it will be of significance to the systems which are thus interconnected; this connection will add a certain amount of unwanted signal in series with the output of the one subsystem which appears at the input of the other. This unwanted signal generally consists of dc and higher frequency components and is sufficiently complex that it approaches complete randomness. Existence of this signal at the input of the receiving subsystem represents a distortion of the data transmitted from the other subsystem and is therefore an error component.

There are several approaches toward elimination of this error source. These approaches are as follows:

- Assume that there will be significant ground potential differences between boxes, and design the system to be insensitive to these voltages. One approach is to make all signal outputs very large with respect to the stray potentials. This is considered impractical for the HDS system since accuracies of 0.1 percent are required. The alternate approach to designing insensitively to ground loops is to make signal output digital in character. Since signal receptors must only be able to differentiate between "0" and "1", ground potentials offer no significant problems. Since this is to be a digital data handling system, no changes in concept are required. The only hardware constraint is that the A/D converters of the instrument be designed to be compatible with the instrument grounding techniques and be physically near the signal sources.

- Require that the signal inputs to each box be differential, thereby eliminating the troublesome flow of signal current. This design approach is sometimes expensive, time consuming, and often leads to coordination problems during the detail design phases of a project.

- A common approach is the employment of transistor-magnetic oscillators to achieve separation of the power system grounds from the signal ground in each black box. This approach permits great freedom to interconnect boxes in any way but is penalized as the result of several characteristics of these oscillators. They add weight, decrease reliability (since certain added parts are necessary), consume added power, and generate large amounts of electromagnetic noise. Suppression of this noise can be a difficult process since the oscillators generate noise in a broad spectrum of frequencies. The transformers in which the noise currents flow set inherent limits on the extent to which spurious capacitive and inductive coupling can be reduced.

A study of the characteristics and requirements of HDS shows that the first approach listed above is definitely the preferable system approach, and that the ultimate can be achieved through transmission of digital signals between boxes. Output of the data storage system will be of digital form and thereby immune from ground problems. Output of the starmapper is digital and, if transmitted at a high enough level, will be immune from the ground noise source. The A/D converter associated with the radiometer can be located near the radiometer and can receive power from the same lead as the radiometer; therefore, the radiometer-to-converter analog signal will not be exposed to the possibility of appreciable error from ground loops.

The system grounding tradeoff will be analyzed further as it applies to spacecraft system status and temperature monitoring. Spacecraft bonding will also be included as it applies to surface potential, circulating currents, and such factors as solar panel reliability.

Eddy Currents

Eddy currents will be induced in the conducting surfaces of the spacecraft due to interaction of the earth's magnetic field and the spinning spacecraft. The eddy current and the magnetic field interact to produce a torque which reduces the spin rate of the spacecraft and also tends to precess the spin axis.

Equations developed in reference 17 for symmetrically spinning thick- and thin-wall cylinders show that the induced torque is dependent on the spacecraft configuration (length, diameter, fineness ratio), the field intensity vector, and the shell conductance.

Spacecraft configuration is largely fixed by the experiment requirements. The field-intensity vector is fixed by the 500 km, near-polar orbit. Therefore, shell conductance is the only factor which is readily available for eddy current control. Further study should be made to determine the feasibility of reducing eddy currents by controlling conductivity of the spacecraft skin. The present study has been conducted with a worst-case model for the eddy current torques.

CONCLUSIONS AND RECOMMENDATIONS

The spacecraft electrical power study has resulted in the following conclusions:

- A solar cell-battery power subsystem is preferrable to all other candidate power sources.
- The recommended solar array configuration is one in which the solar cells are to be mounted on six panels. The panels are folded against the sides of the hexagonal spacecraft at launch and deployed into a common plane at spacecraft separation from the booster.
- The power system concept is tailored to the orbit and injection accuracies specified. However, any further departure of the worst-case nodal crossing of the sun-synchronous orbit toward noon/midnight will require modifications of the concept.
- Reasonable design precautions will ensure that the spacecraft magnetic moment is compatible with attitude determination subsystem requirements.

- Because of reasons stated previously it is recommended that further attention be given to the third-electrode concept, but only as a secondary charge controller. If this concept is proven by flight and additional laboratory experience, it should then be considered as a candidate for the primary controller.

APPENDIX A
SHUNT REGULATOR EFFICIENCY

APPENDIX A
SHUNT REGULATOR EFFICIENCY

$$E_o = E_i - (I_L + I_S)R \tag{A1}$$

$$E_{i\,max.} = K\,E_{i\,min.} \tag{A2}$$

$$I_S = 0 \text{ for } E_i = E_i = E_{i\,min.} \tag{A3}$$

$$E_o = E_{i\,min.} - I_L R \tag{A4}$$

$$E_o = E_{i\,max.} - \left(I_L + I_{S\,max.}\right)R = KE^{*}_{i\,min.} - \left(I_L + I^{*}_{S\,max.}\right)R \tag{A5}$$

$$E_{i\,min.} = K_1 E_o \tag{A6}$$

$$n = \frac{E_o I_L}{KE_{i\,min.}\left(I_L + I_{S\,max.}\right)} \tag{A7}$$

from (A5) and (A6):

$$E_o = KK_1E_o - \left(I_L + I_{S\,max.}\right)\left(\frac{K_1E_o - E_o}{I_L}\right) \tag{A8}$$

$$1 = KK_1 - \frac{I_L + I_{S\,max.}}{I_L}(K_1 - 1) \tag{A9}$$

$$1 + \frac{I_{S\,max.}}{I_L} = \frac{KK_1 - 1}{K_1 - 1} \tag{A10}$$

$$n = \frac{K_1 - 1}{KK_1(KK_1 - 1)} \tag{A11}$$

$$\frac{dn}{dK_1} = \frac{KK_1(KK_1 - 1) - (K_1 - 1)(2K^2K_1 - K)}{(\text{Denom.})^2} = 0 \tag{A12}$$

$$0 = KK_1^2 + 2KK_1 - 1 = K_1^2 - 2K_1 + \frac{1}{K} \tag{A13}$$

$$K_1 = 1 \pm \sqrt{1 - \frac{1}{K}} \text{ for maximum efficiency} \tag{A14}$$

for $K = 1.5$

$$K_1 = 1.577 \tag{A15}$$

APPENDIX B
POWER OUTPUT OF PANELS ROTATED ABOUT THE HINGE LINE

APPENDIX B

POWER OUTPUT OF PANELS ROTATED ABOUT THE HINGE LINE

DISCUSSION

A preliminary power analysis has been performed, and two options have been considered: that of mounting the solar cells directly to the space vehicle on the plane front end and the cylindrical surface, and that of mounting solar cells directly on the plane front end and on plane solar paddles. For the latter case, the optimum orientation of the paddles had to be determined. It is shown that the most obvious orientation, the same plane as the front plane end of the cylindrical vehicle, is the optimum.

The method of determining the optimum paddle orientation is as follows: The variation of power with angle of incidence is closely proportional to the cosine function of angle of incidence. Hence, one wishes to compute the time average value of cosine of angle of incidence for various positions of the sun and for various paddle orientations as the space vehicle spins about its cylindrical axis (Figure B-1).

Let α be the angle the paddle normally makes with the vehicle's cylindrical axis (or the angle the paddle makes with the plane front of the cylinder). The optimum value of α is that which maximizes the time average value of cosine of angle of incidence and turns out to be $\alpha = 0$ for the entire range of vehicle orientation (with respect to the sun) expected. Let ϕ be the angle the sun's position makes with the vehicle cylindrical axis. The angle ϕ is initially 45° but may vary between 31° and 65°. One more angle is needed, θ the angle of spin of the vehicle about its cylindrical axis. Using Euler's treatment of rigid-body motion, ϕ and θ are the first two Euler angles used in specifying the orientation of a body (space vehicle) fixed coordinate system (denoted by double primes) and a space (sun) fixed coordinate system (denoted by no primes), one in which the sun is along the X axis.

The unit normal vector $\underline{m}$ for one such paddle is defined in terms of α and the Cartesian unit vector in the body fixed (double primed) coordinate system. The cosine of angle of incidence on this paddle is, by definition of the dot product, the dot product of the unit normal vector and the unit vector along the space fixed X axis, along which the sun is located. In the mathematical treatment which follows, this dot product is expressed in terms of ϕ, θ, and α.

Since the vehicle spins at a uniform rate about its cylindrical axis, $\frac{d\theta}{dt}$ is constant, and the time average value of cosine of angle of incidence is merely the θ average value of cosine of angle of incidence ($\cos \angle i$) for any given value of α and ϕ. Since $\cos \angle i$ is symmetric about $\theta = 0$, it is only necessary to compute the average value from $\theta = 0$ to $\theta = \pi$, or over one-half

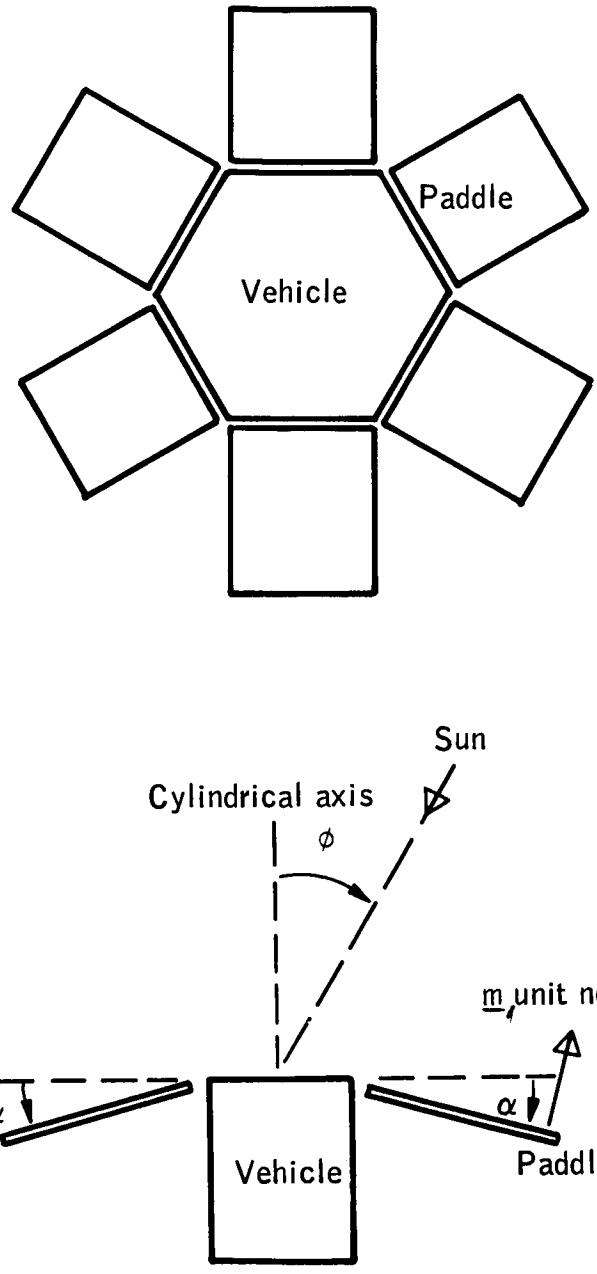

Figure B1. Paddle Angle

cycle. Should cos $\angle i$ become negative, this means the paddle is completely in shadow and no power is obtained, and a zero value must be used rather than a negative value. This requires the introduction of θ', the value beyond which zero is to be used rather than a negative value of cos $\angle i$.

The average of cos $\angle i$ is obtained in the usual way, and it is noted that, for all expected values of ϕ, the average value of cos $\angle i$ is maximum for $\alpha=0$, or for paddles normal to the cylindrical axis or in the same plane as the front plane of the cylinder. Then all cells make the same angle with the sun: cos $\angle i$ = cos ϕ, and the power analysis is simple, once the temperatures are computed.

For the case of cells mounted directly on the cylindrical and plane front surfaces, various cells receive sunlight at different angles of incidence, and the power analysis is a bit more difficult. The plane front surface and cylindrical surface are treated separately. For cells mounted on the cylindrical surfaces the power computed is from experimental data. Here θ denotes the angular position of a cell about the cylindrical axis, and cos $\angle i$ = cos θ sin ϕ.

From previously built cylindrical surface designs, I-V curves were obtained for series strings of cells as the angle of incidence was varied in discrete steps from 0° to 90° (Table B1). The optimum terminal voltage was selected (maximum power voltage for the whole cylindrical array), and the power points for this terminal voltage were plotted as a function of angle of incidence, normalized to be unity at normal incidence. From this curve, the relative power at 4° increments of θ is listed, and the average computed. Hence, the fraction of the power produced by the cylindrical array as opposed to a normal plane array is computed for three values of ϕ, 31°, 45°, 65°. The result of these computations is summarized (Table B1) following the computations.

The final power expected is computed, based on the maximum power point of a typical 2 x 2 cm N/P silicon solar cell in normal incident AMO sunlight at 28°C with allowances for radiation damage and losses due to filtering and assembly. The power is modified according to the average value of cos $\angle i$ and temperature.

DETERMINATION OF OPTIMUM PADDLE ANGLE

It is assumed that the vehicle will spin about its cylindrical axis at a uniform rate, which is fast compared with the variation of the angle position of the sun ϕ, so that time averages of the variation of angle of incidence $\angle i$ with spin angle θ can be computed at given fixed values of ϕ (Figure B2).

A body fixed coordinate system is defined (double primes) and the unit normal vector to the paddle surface is expressed in terms of body fixed axes. (x'' is cylindrical axis.) The first two Euler angles (ϕ, θ) are used to specify the orientation of the body fixed axes with respect to a coordinate system (unprimed) in which the sun is located along the X axis (Figure B-3). The cosine of the angle of incidence is then: cos $\angle i = \underline{i} \cdot \underline{m}$ cos $\angle i = \underline{i} \cdot \underline{m} = \underline{i} \cdot \underline{i}''$ cos α - $\underline{i} \cdot \underline{j}''$ sin α = cos ϕ cos α + cos θ sin ϕ sin α.

TABLE B1. - CYLINDRICAL, MOUNTED SOLAR CELL OUTPUT

θ	cos θ	ϕ = 31° Sin ϕ = 0.515 cos $\angle i$ = cos θ sin ϕ	Relative power	ϕ = 45° Sin ϕ = 0.7071 cos $\angle i$ = cos θ sin ϕ	Relative power	ϕ = 65° Sin ϕ = 0.9063 cos $\angle i$ = cos θ sin ϕ	Relative Power
1°	.9994	.5147	0.492 ($x\frac{1}{2}$ - 0.369)	.7067	0.710 ($x\frac{1}{2}$ - 0.532)	.9057	0.910 ($x\frac{1}{2}$ - 0.682)
5°	.9962	.5131	0.490	.7044	0.708	.9028	0.908
9°	.9877	.5087	0.483	.6984	0.703	.8951	0.900
13°	.9744	.5018	0.475	.6890	0.690	.8831	0.890
17°	.9563	.4925	0.465	.6762	0.675	.8667	0.872
21°	.9336	.4808	0.452	.6601	0.655	.8461	0.853
25°	.9063	.4668	0.434	.6409	0.632	.8214	0.830
29°	.8746	.4505	0.412	.6184	0.605	.7927	0.800
33°	.8387	.4320	0.392	.5930	0.580	.7601	0.766
37°	.7986	.4113	0.362	.5647	0.548	.7238	0.728
41°	.7547	.3887	0.336	.5336	0.522	.6840	0.666
45°	.7071	.3642	0.310	.5000	0.470	.6409	0.633
49°	.6561	.3379	0.277	.4639	0.428	.5946	0.580
53°	.6016	.3099	0.240	.4254	0.378	.5452	0.524
57°	.5446	.2805	0.205	.3851	0.325	.4936	0.438
61°	.4848	.2497	0.170	.3428	0.277	.4394	0.396
65°	.4226	.2177	0.153	.2988	0.225	.3830	0.328
69°	.3584	.1846	0.095	.2534	0.175	.3248	0.257
73°	.2924	.1506	0.066	.2067	0.120	.2650	0.160
77°	.2250	.1158	0.041	.1591	0.070	.2039	0.115
81°	.1564	.0806	0.025	.1106	0.037	.1418	0.058
85°	.0872	.0449	0.011	.0616	0.022	.0790	0.023
89°	.0174	.0090	0.002	.0123	0.003	.0158	0.005
			6.145		9.203		12.185
			$\frac{6.145}{45}$ = 0.136		$\frac{9.203}{45}$ = 0.202		$\frac{12.185}{45}$ = 0.270
		Convervatively	0.130		0.200		0.260

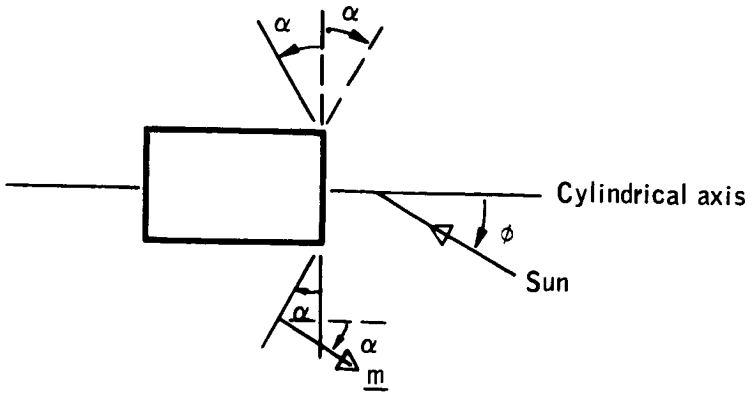

Figure B2. Paddle Sun Angles

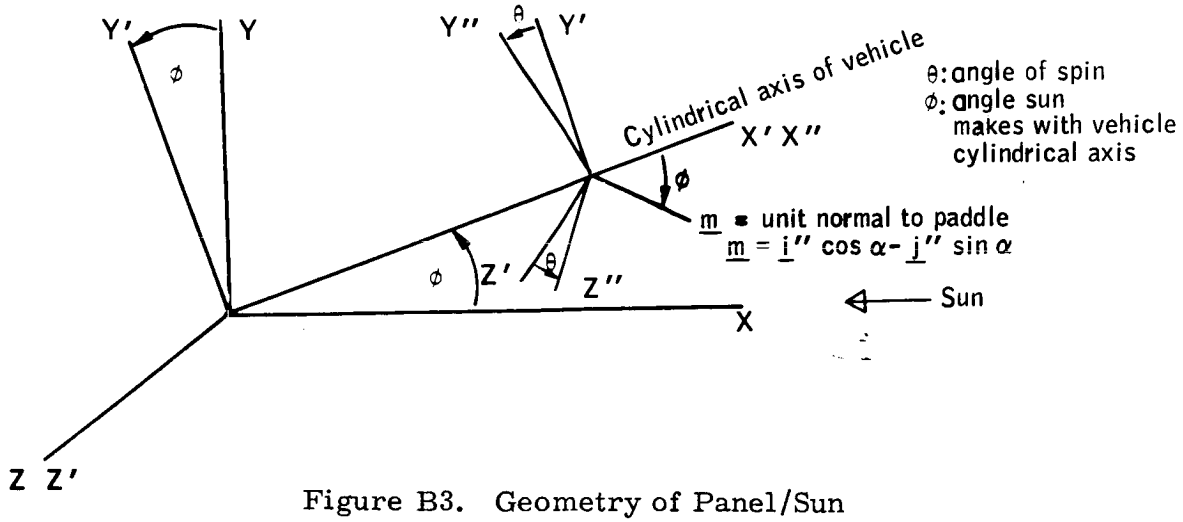

Figure B3. Geometry of Panel/Sun

$$\underline{i} \cdot \underline{i}'' = \cos \phi$$
$$\underline{i} \cdot \underline{j}'' = \cos \theta \ (-\sin \phi)$$
$$\underline{i} \cdot \underline{k}'' = \sin \theta \sin \phi$$

The time average cos $\angle i$ is

$$\overline{\cos \angle i} = \frac{1}{\pi} \int_{\theta = 0}^{\theta = \pi \cdot R\theta = \theta'} \cos \angle i \, d\theta$$

θ' is introduced to prevent negative contributions to the average $(\frac{\pi}{2} \leq \theta' \leq \pi)$. $\theta' = \pi$ if cos $\angle i$ is always positive, otherwise θ' is the value of θ at which cos $\angle i = 0$ (see Figure B4).

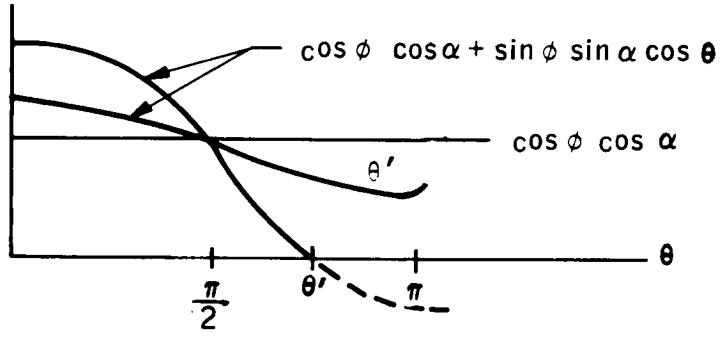

Figure B4. Value of θ'

$$\overline{\cos \angle i} = \frac{1}{\pi} \int_0^{\theta'} \cos \phi \cos \alpha \, d\theta + \frac{1}{\pi} \int_0^{\theta'} \sin \phi \sin \alpha \cos \theta \, d\theta$$

$$= \frac{\theta'}{\pi} \cos \phi \cos \alpha + \frac{1}{\pi} \sin \phi \sin \alpha \sin \theta \Big|_0^{\theta'}$$

Value of θ':

$$\cos \phi \cos \alpha + \sin \phi \sin \alpha \cos \theta' = 0$$

$$\cos \theta' = \frac{\cos \phi \cos \alpha}{\sin \phi \sin \alpha} = \frac{-1}{\tan \phi \tan \alpha}$$

Therefore, for the limiting cases,

$$\theta' = \pi \quad \text{if } (\tan \phi \tan \alpha) \leq 1$$

$$\theta' = \frac{\pi}{2} \quad \text{if } \tan \alpha = \infty \text{ or } \alpha = \frac{\pi}{2}$$

Thus:

$$\overline{\cos \angle i} = \cos \phi \cos \alpha \quad , \quad \text{if } (\tan \phi \tan \alpha) \leq 1$$

$$\overline{\cos \angle i} = \frac{\sin \phi}{\pi} \quad , \quad \text{if } \alpha = \frac{\pi}{2} \text{ (as for the cylindrical surface)}$$

So, at least for the case $(\tan \phi \tan \alpha) \leq 1$, the maximum value of $\cos \angle i$ occurs for $\alpha = 0$.

$$\overline{\cos \angle i} = \cos \phi \cos \alpha = \cos \phi$$

Hence, the paddles should be normal to vehicle cylindrical axis.

The optimum paddle angle is $\alpha = 0$, at least for the cases:

$$\alpha \leq 45°, \quad \phi \leq 45°$$
$$\alpha \leq 59°, \quad \phi \leq 31°$$
$$\alpha \leq 25°, \quad \phi \leq 65°$$

Since $\phi = 65°$ is the largest expected value of ϕ, let us examine $\overline{\cos \angle i}$ for values of $\alpha > 25°$, for $\phi = 65°$

α	$\overline{\cos \angle i}$
0°	.423
35°	.375
45°	.377
55°	.368
65°	.362

Hence, $\alpha = 0°$ still optimizes the value of $\overline{\cos \angle i}$ for the case of $(\tan \phi \tan \alpha) \leq 1$, $\phi \leq 65°$.

APPENDIX C

POWER OUTPUT OF PANELS ROTATED ABOUT A LINE RADIAL FROM SPIN AXIS

APPENDIX C

POWER OUTPUT OF PANELS ROTATED ABOUT A LINE RADIAL FROM SPIN AXIS

For very large values of sun-line/spin-axis angle, power output from panels normal to the spin axis will be small. One means of correcting this situation would be to rotate each panel about a line radial from the spin axis (Figure C1). Although such a rotation may cause the panel output to drop to zero during part of each spacecraft rotation, it allows the panel to view the sun more directly during another part of each rotation.

In order to compute the average power output for an array which is rotated about a radial line, the coordinates as shown in Figure C2 are used. The direction of the sun is

$$\hat{s} = \cos\theta\,\hat{i} + \sin\theta\,\hat{j} \tag{C1}$$

and the direction of the normal-to-panel vector is:

$$\hat{n} = \cos\lambda\,\hat{I} + \sin\lambda\,\hat{J} \tag{C2}$$

From the geometry

$$\left.\begin{aligned} \hat{I} &= \hat{i} \\ \hat{J} &= \cos\phi\,\hat{j} - \sin\phi\,\hat{k} \\ \hat{K} &= \sin\phi\,\hat{j} + \cos\phi\,\hat{k} \end{aligned}\right] \tag{C3}$$

it may be seen that

$$\hat{n} = \cos\lambda\,\hat{i} + \sin\lambda\cos\phi\,\hat{j} - \sin\lambda\sin\phi\,\hat{k} \tag{C2a}$$

The angle between $\hat{n}$ and $\hat{s}$ is then determined from

$$\cos(\hat{n},\hat{s}) = \hat{n}\cdot\hat{s} = \cos\theta\cos\lambda + \sin\theta\sin\lambda\cos\phi \tag{C4}$$

The simplifying assumption is made that panel power output is proportional to $\cos(\hat{n},\hat{s})$ for positive values and zero for negative values. The average relative power output of a panel over one spacecraft rotation is then

$$\overline{P} = \frac{1}{2\pi}\int_L^U (\hat{n}\cdot\hat{s})\,d\phi = \frac{1}{2\pi}\int_L^U (\cos\theta\cos\lambda + \sin\theta\sin\lambda\cos\phi)\,d\phi \tag{C5}$$

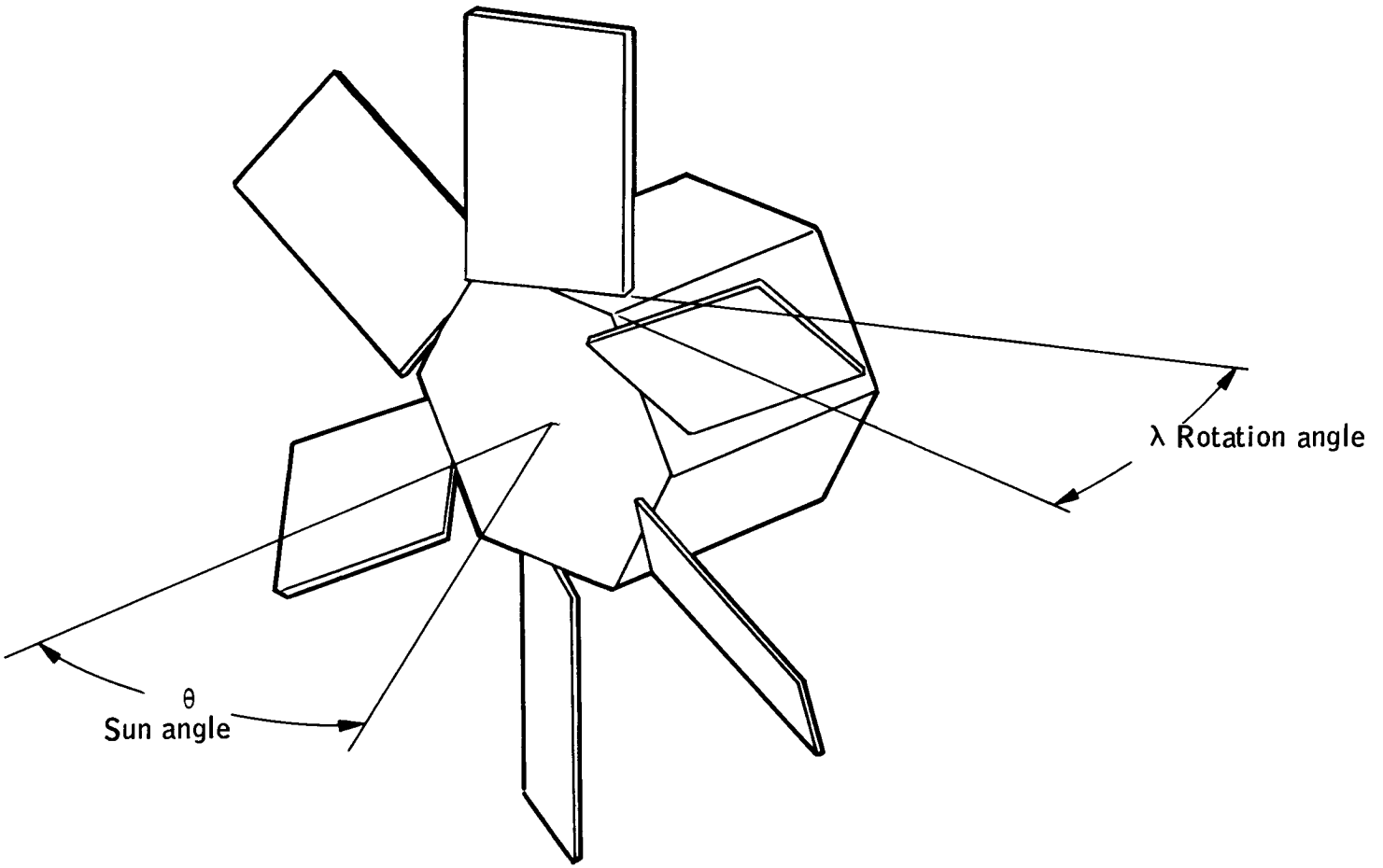

Figure C1. Paddle Configuration

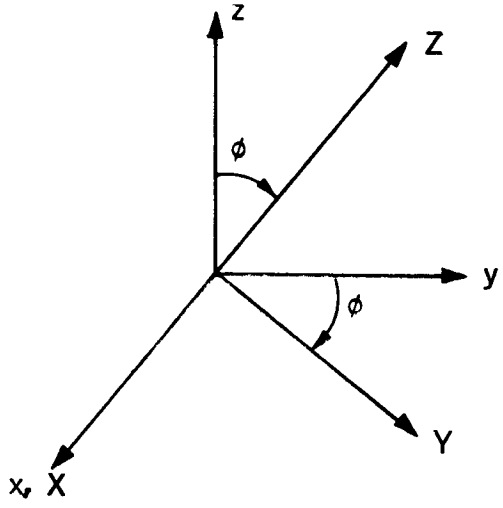

xyz: Space-fixed coordinates (corresponds to spacecraft spin axis, sun is in xy plane)

XYZ: Spacecraft coordinates (Z corresponds to line about which panel is rotated, X is spin axis)

$\hat{i}, \hat{j}, \hat{k}$: Unit vectors along x, y, z

$\hat{I}, \hat{J}, \hat{K}$: Unit vectors along X, Y, Z

ϕ : Angle of spacecraft rotation about spin axis

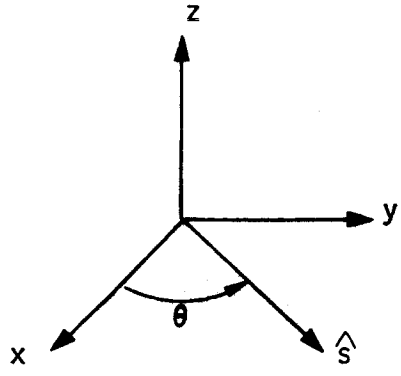

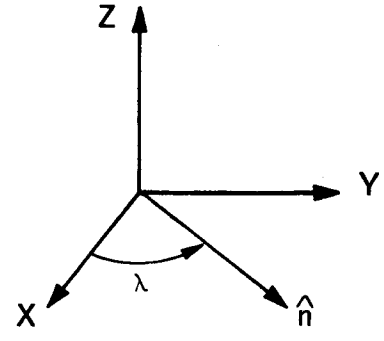

$\hat{s}$: Unit vector toward sun

θ: Sun-line/spin-axis angle

$\hat{n}$: Unit vector normal to panel

λ: Angle of panel rotation about line radial from spin axis.

Figure C2. Geometry of Sun/Panel

where

$$\left.\begin{aligned} U &= \cos^{-1}\left(\frac{-\cos\theta\cos\lambda}{\sin\theta\sin\lambda}\right) \\ L &= -U \end{aligned}\right\} \text{for } \lambda > \tan^{-1}(\cot\theta)$$

or

$$\left.\begin{aligned} U &= \pi \\ L &= -\pi \end{aligned}\right\} \text{for } \lambda \leq \tan^{-1}(\cot\theta)$$

Note that for $\lambda \leq \tan^{-1}(\cot\theta)$ the average relative power becomes

$$\bar{P}_{\lambda \leq \tan^{-1}(\cot\theta)} = \cos\theta\cos\lambda \qquad \text{(C6)}$$

which indicates that power is maximized, for this regime only, by keeping λ at zero (no panel rotation). For greater λ values, the average relative power becomes:

$$\bar{P}_{\lambda > \tan^{-1}(\cot\theta)} = \frac{1}{\pi}\left[U\cos\theta\cos\lambda + \sin\theta\sin\lambda\sin U\right] \qquad \text{(C7)}$$

where

$$U = \cos^{-1}\left(\frac{-\cos\theta\cos\lambda}{\sin\theta\sin\lambda}\right)$$

The average relative power based on these equations is plotted in Figure C3 as a function of λ for values of θ from zero to 90 degrees. Note that for sun-line/spin-axis angles less than about 70 degrees no advantage is gained by panel rotation; usually power is lost. If sun angles in excess of about 70 degrees were expected, provision for a panel rotation to about 70 degrees would then allow a nearly constant power output at about 30 percent of full normal illumination with little change as sun-line/spin-axis angle changes.

Since the mean sun-line/spin-axis angle for the HDS mission as presently envisioned is 45 degrees, with a 3-sigma expected high value of 65 degrees within a year's mission (based on two-stage Delta launch vehicle), there does not appear to be any good reason to provide for panel rotation. Alteration of either the mean value, or of expected dispersions, could alter this conclusion. It should be mentioned that the error in the assumption regarding power being proportioned to $\cos(\hat{n}, \hat{s})$ does not really change the conclusion. Panel power will fall below the cosine law value in the vicinity of $(\hat{n}, \hat{s}) = 90$ degrees. All cases below the broken line left of 65 degrees panel rotation and those immediately above it in Figure C3 will pass through this condition during each spacecraft revolution and will therefore generate less power than shown.

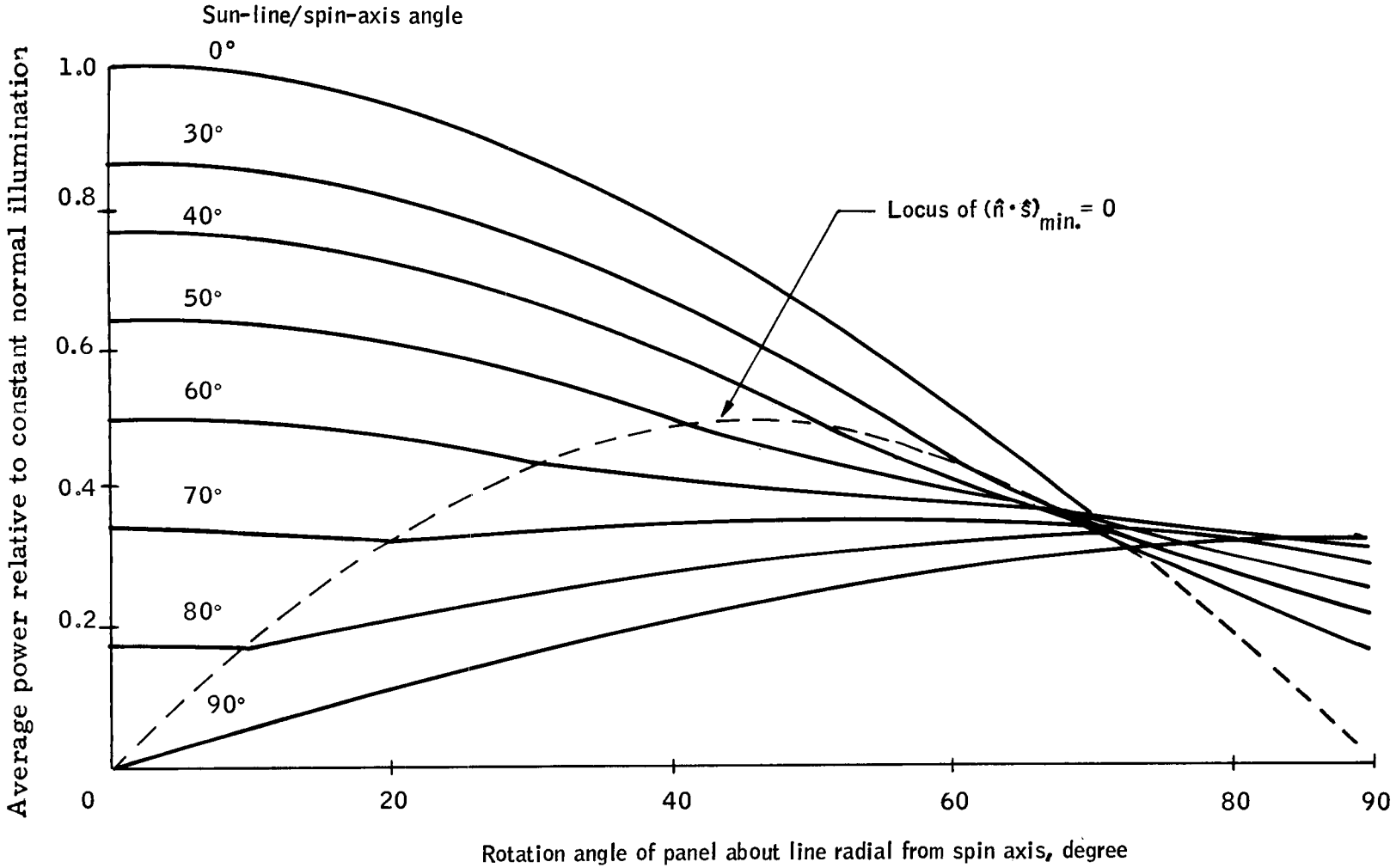

Figure C3. Average Relative Power versus Panel Rotation Angle

APPENDIX D
SOLAR ARRAY RADIATION DEGRADATION

APPENDIX D
SOLAR ARRAY RADIATION DEGRADATION

The damage to solar cells by high energy electrons and protons is caused by defects produced in the silicon crystal lattice. These effects cause current and voltage degradation which has been investigated during the past few years. Different particles and varying energy levels produce different effects in the cells. When dealing with heterogenous particles with complex spectra, it is necessary to reduce the flux components to a common base so that they can be integrated. Thus, the flux equivalents may be combined, whereas the damage effects cannot be simply added. The laboratory experiments have usually been made with 1 MeV electrons, so that the best data are based on equivalent 1 MeV electron radiation damage rates. In utilizing the results typical radiation environments must, therefore, first be converted to the equivalent 1 MeV electron fluxes. Upon conversion, the individual sources can be simply added together to obtain the total of 1 MeV equivalent electron flux which determines the solar cell damage values.

For this radiation analysis three high-energy sources of particle radiation were considered, including trapped electrons with energies from 0.5 MeV to 7 MeV; trapped protons with energies from about 4 MeV to greater than 300 MeV; and solar protons whose effect on the trapped particles is included in the first groups and which otherwise can be neglected for this orbit due to shielding by the earth's magnetic field. Each of these radiation sources must be converted to an equivalent of 1 MeV electron flux before the total solar cell damage value can be determined.

The conversion can be made by determining the damage caused by the particular radiation spectrum and correlating such losses with the quantity of 1 MeV electrons needed to produce the same result. Because of the practical problems involved in simulating such spectra, a more convenient method has been developed which makes it possible to make these conversions by semi-theoretical - semi-experimental methods.

The technique for converting electron and proton fluxes into an equivalent 1 MeV electron flux which in turn determines the solar cell degradation is summarized in the five-step procedure given below.

Step 1. Determine the coverglass shield value (g/cm^2) for the type and thickness coverglass to be used. This factor can be taken from Figure D1.

Step 2. Determine the equivalent 1 MeV electron flux ϕ_{EE} corresponding to the omnidirectional electron flux ϕ_F for the particular electron energy F considered.

Flux ϕ_F is obtained at 90° inclination from the orbital radiation environment data from Table D1. The equivalent 1 MeV electron flux due to trapped electrons ϕ_{EE} is determined using the equation

$$\phi_{EE} = \sum_{F=0}^{F=\infty} R_F \phi_F$$

where R_F is the conversion ratio (equivalent 1 MeV normal incident electrons per unit omindirectional electron flux for the electron energy F considered from Figure D2). This calculation is summarized in Table D2.

Step 3. Determine the equivalent 1 MeV electron flux ϕ_{EP} corresponding to the omnidirectional portion flux ϕ_K for the proton energy K considered. The value of ϕ_K is obtained from the orbital radiation data from Tables D3 through D6. The equivalent 1 MeV flux due to trapped protons ϕ_{EP} is determined using the equation

$$\phi_{EP} \sum_{K=0}^{K=\infty} N_K \phi_K$$

where N_K is the conversion ratio (equivlent 1 MeV electrons per unit omnidirectional proton flux for the proton energy K considered from Figure D3). This calculation is shown in Table D7.

Step 4. Determine the total equivalent 1 MeV electron flux by adding the 1 MeV equivalent flux values due to electrons and protons.

$$\phi_{Total} = \phi_{EE} + \phi_{EP}$$

Step 5. Determine solar cell degradation corresponding to the total equivalent 1 MeV integrated flux ϕ_{Total} from Figure D4, the experimental solar cell degradation curves. Degradation calculations are shown below.

For one day the equivalent 1 MeV flux is:

Proton	397.67×10^8
Electron	31.36×10^8
Total	429.03×10^8

Thus, for one year the equivalent 1 MeV flux is 1.566×10^{13}.

The power at the maximum power point is:

Power (with no radiation) = 59.6

Power (with one year's radiation) = 57.8

Consequently, the power loss is:

$$\text{Power loss} = \frac{59.6 - 57.8}{59.6}(100) = 3.02\%$$

while the voltage and current losses are:

$$\text{Voltage loss} = \frac{460 - 455}{460}(100) = 1.09\%$$

$$\text{Current loss} = \frac{64.8 - 63.5}{64.8}(100) = 2.01\%$$

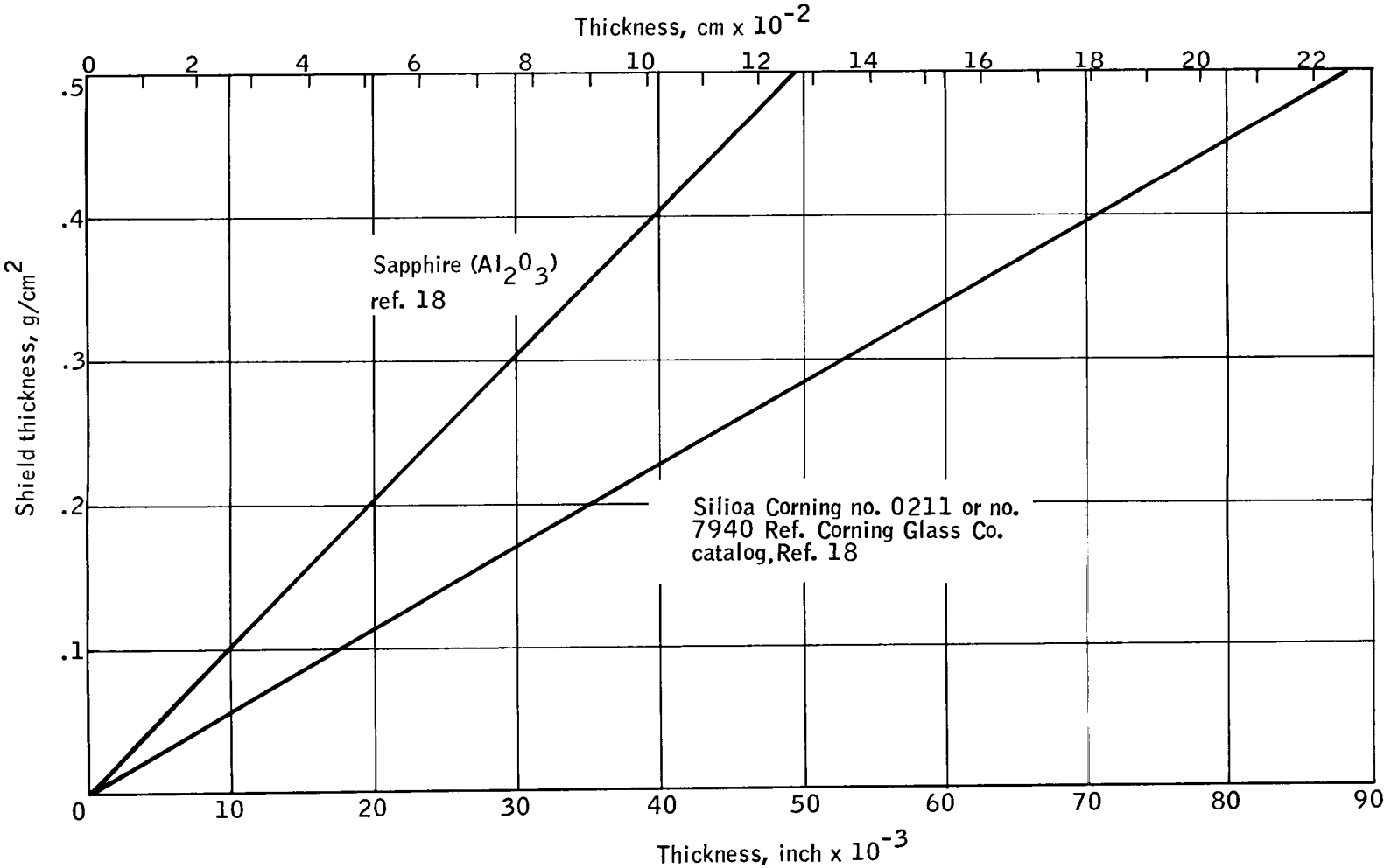

Figure D1. Solar Cell Coverglass Shield Thickness as a Function of Thickness of Coverglass

TABLE D1. - ORBITAL INTEGRATION FOR PROJECTED 1968 ELECTRON ENVIRONMENT

Orbit altitude = 300 n. mi. Total time = 24 hours Time interval = 1 minute

Energy, MeV		Orbital flux, 0 deg.		Orbital flux, 30 deg.		Orbital flux, 60 deg.		Orbital flux, 90 deg.	
E1	E2	E1	E1-E2	E1	E1-E2	E1	E1-E2	E1	E1-E2
0.	0.25	4.51E 06	3.41E 06	6.37E 10	5.35E 10	7.92E 10	6.29E 10	6.82E 10	5.31E 10
0.25	0.50	1.10E 06	8.30E 05	1.02E 10	8.56E 09	1.63E 10	1.16E 10	1.51E 10	1.04E 10
0.50	0.75	2.67E 05	2.02E 05	1.69E 09	1.40E 09	4.71E 09	2.63E 09	4.67E 09	2.57E 09
0.75	1.00	6.48E 04	4.91E 04	2.87E 08	2.36E 08	2.08E 09	9.92E 08	2.10E 09	1.01E 09
1.00	1.25	1.58E 04	1.19E 04	5.09E 07	3.65E 07	1.09E 09	4.77E 08	1.09E 09	4.91E 08
1.25	1.50	3.84E 03	2.78E 03	1.44E 07	4.35E 06	6.12E 08	2.58E 08	5.97E 08	2.59E 08
1.50	1.75	1.06E 03	3.09E 02	1.00E 07	7.85E 05	3.54E 08	1.46E 08	3.37E 08	1.44E 08
1.75	2.00	7.50E 02	2.19E 02	9.22E 06	6.64E 05	2.09E 08	8.35E 07	1.93E 08	8.05E 07
2.00	2.25	5.31E 02	1.55E 02	8.56E 06	5.81E 05	1.25E 08	4.85E 07	1.13E 08	4.54E 07
2.25	2.50	3.76E 02	1.10E 02	7.98E 06	5.15E 05	7.67E 07	2.87E 07	6.72E 07	2.63E 07
2.50	2.75	2.66E 02	7.76E 01	7.46E 06	4.82E 05	4.81E 07	1.69E 07	4.09E 07	1.51E 07
2.75	3.00	1.88E 02	5.49E 01	6.98E 06	4.38E 05	3.11E 07	1.02E 07	2.58E 07	8.92E 06
3.00	3.25	1.33E 02	3.89E 01	6.54E 06	4.04E 05	2.09E 07	6.23E 06	1.69E 07	5.31E 06
3.25	3.50	9.42E 01	2.75E 01	6.14E 06	3.72E 05	1.47E 07	3.84E 06	1.16E 07	3.19E 06
3.50	3.75	6.67E 01	1.95E 01	5.76E 06	3.43E 05	1.08E 07	2.42E 06	8.39E 06	1.97E 06
3.75	4.00	4.72E 01	1.39E 01	5.42E 06	3.19E 05	8.40E 06	1.56E 06	6.42E 06	1.24E 06
4.00	4.25	3.33E 01	9.66E 00	5.10E 06	2.94E 05	6.85E 06	1.04E 06	5.18E 06	8.12E 05
4.25	4.50	2.37E 01	6.93E 00	4.81E 06	2.80E 05	5.81E 06	7.14E 05	4.36E 06	5.52E 05
4.50	4.75	1.68E 01	4.88E 00	4.53E 06	2.58E 05	5.10E 06	5.10E 05	3.81E 06	3.90E 05
4.75	5.00	1.19E 01	3.47E 00	4.27E 06	2.36E 05	4.58E 06	3.83E 05	3.42E 06	2.90E 05
5.00	5.25	8.40E 00	2.45E 00	4.03E 06	2.26E 05	4.20E 06	3.00E 05	3.13E 06	2.28E 05
5.25	5.50	5.95E 00	1.73E 00	3.81E 06	2.11E 05	3.90E 06	2.52E 05	2.90E 06	1.90E 05
5.50	5.75	4.21E 00	1.23E 00	3.60E 06	1.92E 05	3.65E 06	2.07E 05	2.71E 06	1.57E 05
5.75	6.00	2.99E 00	8.78E-01	3.40E 06	1.93E 05	3.44E 06	1.94E 05	2.56E 06	1.47E 05
6.00	6.25	2.11E 00	6.16E-01	3.21E 06	1.68E 05	3.25E 06	1.62E 05	2.41E 06	1.23E 05
6.25	6.50	1.49E 00	4.37E-01	3.04E 06	1.62E 05	3.09E 06	1.53E 05	2.29E 06	1.16E 05
6.50	6.75	1.06E 00	3.07E-01	2.88E 06	1.58E 05	2.93E 06	1.46E 05	2.17E 06	1.12E 05
6.75	7.00	7.50E-01	2.19E-01	2.72E 06	1.39E 05	2.79E 06	1.29E 05	2.06E 06	9.80E 04
7.00		5.31E-01	5.31E-01	2.58E 06	2.58E 06	2.66E 06	2.66E 06	1.96E 06	1.96E 06

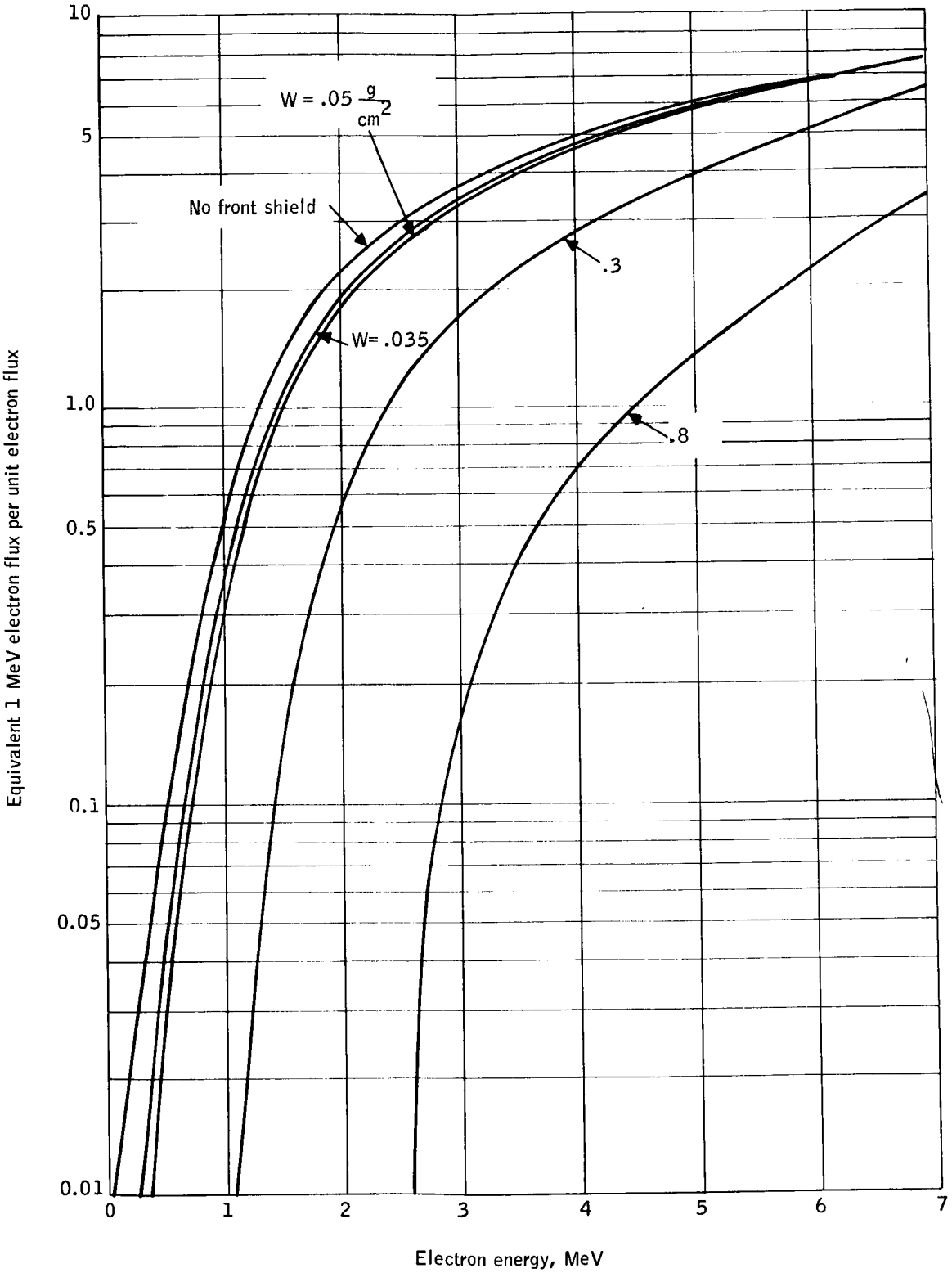

Figure D2. Equivalent 1 MeV Electron Flux per Unit Electron Flux as a Function of Electron Energy in MeV

[From ref. 19]

TABLE D2. - ELECTRON ENVIRONMENT WITH 90° ORBITAL FLUX

Energy, MeV		Orbital flux	Conversion ratio	Equivalent 1 MeV flux
E_1	E_2			
0	0.25	5.31×10^{10}	0.011	53.1×10^{7}
0.25	0.50	1.04×10^{10}	0.05	52.0
0.50	0.75	2.57×10^{9}	0.16	41.12
0.75	1.00	1.01×10^{9}	0.36	36.36
1.00	1.25	4.91×10^{8}	0.68	33.39
1.25	1.50	2.59×10^{8}	1.07	27.71
1.50	1.75	1.44×10^{8}	1.47	21.17
1.75	2.00	8.05×10^{7}	1.90	15.30
2.00	2.25	4.54×10^{7}	2.30	10.44
2.25	2.50	2.63×10^{7}	2.68	7.05
2.50	2.75	1.51×10^{7}	3.03	4.58
2.75	3.00	8.92×10^{6}	3.38	3.01
3.00	3.25	5.31×10^{6}	3.75	1.99
3.25	3.50	3.19×10^{6}	4.07	1.30
3.50	3.75	1.97×10^{6}	4.75	0.94
3.75	4.00	1.24×10^{6}	5.05	0.63
4.00	4.25	8.12×10^{5}	5.35	0.43
4.25	4.50	5.52×10^{5}	5.65	0.31
4.50	4.75	3.90×10^{5}	5.95	0.23
4.75	5.00	2.90×10^{5}	6.20	0.18
5.00	5.25	2.28×10^{5}	6.40	0.15
5.25	5.50	1.90×10^{5}	6.55	0.12
5.50	5.75	1.57×10^{5}	6.75	0.11
5.75	6.00	1.47×10^{5}	7.00	0.10
6.00	6.25	1.23×10^{5}	7.25	0.09
6.25	6.50	1.16×10^{5}	7.40	0.09
6.50	6.75	1.12×10^{5}	7.70	0.09
6.75	7.00	9.50×10^{4}	8.00	0.08
7.00	+	1.96×10^{6}	8.00	1.57
		Total		313.64×10^{7}

TABLE D3. - ORBITAL INTEGRATION MAP AP 4

Orbit altitude = 300 n. mi. Total time = 24 hours Time interval = 1 minute

Orbit inclination, degrees		0		30		60		90	
E_K	E_{K+1}	$\Phi(>E_K)$	$\Phi(E_{K+1}-E_K)$	$\Phi(>E_K)$	$\Phi(E_{K+1}-E_K)$	$\Phi(>E_K)$	$\Phi(E_{K+1}-E_K)$	$\Phi(>E_K)$	$\Phi(E_{K+1}-E_K)$
1	2	0.601E 05	0.154E 03	0.494E 08	0.737E 07	0.310E 08	0.454E 07	0.248E 08	0.365E 07
2	3	0.599E 05	0.154E 03	0.421E 08	0.624E 07	0.264E 08	0.386E 07	0.211E 08	0.310E 07
3	4	0.598E 05	0.153E 03	0.358E 08	0.529E 07	0.225E 08	0.329E 07	0.180E 08	0.264E 07
4	5	0.596E 05	0.152E 03	0.305E 08	0.449E 07	0.193E 08	0.280E 07	0.154E 08	0.224E 07
5	6	0.595E 05	0.152E 03	0.260E 08	0.381E 07	0.165E 08	0.238E 07	0.131E 08	0.191E 07
6	7	0.593E 05	0.151E 03	0.222E 08	0.324E 07	0.141E 08	0.203E 07	0.112E 08	0.162E 07
7	8	0.592E 05	0.150E 03	0.190E 08	0.275E 07	0.120E 08	0.173E 07	0.962E 07	0.138E 07
8	9	0.590E 05	0.150E 03	0.162E 08	0.234E 07	0.103E 08	0.147E 07	0.824E 07	0.117E 07
9	10	0.589E 05	0.149E 03	0.139E 08	0.199E 07	0.888E 07	0.125E 07	0.706E 07	0.100E 07
10	11	0.587E 05	0.148E 03	0.119E 08	0.169E 07	0.762E 07	0.107E 07	0.605E 07	0.856E 06
11	12	0.586E 05	0.148E 03	0.102E 08	0.144E 07	0.655E 07	0.917E 06	0.520E 07	0.731E 06
12	13	0.584E 05	0.147E 03	0.878E 07	0.123E 07	0.563E 07	0.784E 06	0.446E 07	0.624E 06
13	14	0.583E 05	0.146E 03	0.755E 07	0.105E 07	0.484E 07	0.670E 06	0.384E 07	0.533E 06
14	15	0.581E 05	0.146E 03	0.650E 07	0.897E 06	0.417E 07	0.573E 06	0.331E 07	0.455E 06
15	20	0.580E 05	0.721E 03	0.560E 07	0.287E 07	0.360E 07	0.184E 07	0.285E 07	0.146E 07
20	25	0.573E 05	0.706E 03	0.273E 07	0.133E 07	0.175E 07	0.864E 06	0.139E 07	0.682E 06
25	30	0.566E 05	0.691E 03	0.139E 07	0.638E 06	0.893E 06	0.413E 06	0.710E 06	0.325E 06
30	35	0.559E 05	0.676E 03	0.754E 06	0.314E 06	0.479E 06	0.203E 06	0.385E 06	0.159E 06
35	40	0.552E 05	0.662E 03	0.439E 06	0.161E 06	0.275E 06	0.104E 06	0.226E 06	0.811E 05
40	45	0.545E 05	0.649E 03	0.277E 06	0.866E 05	0.171E 06	0.555E 05	0.144E 06	0.432E 05
45	50	0.539E 05	0.636E 03	0.191E 06	0.490E 05	0.116E 06	0.312E 05	0.101E 06	0.244E 05
50	60	0.532E 05	0.123E 04	0.142E 06	0.482E 05	0.849E 05	0.306E 05	0.771E 05	0.242E 05
60	∞	0.520E 05	0.520E 05	0.938E 05	0.938E 05	0.543E 05	0.543E 05	0.529E 05	0.529E 05

TABLE D4. - ORBITAL INTEGRATION MAP AP 2

Orbit altitude = 300 n. mi. Total time = 24 hours Time interval = 1 minute

Orbit inclination, degrees		0		30		60		90	
E_K	E_{K+1}	$\Phi(>E_K)$	$\Phi(E_{K+1}-E_K)$	$\Phi(>E_K)$	$\Phi(E_{K+1}-E_K)$	$\Phi(>E_K)$	$\Phi(E_{K+1}-E_K)$	$\Phi(>E_K)$	$\Phi(E_{K+1}-E_K)$
5	10	0.581E 05	0.292E 03	0.594E 07	0.330E 06	0.497E 07	0.112 07	0.388E 07	0.851E 06
10	15	0.578E 05	0.290E 03	0.561E 07	0.309E 06	0.384E 07	0.328 06	0.303E 07	0.252E 06
15	20	0.575E 05	0.289E 03	0.530E 07	0.290E 06	0.351E 07	0.272 06	0.277E 07	0.206E 06
20	25	0.572E 05	0.287E 03	0.501E 07	0.271E 06	0.324E 07	0.242 06	0.257E 07	0.184E 06
25	30	0.570E 05	0.286E 03	0.474E 07	0.255E 06	0.300E 07	0.217E 06	0.238E 07	0.166E 06
30	35	0.567E 05	0.284E 03	0.448E 07	0.239E 06	0.278E 07	0.196E 06	0.222E 07	0.150E 06
35	40	0.564E 05	0.283E 03	0.424E 07	0.224E 06	0.259E 07	0.178E 06	0.207E 07	0.137E 06
40	45	0.561E 05	0.282E 03	0.402E 07	0.210E 06	0.241E 07	0.162E 06	0.193E 07	0.125E 06
45	50	0.558E 05	0.280E 03	0.381E 07	0.198E 06	0.225E 07	0.148E 06	0.180E 07	0.114E 06
50	60	0.555E 05	0.556E 03	0.361E 07	0.360E 06	0.210E 07	0.260E 06	0.169E 07	0.202E 06
60	70	0.550E 05	0.551E 03	0.325E 07	0.318E 06	0.184E 07	0.220E 06	0.149E 07	0.171E 06
70	80	0.544E 05	0.545E 03	0.293E 07	0.282E 06	0.162E 07	0.187E 06	0.131E 07	0.146E 06
80	90	0.539E 05	0.540E 03	0.265E 07	0.250E 06	0.143E 07	0.160E 06	0.117E 07	0.126E 06
90	100	0.533E 05	0.534E 03	0.240E 07	0.221E 06	0.127E 07	0.137E 06	0.104E 07	0.109E 06
100	110	0.528E 05	0.529E 03	0.217E 07	0.197E 06	0.113E 07	0.119E 06	0.937E 06	0.949E 05
110	120	0.523E 05	0.524E 03	0.198E 07	0.175E 06	0.101E 07	0.103E 06	0.842E 06	0.829E 05
120	130	0.518E 05	0.519E 03	0.180E 07	0.156E 06	0.913E 06	0.901E 05	0.759E 06	0.726E 05
130	140	0.512E 05	0.513E 03	0.164E 07	0.139E 06	0.823E 06	0.788E 05	0.686E 06	0.639E 05
140	150	0.507E 05	0.508E 03	0.151E 07	0.125E 06	0.744E 06	0.691E 05	0.622E 06	0.564E 05
150	200	0.502E 05	0.246E 04	0.138E 07	0.457E 06	0.675E 06	0.241E 06	0.566E 06	0.201E 06
200	250	0.477E 05	0.234E 04	0.927E 06	0.274E 06	0.434E 06	0.135E 06	0.365E 06	0.117E 06
250	300	0.454E 05	0.223E 04	0.653E 06	0.171E 06	0.298E 06	0.804E 05	0.247E 06	0.724E 05
300	∞	0.432E 05	0.432E 05	0.481E 06	0.481E 06	0.218E 06	0.218E 06	0.175E 06	0.175E 06

TABLE D5. - ORBITAL INTEGRATION MAP AP 1

Orbit altitude = 300 n. mi. Total time = 24 hours Time interval = 1 minute

Orbit inclination, degrees		0		30		60		90	
E_K	E_{K+1}	$\Phi(>E_K)$	$\Phi(E_{K+1}-E_K)$	$\Phi(>E_K)$	$\Phi(E_{K+1}-E_K)$	$\Phi(>E_K)$	$\Phi(E_{K+1}-E_K)$	$\Phi(>E_K)$	$\Phi(E_{K+1}-E_K)$
5	10	0.593E 05	0.397E 03	0.648E 07	0.504E 06	0.867E 08	0.650E 08	0.447E 08	0.324E 08
10	15	0.589E 05	0.395E 03	0.597E 07	0.458E 06	0.217E 08	0.142E 08	0.122E 08	0.737E 07
15	20	0.585E 05	0.392E 03	0.551E 07	0.416E 06	0.744E 07	0.336E 07	0.490E 07	0.185E 07
20	25	0.581E 05	0.389E 03	0.510E 07	0.379E 06	0.408E 07	0.950E 06	0.304E 07	0.588E 06
25	30	0.577E 05	0.387E 03	0.472E 07	0.346E 06	0.313E 07	0.387E 06	0.245E 07	0.273E 06
30	35	0.573E 05	0.384E 03	0.437E 07	0.316E 06	0.275E 07	0.237E 06	0.218E 07	0.181E 06
35	40	0.569E 05	0.381E 03	0.406E 07	0.288E 06	0.251E 07	0.186E 06	0.200E 07	0.146E 06
40	45	0.566E 05	0.379E 03	0.377E 07	0.264E 06	0.232E 07	0.161E 06	0.185E 07	0.127E 06
45	50	0.562E 05	0.376E 03	0.350E 07	0.242E 06	0.216E 07	0.145E 06	0.172E 07	0.115E 06
50	60	0.558E 05	0.745E 03	0.326E 07	0.426E 06	0.201E 07	0.252E 06	0.161E 07	0.202E 06
60	70	0.551E 05	0.735E 03	0.283E 07	0.361E 06	0.176E 07	0.213E 06	0.141E 07	0.171E 06
70	80	0.543E 05	0.725E 03	0.247E 07	0.306E 06	0.155E 07	0.182E 06	0.124E 07	0.147E 06
80	90	0.536E 05	0.715E 03	0.217E 07	0.261E 06	0.136E 07	0.157E 06	0.109E 07	0.126E 06
90	100	0.529E 05	0.705E 03	0.190E 07	0.224E 06	0.121E 07	0.136E 06	0.966E 06	0.109E 06
100	110	0.522E 05	0.696E 03	0.168E 07	0.193E 06	0.107E 07	0.118E 06	0.856E 06	0.953E 05
110	120	0.515E 05	0.686E 03	0.149E 07	0.166E 06	0.958E 06	0.103E 06	0.760E 06	0.830E 05
120	130	0.508E 05	0.677E 03	0.132E 07	0.144E 06	0.855E 06	0.902E 05	0.677E 06	0.724E 05
130	140	0.501E 05	0.668E 03	0.117E 07	0.125E 06	0.764E 06	0.791E 05	0.605E 06	0.634E 05
140	150	0.494E 05	0.659E 03	0.105E 07	0.109E 06	0.685E 06	0.697E 05	0.542E 06	0.556E 05
150	200	0.488E 05	0.316E 04	0.944E 06	0.378E 06	0.615E 06	0.245E 06	0.486E 06	0.193E 06
200	250	0.456E 05	0.295E 04	0.566E 06	0.207E 06	0.370E 06	0.137E 06	0.292E 06	0.106E 06
250	300	0.427E 05	0.275E 04	0.358E 06	0.119E 06	0.232E 06	0.805E 05	0.186E 06	0.616E 05
300	∞	0.399E 05	0.399E 05	0.239E 06	0.239E 06	0.152E 06	0.152E 06	0.124E 06	0.124E 06

TABLE D6. - ORBITAL INTEGRATION MAP AP 3

Orbit altitude = 300 n. mi. Total time = 24 hours Time interval = 1 minute

Orbit inclination, degrees		0		30		60		90	
E_K	E_{K+1}	$\Phi(>E_K)$	$\Phi(E_{K+1}-E_K)$	$\Phi(>E_K)$	$\Phi(E_{K+1}-E_K)$	$\Phi(>E_K)$	$\Phi(E_{K+1}-E_K)$	$\Phi(>E_K)$	$\Phi(E_{K+1}-E_K)$
5	10	0.904E 05	0.450E 04	0.582E 07	0.396E 06	0.464E 07	0.473E 06	0.363E 07	0.360E 06
10	15	0.859E 05	0.427E 04	0.542E 07	0.364E 06	0.416E 07	0.409E 06	0.327E 07	0.313E 06
15	20	0.816E 05	0.406E 04	0.505E 07	0.336E 06	0.375E 07	0.356E 06	0.295E 07	0.273E 06
20	25	0.776E 05	0.385E 04	0.472E 07	0.309E 06	0.340E 07	0.312E 06	0.268E 07	0.241E 06
25	30	0.737E 05	0.366E 04	0.441E 07	0.285E 06	0.308E 07	0.275E 06	0.244E 07	0.213E 06
30	35	0.701E 05	0.347E 04	0.412E 07	0.263E 06	0.281E 07	0.244E 06	0.223E 07	0.189E 06
35	40	0.666E 05	0.330E 04	0.386E 07	0.244E 06	0.256E 07	0.217E 06	0.204E 07	0.169E 06
40	45	0.633E 05	0.313E 04	0.361E 07	0.225E 06	0.235E 07	0.194E 06	0.187E 07	0.151E 06
45	50	0.601E 05	0.297E 04	0.339E 07	0.209E 06	0.215E 07	0.174E 06	0.172E 07	0.136E 06
50	60	0.572E 05	0.551E 04	0.318E 07	0.374E 06	0.198E 07	0.298E 06	0.158E 07	0.234E 06
60	70	0.516E 05	0.497E 04	0.280E 07	0.322E 06	0.168E 07	0.244E 06	0.134E 07	0.192E 06
70	80	0.467E 05	0.449E 04	0.248E 07	0.279E 06	0.144E 07	0.201E 06	0.115E 07	0.159E 06
80	90	0.422E 05	0.405E 04	0.220E 07	0.242E 06	0.123E 07	0.167E 06	0.997E 06	0.133E 06
90	100	0.381E 05	0.365E 04	0.196E 07	0.211E 06	0.107E 07	0.140E 06	0.864E 06	0.112E 06
100	110	0.345E 05	0.330E 04	0.175E 07	0.184E 06	0.929E 06	0.118E 06	0.752E 06	0.948E 05
110	120	0.312E 05	0.298E 04	0.156E 07	0.161E 06	0.810E 06	0.100E 06	0.657E 06	0.806E 05
120	130	0.282E 05	0.269E 04	0.140E 07	0.142E 06	0.710E 06	0.858E 05	0.576E 06	0.688E 05
130	140	0.255E 05	0.243E 04	0.126E 07	0.125E 06	0.624E 06	0.735E 05	0.507E 06	0.591E 05
140	150	0.230E 05	0.220E 04	0.113E 07	0.110E 06	0.550E 06	0.631E 05	0.448E 06	0.509E 05
150	200	0.208E 05	0.821E 04	0.102E 07	0.391E 06	0.487E 06	0.209E 06	0.397E 06	0.169E 06
200	250	0.126E 05	0.496E 04	0.636E 06	0.224E 06	0.277E 06	0.108E 06	0.227E 06	0.885E 05
250	300	0.771E 04	0.301E 04	0.412E 06	0.135E 06	0.169E 06	0.598E 05	0.139E 06	0.474E 05
300	∞	0.470E 04	0.470E 04	0.277E 06	0.277E 06	0.109E 06	0.109E 06	0.898E 05	0.898E 05

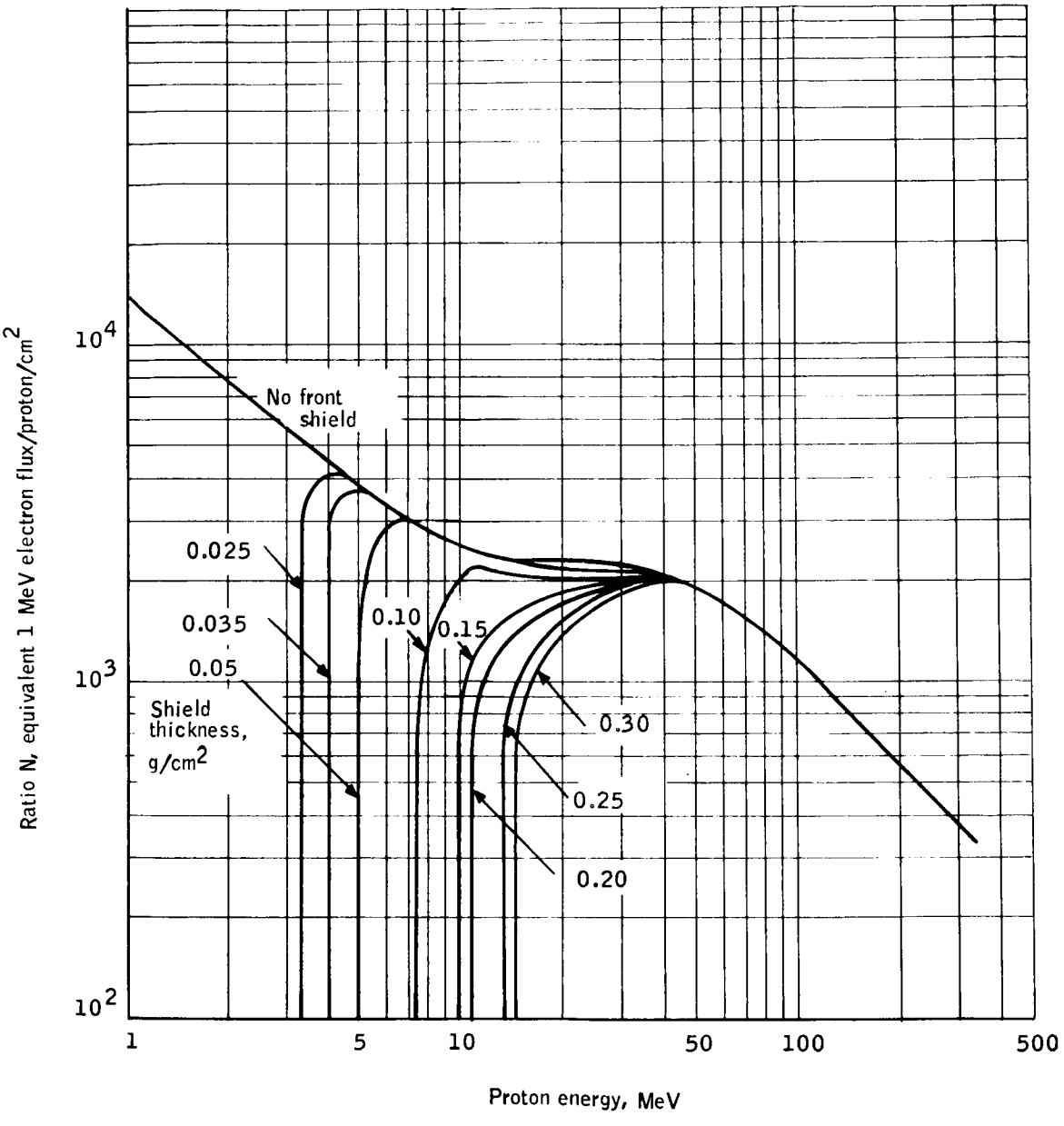

Figure D3. Solar Cell Damage Equivalent to 1 MeV Electrons as Functions of Proton Energy Infinite Back Shielding [From ref. 8]

TABLE D7. - PROTON ENVIRONMENT WITH 90° ORBITAL FLUX

Energy, MeV		Orbital flux	Conversion ratio	Equivalent 1 MeV flux
E_1	E_2			
4	5	0.224×10^7	3.70×10^3	82.88×10^8
5	6	0.191×10^7	3.35	63.99
6	7	0.162×10^7	3.0	48.60
7	8	0.138×10^7	2.8	38.64
8	9	0.117×10^7	2.65	21.01
9	10	0.100×10^7	2.55	25.50
10	11	0.856×10^6	2.47	21.14
11	12	0.731×10^6	2.40	17.54
12	13	0.624×10^6	2.36	14.73
13	14	0.533×10^6	2.30	12.26
14	15	0.455×10^6	2.27	10.33
15	20	0.206×10^6	2.19	4.51
20	25	0.184×10^6	2.15	3.96
25	30	0.166×10^6	2.13	3.54
30	35	0.181×10^6	2.10	3.80
35	40	0.146×10^6	2.05	2.99
40	45	0.127×10^6	2.00	2.54
45	50	0.115×10^6	1.93	2.22
50	60	0.234×10^6	1.75	4.10
60	70	0.192×10^6	1.58	3.03
70	80	0.159×10^6	1.42	2.26
80	90	0.133×10^6	1.28	1.70
90	100	0.112×10^6	1.16	1.30
100	110	0.948×10^5	1.05	1.00
110	120	0.806×10^5	0.96	0.77
120	130	0.688×10^5	0.88	0.61
130	140	0.591×10^5	0.82	0.48
140	150	0.509×10^5	0.76	0.39
150	200	0.109×10^6	0.56	0.95
200	250	0.885×10^5	0.445	0.39
250	300	0.494×10^5	0.300	0.18
300	∞	0.898×10^5	0.370	0.33
		Total		397.67×10^8

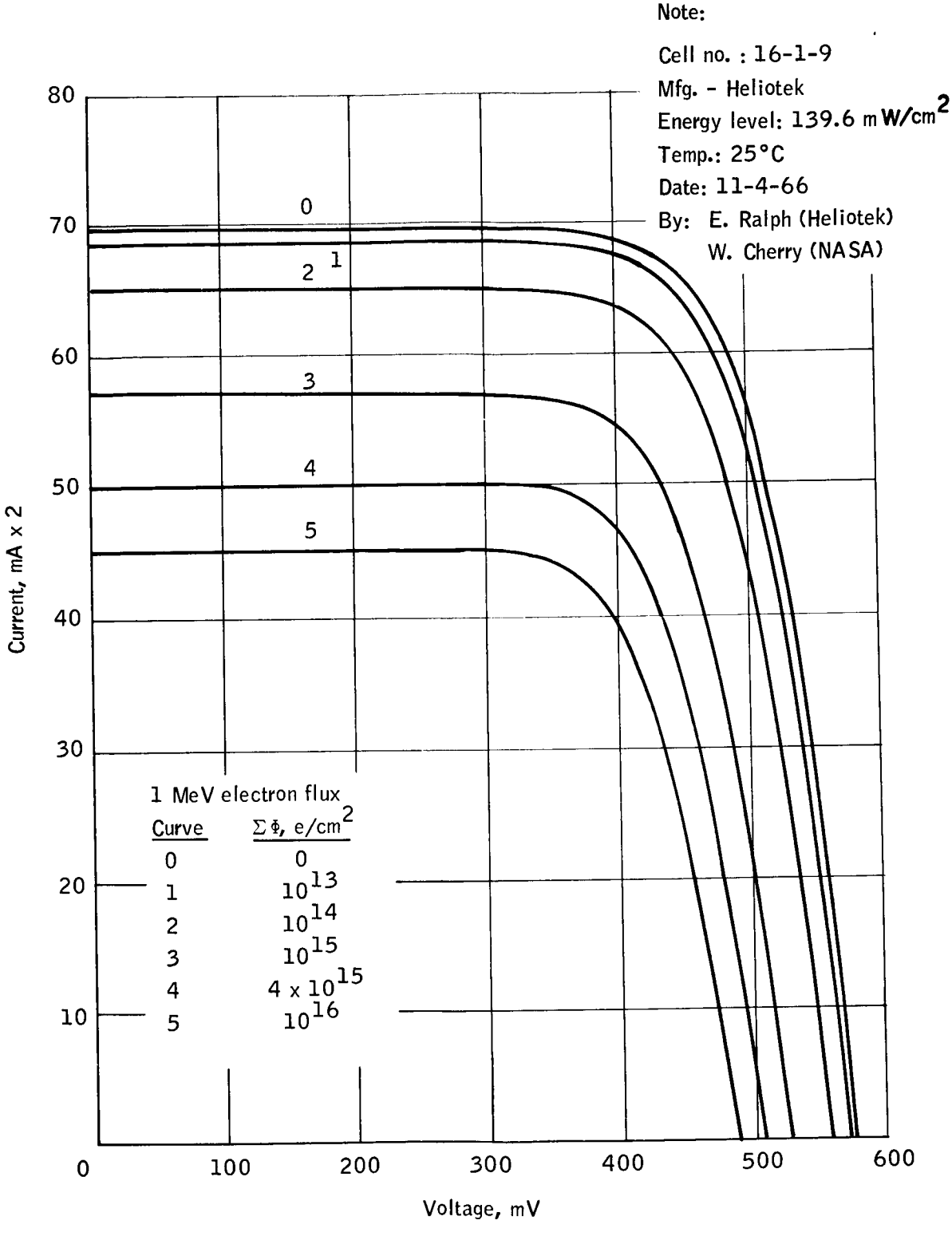

Figure D4. I-V Characteristic

APPENDIX E
SOLAR ARRAY RELIABILITY ANALYSIS

APPENDIX E
SOLAR ARRAY RELIABILITY ANALYSIS

INTRODUCTION

Reported herein are the results of the reliability analysis performed on the proposed design of a solar cell power supply for the HDS satellite.

Included is a failure effect analysis and reliability model with appropriate calculations of system reliability and maximum anticipated power degradation.

ARRAY CONFIGURATION

The array consists of six identical solar panels which fold outward from the sides of the hexagonal shaped satellite. In this position all solar cells will lie in the same plane. Each panel will consist of two circuits comprising 108 series bu eight parallel connected solar cells. Each solar cell circuit is connected in series with an array of two parallel blocking diodes. All wiring and connections are redundant. The array will consist of a total of 10 368 solar cells.

SOLAR CELL FAILURE ANALYSIS

Failures Resulting in Complete Loss of Solar Cell Power

Short-circuit failures.-- A short circuit of a solar cell results when a conducting path exists between the upper and lower surfaces of the cell.

The most probable cause for this type of failure is a contact between the lower surface of the cell and the lead from the submodule bus bar which is connected to the top surface of the same cell. This will result in a short circuit of the affected cell and will also short circuit the other cells in that submodule. There will be a slight variation in the operating voltage and current for the other cells in that string resulting in a correspondingly small power degradation. This power degradation will be of the order of one percent for the affected string when operating at no-failure maximum power voltage. A total power degradation of the order of 1/10 percent per failure will result for the entire array. Quality control inspection of the intercell connections substantially reduces the possibility of such a failure under normal operating conditions. The probability that such a failure will occur is, therefore, assumed to be zero.

Open-circuit failures. -- Each solar cell is soldered at three points on its lower surface to a submodule bus bar. The series connection to the next submodule bus bar is completed by four solder joints on the top surface of each cell. For soldering performed with a high degree of workmanship, the

solder joint failure rate is 1.0×10^{-8} failures per hour and the probability of failure of a solder joint is 8.8×10^{-5} per year. Since the four solder connections on the upper surface represent threefold solder joint redundancy, the probability that the cell will open circuit as a result of failure of all solder joints at the upper surface will be of the order of 10^{-16} per year. The probability that a cell will open circuit as a result of a solder joint failure on the lower surface will be of the order of 10^{-12} per year.

An open-circuit cell failure may result from the fracture of a cell. The probability is extremely remote that such failure would not be detected during preliminary inspections or that it would occur under normal operating conditions. An open-circuit failure caused by the separation of the electrode grid from the upper surface of a cell may result from thermal cycling of the cell and/or vibration of the cell. Engineering studies and conclusions to date indicate that, in this case, the solar cell failure rate would have an upper limit of 1.75×10^{-4} per year. If all possibilities of open-circuit failure for normal operation are considered, the probability of an open-circuit failure of an individual solar cell is no greater than 1.76×10^{-4} per year.

Cell Failure Probabilities

If $P = 1.76 \times 10^{-4}$ per year is the probability of failure of an individual solar cell during one year, for eight solar cells connected in a parallel submodule array, the probability of n failures within the submodule will be

$$ {}^{n}P_{8} = \frac{8!}{(8-n)!\,n!} P^{n} (1-P)^{8-n} \text{ per year} \qquad \text{(E1)} $$

The values of ${}^{1}P_{8}$ and ${}^{2}P_{8}$ are:

$$ {}^{1}P_{8} = 1.40 \times 10^{-3} \text{ per year} $$

$$ {}^{2}P_{8} = 8.61 \times 10^{-7} \text{ per year} $$

It is seen that the probability of two failures occurring within one submodule is remote as compared to the occurrence of a single failure. Therefore, this analysis is restricted to single solar cell failures within a submodule.

If ${}^{1}P_{8}$ is the probability of having a single submodule failure, the probability of having n cell failures within an eight-parallel by 108-series solar cell circuit will be

$$ {}^{n}P_{108} = \frac{108!}{(108-n)!\,n!} \left({}^{1}P_{8}\right)^{n} \left(1-{}^{1}P_{8}\right)^{108-n} \qquad \text{(E2)} $$

The values of ${}^{n}P_{108}$ for n = 1 and for n = 2 are

$$ {}^{1}P_{108} = 0.13 $$

$$ {}^{2}P_{108} = 0.0098 $$

Once again it can be seen that the probability of two such failures is less by at least an order of magnitude than that for a single failure. It is therefore assumed that there will be no more than one cell failure within any string, by no means an unreasonable assumption.

If the power degradation computed for a single cell failure within a string is compared with the power degradation resulting from two cell failures occurring in different submodules, no appreciable difference will be found. This is the result of the current-limiting actions imposed by the first failure. Thus, the first cell failure within any string is the critical failure with respect to power degradation of the solar cell array.

Total Solar Cell Reliability

The total solar cell reliability ${}^{x}R$ is the probability that there will be no more than x failures out of a total of N solar cells for the array.

For a binomial distribution, the probability that x failures will occur is

$$ {}^{x}P = \frac{N!}{(N-x)!\,x!}\, P^{x} (1-P)^{N-x} \qquad \text{(E3)} $$

where P is the probability of failure of a single solar cell.

The gaussian distribution is approximately equal to the binomial distribution when N is large and P is small. For the gaussian distribution

$$ {}^{x}P = \frac{1}{\sqrt{2\pi}\sigma} e^{-(x-m)^2/2\sigma^2} \qquad \text{(E4)} $$

where

$$ m = N \cdot P $$

$$ \sigma = \sqrt{N \cdot P\,(1-P)} $$

Using the gaussian distribution ^{x}R may be evaluated as

$$^{x}R = \int_{-\infty}^{x} x_P \cdot dx \qquad \text{(E5)}$$

Evaluation of Solar Cell Reliability

The array has a total number of solar cells, N = 10 368 cells. The probability of failure of each solar cell is $P = 1.76 \times 10^{-4}$ per year, so that $m = 1.60$ and $\sigma = 1.26$. Values of ^{x}R (the solar cell reliability) and corresponding values of x (the total number of solar cell failures) are given in the table below.

x	^{x}R
2	.5529
3	.8094
4	.9468
5	.9908
6	.9987

Power Degradation Resulting from Solar Cell Failures

In the previous sections of the solar cell failure analysis all open circuit failures were assumed to be complete, that is, the entire cell was considered to be an open circuit if a fracture occurred at any place on the solar cell. In reality, as a result of use of extended solder tabs, such a fracture would not result in the complete loss of the solar cell, but only a partial loss depending upon the position of the fracture. It is the purpose of this analysis to evaluate the anticipated circuit power degradation on the basis of fractional loss of solar cells.

Procedure. -- Values of current and corresponding voltage are taken for 53 points on the typical I-V curve for a 2 x 2 cm N/P solar cell. This curve is displayed in Figure E1.

The current-voltage points selected are given in Table E1.

No failures - composite characteristic curve: Since the voltage drop for all cells in any submodule will be equal, so also will be the currents through each individual cell, if the cells are assumed to have identical characteristics. Therefore, the total current through any submodule will be equal to the product of the individual cell current at a given voltage and the number of cells per submodule. Likewise, all submodules being in series will have identical currents, and the total voltage drop for a module will be the product of the voltage drop per submodule and the number of submodules per module.

TABLE E1. - CHARACTERISTIC CURVE COORDINATES, N/P 2 x 2 CM HTA 625 SOLAR CELL

Voltage, volts	Current, amps	Voltage, volts	Current, amps
-20.0127	0.1438	0.4374	0.1315
-16.0127	0.1425	0.4472	0.1308
-12.0127	0.1412	0.4550	0.1300
-8.0127	0.1399	0.4622	0.1293
-4.0127	0.1386	0.4711	0.1281
-0.0127	0.1372	0.4772	0.1272
0.0372	0.1372	0.4828	0.1263
0.0872	0.1370	0.4872	0.1251
0.1372	0.1367	0.4920	0.1245
0.1872	0.1365	0.4947	0.1240
0.2040	0.1363	0.4976	0.1232
0.2200	0.1361	0.5002	0.1221
0.2372	0.1360	0.5082	0.1200
0.2540	0.1359	0.5152	0.1169
0.2700	0.1358	0.5202	0.1143
0.2872	0.1355	0.5262	0.1120
0.3010	0.1351	0.5297	0.1104
0.3122	0.1348	0.5362	0.1067
0.3250	0.1346	0.5472	0.0983
0.3372	0.1343	0.5562	0.0892
0.3500	0.1341	0.5652	0.0767
0.3622	0.1340	0.5737	0.0602
0.3750	0.1338	0.5822	0.0400
0.3872	0.1335	0.5972	-0.0162
0.3974	0.1332	0.6132	-0.1434
0.4072	0.1329		
0.4173	0.1323		
0.4272	0.1319		

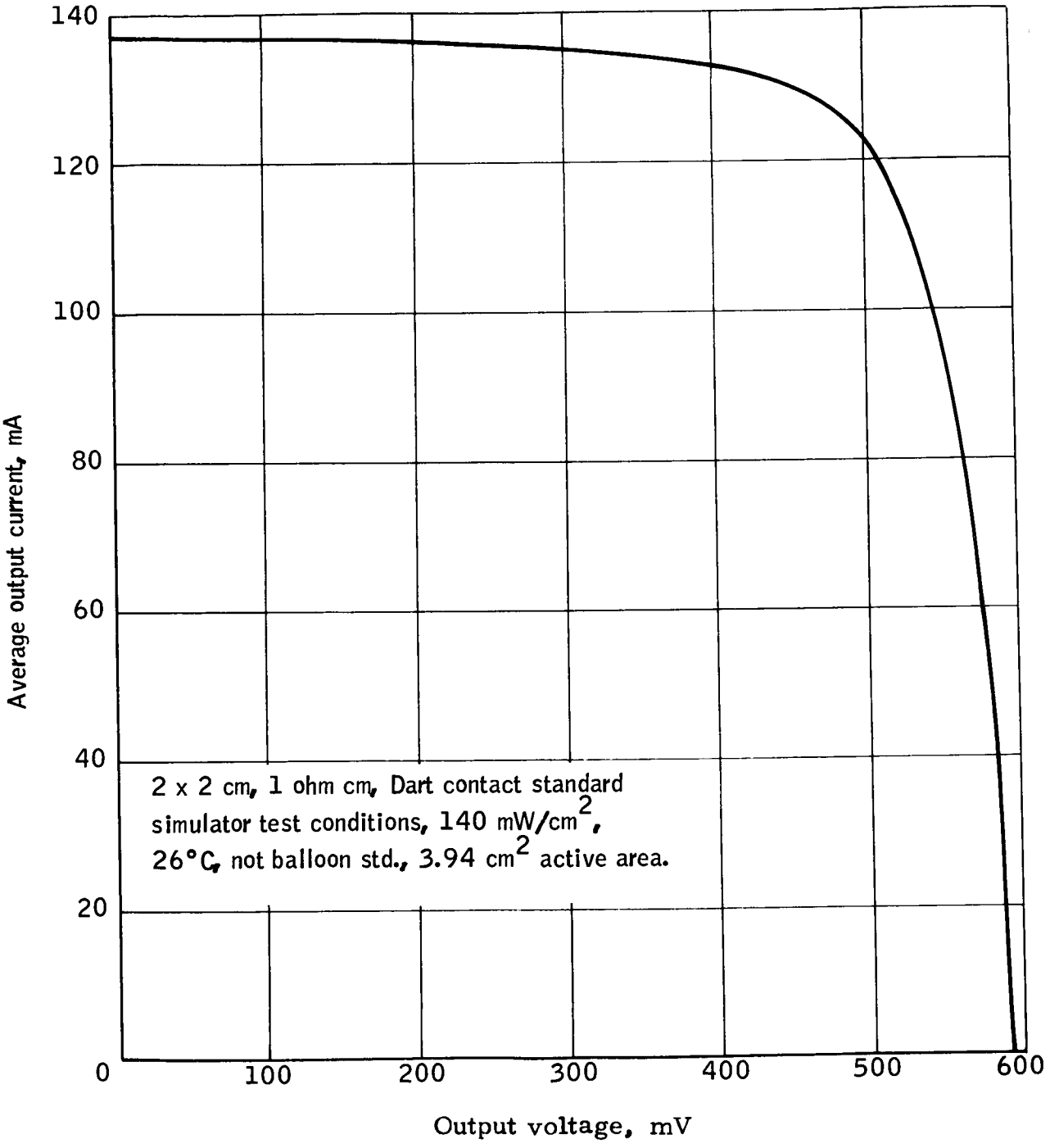

Figure E1. Average Electrical Out-put, HTA 625 Cell

Therefore, to form composite characteristic curves for a module with no failures, it is necessary only to multiply the values of the current given in Table D1 by the number of cells per submodule and the voltages by the number of submodules. Using these data, an I-V curve can be plotted for the module. For this module, the power at any voltage can be computed as the product of the voltage and current.

Open-circuit failure - composite characteristic curve: For a worst-case analysis, it was assumed that the fraction of the solar cell lost as a result of a fracture would be random. Thus, for example, the chance of loss of between 1/8 and 1/4 of a solar cell would be the same as the loss of from 7/8 to a full solar cell. This is an assumption which is severe in the light of the fact that observed failures in general result in a small fractional loss of the solar cell. Since sufficient statistical information is not available concerning the problem of solar cell fractures, the severest condition, that of random loss, is used in this analysis.

For the case of a circuit which has a fracture in the fractional region such that, for example, between 1/2 and 5/8 of the solar cell remains for circuit continuity, the fractured-cells characteristic curve must be formed by reducing the current to an average current factor $\frac{1/2 + 5/8}{2} = 9/16$ of the no failure current, while the voltage remains the same.

Then composite characteristic curves for the complete circuit with failure are formed in the following manner: Composite characteristic curves are constructed for a "short string" of 8-parallel by 107-series cells. Also, a characteristic curve for a single submodule of 7 cells plus one failed cell is constructed.

For this submodule, the current will be 7-9/16 of that for a single solar cell. The composite characteristic curve for circuit failure is then formed by adding together the values of voltage for equal values of current.

Analysis of data. -- The following configurations were examined:

Between, 0 and 1/8 cell remaining with average current - 1/16 of that of a normal cell,

1/8 and 1/4 cell remaining with average current - 3/16 of that of a normal cell

1/4 and 3/8 cell remaining with average current - 5/16 of that of a normal cell,

3/8 and 1/2 cell remaining with average current - 7/16 of that of a normal cell,

1/2 and 5/8 cell remaining with average current - 9/16 of that of a normal cell,

5/8 and 3/4 cell remaining with average current - 11/16 of that of a normal cell,

3/4 and 7/8 cell remaining with average current - 13/16 of that of a normal cell,

7/8 and a complete cell remaining with average current - 15/16 of that of a normal cell.

For each case, the single failure percent power degradation was evaluated. The results are given in Table E2.

Power Degradation. -- Under the assumption of random fracture, the average current degradation per circuit for each failure would be equal to the average of those failures indicated in Table E2. Thus, an average power degradation of 0.53 percent of the affected strings power output at no-failure maximum power voltage will result for each solar cell failure.

This corresponds to a total power degradation for the entire array of 0.054 percent/failure-year.

TABLE E2. - CIRCUIT POWER DEGRADATION AS RELATED TO FRACTIONAL LOSS OF A SOLAR CELL

Cell fraction lost	Current at max. power voltage of 53.4 V, mA	Current degradation, Δi, mA
0 - 1/8	> 991	< 1
1/8 - 1/4	> 991	< 1
1/4 - 3/8	> 991	< 1
3/8 - 1/2	991	1
1/2 - 5/8	990	2
5/8 - 3/4	988	4
3/4 - 7/8	982	10
7/8 - 8/8	970	22

Maximum power current = 992 mA.
Average current degradation = 5.3 mA.

A tabulation of solar cell failures x, corresponding reliability ^{x}R, and power degradation ^{x}D is given below.

x	^{x}R	^{x}D
2	.5529	.088
3	.8044	.132
4	.9468	.176
5	.9908	.220
6	.9987	.269

WIRING RELIABILITY MODEL AND FAILURE ANALYSIS

Total Array Wiring Reliability, R_1

The total array wiring reliability, R_1 will depend upon the wiring reliability of each identical solar cell panel R_2 such that

$$R_1 = (R_2)^6 \qquad \text{(E6)}$$

as represented by the block diagram (Figure E2).

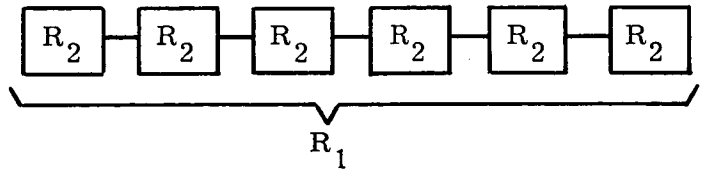

Figure E2. Total Array Wiring Reliability

Solar Panel Wiring Reliability, R_2

The reliability of a solar panel R_2 will depend upon the wiring reliability of each of the two circuits upon that panel R_3 such that

$$R_2 = (R_3)^2 \qquad \text{(E7)}$$

as represented by the block diagram (Figure E3) below.

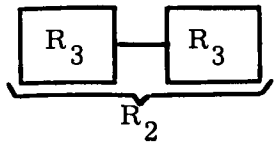

Figure E3. Solar Panel Wiring Reliability, R_2

Circuit Wiring Reliability, R_3

The circuit wiring reliability R_3 will depend upon the following reliability factors:

- R_4, the circuit negative termination reliability
- R_5, the intra-circuit connection reliability
- R_6, the circuit positive termination reliability
- R_7, the diode array and positive bus connection reliability

A block diagram which represents the circuit wiring reliability R_3 is shown in Figure E4 and is represented by the expression:

$$R_3 = R_4 \cdot R_5 \cdot R_6 \cdot R_7 \qquad \text{(E8)}$$

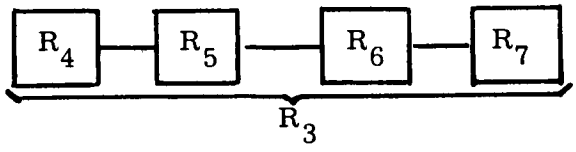

Figure E4. Circuit Wiring Reliability, R_3.

Reliability of the Circuit Negative Termination, R_4

As shown in Figure E5, redundant braided wire passes from each of two solder tabs to a stand-off connector. Insulated stranded wire passes from this standoff to the array negative bus bar.

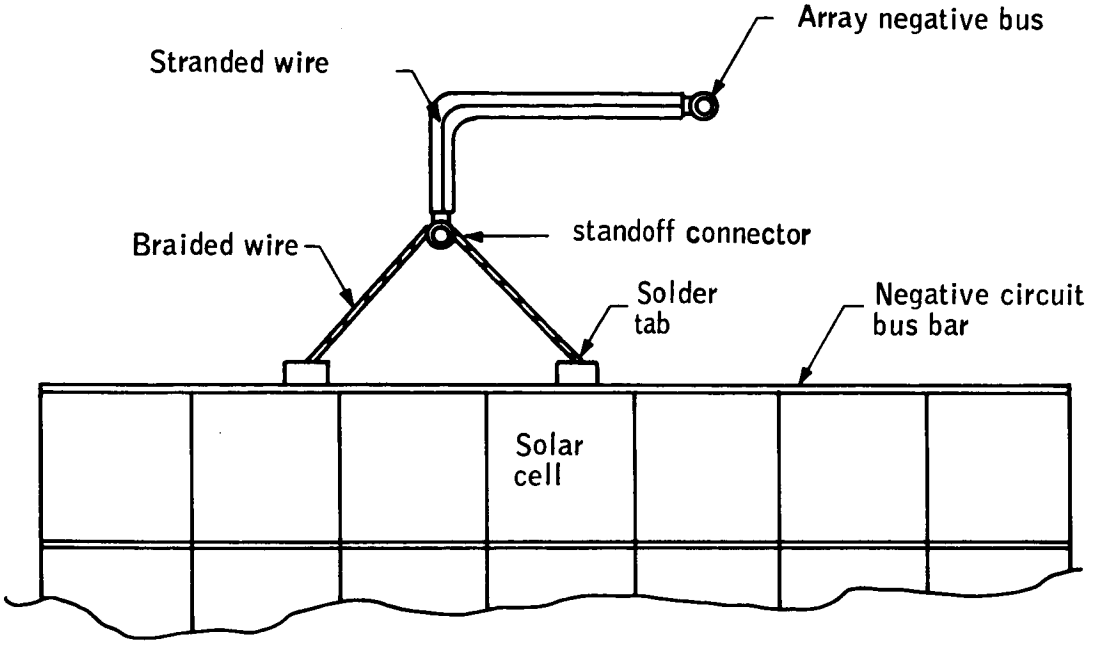

Figure E5. Circuit Negative Termination

Open-circuit failure of this connection will result in complete loss of power for the affected circuit. This will result in an 8.5-percent power degradation for the array. The probability of occurrence of such a failure is 4.8×10^{-8} per year.

A short-circuit failure to panel substrate for this connection will have no effect provided the power system is grounded at this B- potential.

The reliability of this connection will depend upon the following factors:

R_8 - Reliability of the solder tab-bus bar and solder connection. The bus tab is a rectangular piece of bus metal which measures approximately 0.125" by 0.250". The tab which is soldered to the bottom of the solar cell bus bar (in pairs) is used for the purpose of terminating a module. A braided wire is in turn soldered to this tab and is connected to a standoff connector.

R_9 - Reliability of the solder tab.

R_{10} - No "short" reliability of the braided wire.

R_{11} - No "open circuit" reliability of the braided wire.

R_{12} - Reliability of the braided wire to solder-tab solder connection.

R_{13} - Reliability of the standoff connection.

R_{14} - Reliability of braided wire to standoff solder joint.

R_{15} - No "open" circuit reliability of insulated stranded wire.

R_{16} - No "short" circuit reliability of insulated stranded wire.

R_{17} - Reliability of a stranded wire solder joint.

The reliability model for the circuit negative termination is shown in Figure E6.

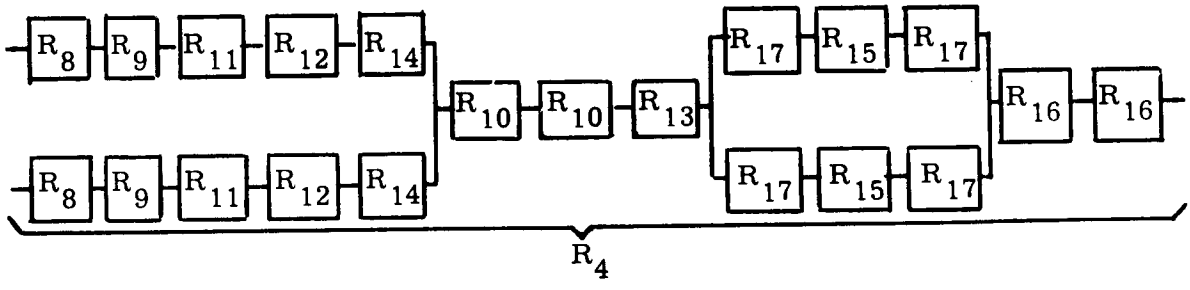

Figure E6. Circuit Negative Termination Reliability Model

Let:

$$R_{18} = R_8 \cdot R_9 \cdot R_{11} \cdot R_{12} \cdot R_{14}$$

and: $R_{19} = R_{17}^2 \cdot R_{15}$, such that the expression for this reliability is

$$R_4 = \left(R_{10} \cdot R_{16}\right)^2 R_{13} \left[1 - (1-R_{18})^2\right]\left[1 - (1-R_{19})^2\right]$$

Intra-Circuit Connection Reliability

The laydown of each individual circuit allows for two 7x54 groups of solar cells which transverse the length of the panel. These are joined at the center by the intra-circuit connection. This connection is shown in Figure E7.

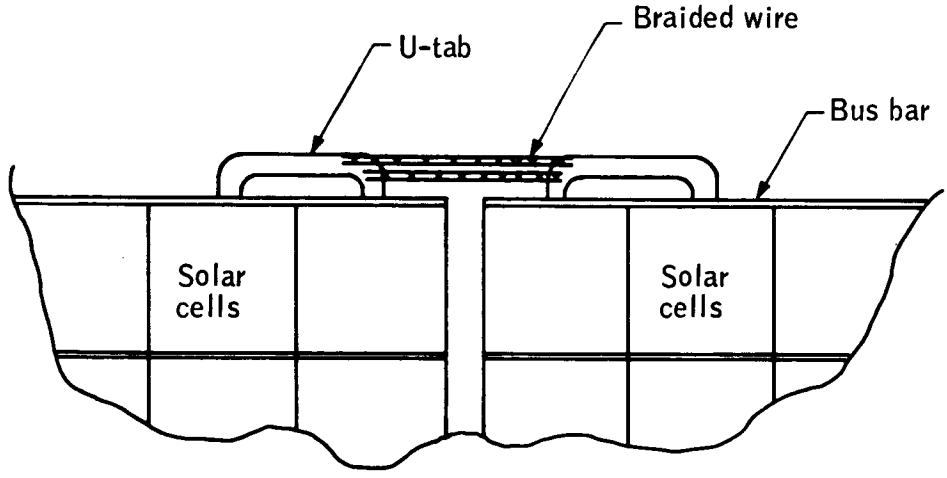

Figure E7. Intracircuit Connection

An open circuit failure of this connection will result in complete loss of power for the affected circuit. This will result in a 8.5 percent power degradation for the entire array. The probability of occurrence of such a failure is 8.8×10^{-8} per year.

A short-circuit of this connection will result in complete or partial loss of circuit power depending upon the position of any additional ground points in the circuit. The probability of occurrence of this failure is 1.76×10^{-7} per year.

The reliability R_5 of this connection will depend upon the following reliability factors in addition to those mentioned previously.

R_{20} = U-solder-tab reliability.

A model for this reliability is as shown in Figure E8.

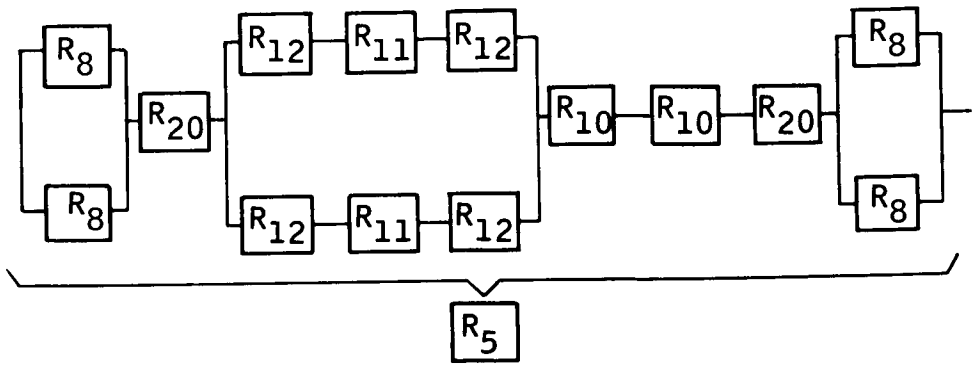

Figure E8. Reliability of an Intracircuit Connection

The expression for this reliability is:

$$R_5 = \left[1 - (1-R_8)^2\right]^2 \left(R_{10}\right)^2 \left[1 - (1-R_{11}\, R_{12}^2)^2\right] \left(R_{20}\right)^2 \qquad \text{(E10)}$$

Reliability of a Positive Circuit Termination

As shown in Figure E9, redundant, braided wires pass from each of two solder tabs to a feed-through connector.

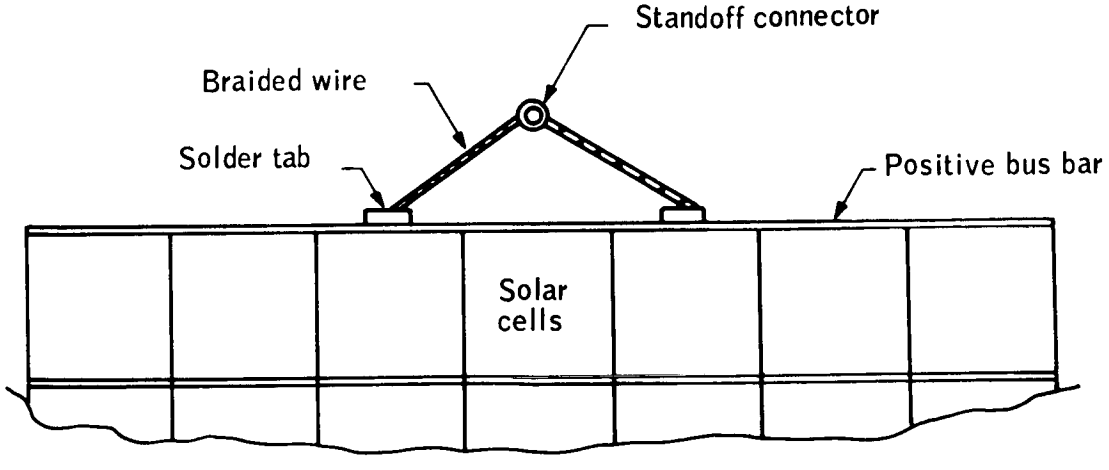

Figure E9. Circuit Positive Termination

Open-circuit failure of this connection will result in complete loss of power for the affected circuit. This will result in an 8.5-percent power degradation for the array. The probability of occurrence of such a failure is 7.1×10^{-8} per year.

A single short-circuit failure to the panel substrate will result in complete loss of power in that circuit. The probability of occurrence of this failure is 1.76×10^{-7} per year.

The reliability of a positive circuit termination R_6 will depend upon those reliability factors previously indicated. The appropriate reliability model is shown in Figure E10.

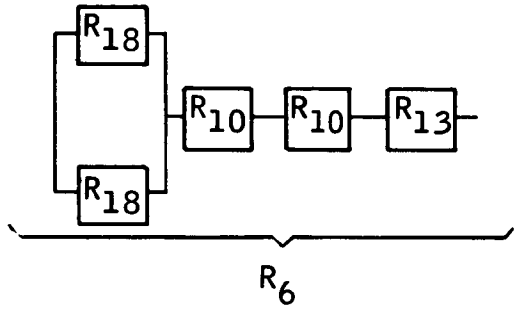

Figure E10. Reliability of a Positive Circuit Termination

The expression for this reliability is:

$$R_6 = \left(R_{10}\right)^2 R_{13}\left[1 - (1-R_{18})^2\right] \qquad \text{(E11)}$$

Reliability of the Diode Array and Positive Bus Connection

As shown in Figure E11, a redundant, insulated stranded wire passes from the positive circuit termination standoff to the diode negative standoff. Connected between the diode negative standoff and the diode positive standoff are two redundant diodes. A redundant, insulated stranded wire passes from this point to the array positive bus. One diode is sufficient to carry the current of the circuit.

An open-circuit failure of both diodes and diode connections will result in a complete loss of power for the affected circuit, an 8.5-percent power degradation resulting for the array. The probability of occurrence of this failure is 1.06×10^{-5} per year.

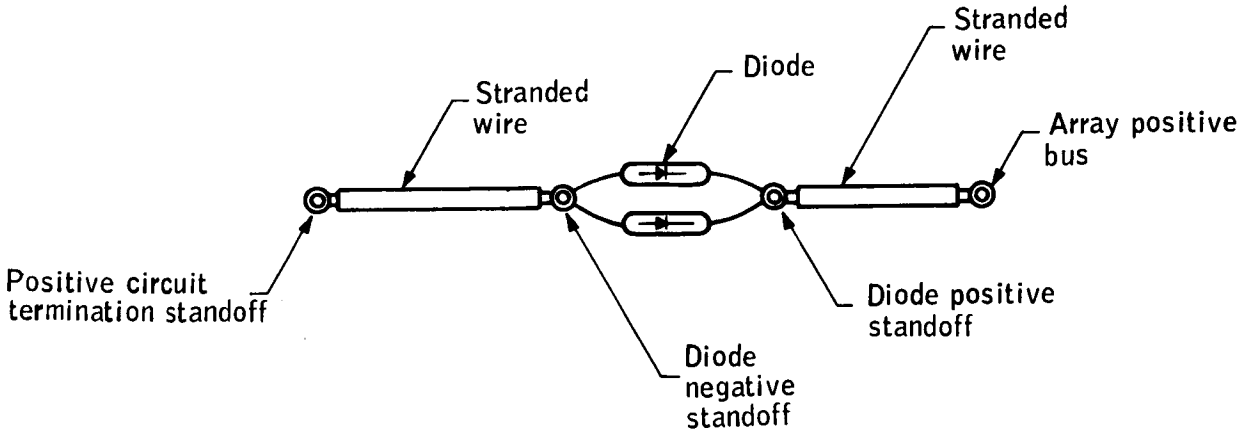

Figure E11. Diode Array and Positive Bus Connection

A short circuit to the substrate of this connection on the cell side of the diodes will result in a complete loss of power for that circuit as indicated previously. A ground on the array bus side of the diode will result in a complete loss of power for the array. The probability of occurrence of such failures is 1.76×10^{-7} per year. A short-circuit failure of either diode will cause no effect unless coupled with a short circuit in the associated circuit. The probability of both failures occurring is negligible.

The reliability R_7 of the diode array and positive bus connection will depend upon those reliability factors indicated previously and in addition:

R_{21} - the diode reliability

R_{22} - the diode solder-joint reliability

The reliability model for the diode array and positive bus connection is shown in Figure E12.

Let $R_{23} = R_{21}\left(R_{22}\right)^2$ represent the reliability of a diode and solder connection such that the reliability of the diode array and positive bus connection is given by the expression

$$R_7 = \left(R_{16}\right)^4 \left(R_{13}\right)^2 \cdot \left[1-(1-R_{19})^2\right]^2 \cdot \left[1-(1-R_{23})^2\right] \qquad \text{(E12)}$$

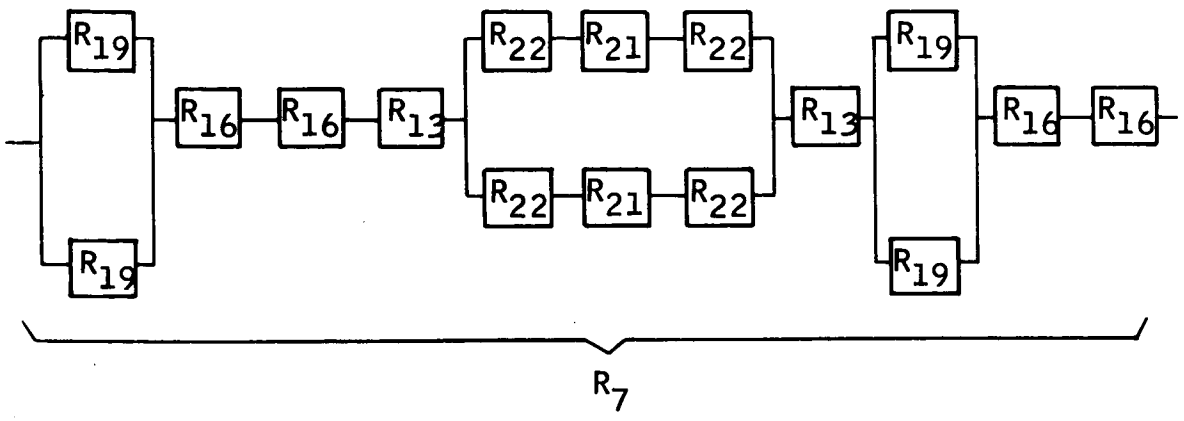

Figure E12. Diode Array and Positive Bus Connection Reliability Model

WIRING RELIABILITY CALCULATIONS

Using the latest available component failure rates as tabulated in Table E3. the reliability factors indicated in the previous section are evaluated. It should be noted that these failure rates are generated from environmental testing in some cases, while others are a result of engineering judgment. These factors have been used in previous reliability analyses on solar cell power supplies, of which no failures of the power supply have been recorded in flight. All reliability factors assume comprehensive quality control inspection and environmental testing to detect preflight failures resulting from fabrication or handling.

The reliability factors were computed and indicated in reverse numerical order in Table E4.

The array wiring reliability was calculated to be 0.99985.

TABLE E3. - FAILURE RATES

Symbol	Element	Failure rate per year	Reliability per year
R_8	Solder tab-bus solder connection	1.0×10^{-8}	.999 912
R_9	Solder tab	1×10^{-12}	.999 999 999
R_{10}	No short - braided wire	1.0×10^{-11}	.999 999 912
R_{11}	No open - braided wire	1.0×10^{-8}	.999 912
R_{12}	Braided wire to tab solder connection	1.0×10^{-8}	.999 912
R_{13}	Standoff connector	1×10^{-12}	.999 999 999
R_{14}	Braided wire to standoff solder connection	1.0×10^{-11}	.999 999 912
R_{15}	No open - stranded wire	1.0×10^{-8}	.999 912
R_{16}	No short - stranded wire	1.0×10^{-11}	.999 999 912
R_{17}	Stranded wire to standoff solder connection	1.0×10^{-11}	.999 999 912
R_{20}	U tab	1×10^{-12}	.999 999 999
R_{21}	Diode	3.5×10^{-7}	.996 93
R_{22}	Diode to standoff solder connection	1.0×10^{-8}	.999 912

TABLE E4. - RELIABILITY FACTORS AND EQUATIONS

Factor	Value/year
$R_{23} = R_{21}\left(R_{22}\right)^2$	.996 76
$R_{19} = R_{15}\left(R_{17}\right)^2$	.999 911
$R_{18} = R_8 \cdot R_9 \cdot R_{11} \cdot R_{12} \cdot R_{14}$	.999 735
$R_7 = \left(R_{16}\right)^4\left(R_{13}\right)^2\left[1 - (1-R_{19})^2\right]^2\left[1 - (1-R_{23})^2\right]$	.999 989
$R_6 = \left(R_{10}\right)^2 R_{13}\left[1 - (1-R_{18})^2\right]$	.999 999 74
$R_5 = \left[1 - (1-R_8)^2\right]^2\left(R_{10}R_{20}\right)^2\left[1 - (1-R_{11}R_{12})^2\right]^2$	.999 999 73
$R_4 = \left(R_{10}R_{16}\right)^2 R_{13}\left[1 - (1-R_{18})^2\right]\left[1 - (1-R_{19})^2\right]$	.999 999 70
$R_3 = R_4 \cdot R_5 \cdot R_6 \cdot R_7$	.999 988
$R_2 = \left(R_3\right)^2$	.999 976
$R_1 = \left(R_2\right)^6$	.999 85

TOTAL ARRAY RELIABILITY

The total array reliability is the product of the array wiring reliability and the solar cell reliability

$$R = R_1 \cdot {}^{x}R \tag{E13}$$

as represented by the diagram Figure E13.

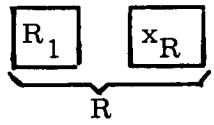

Figure E13. Total Array Reliability

For a maximum of five anticipated solar cell failures corresponding to a maximum anticipated power degradation of 0.22 percent, there is a probability of successful operation for one year of the solar cell array of $R = 0.99985 \times 0.9908 = 0.9906$.

For a maximum of six anticipated solar cell failures, corresponding to a maximum anticipated power degradation of 0.26 percent, there is a probability of successful operation for one year of the solar cell array of $R = 0.99985 \times 0.9987 = 0.9986$.

It must be noted that the relatively high reliability is the result of the fact that each circuit has seven solar cells in parallel, thus minimizing the current-limiting effect of a solar cell failure. Also, the minimization of circuit wiring and use of redundancy contributes greatly to the favorable results.

REFERENCES

1. Bauer, P.; and Sparks, R.H.: Nickel-Cadmium for the Orbiting Geophysical Laboratory. Vol. 2. NASA Goddard Contract No. NASS - 899 TRW, 12 February 1964.

2. Bruess, E.C.: The Evaluation Program for Secondary Spacecraft Cells. Second Annual Report, Quality Evaluation Laboratory, U.S. Naval Ammunition Depot, Crane, Indiana. NASA Goddard Contract No. W-11, 252B, 13 May 1966.

3. Anon.: Life Cycle Tests. Monthly Progress Report, U.S. Naval Ammunition Depot, Crane, Indiana, November 1966.

4. Hennigan, Thomas J.; and Sizemore, Kenneth O.: Charge Control Devices, Charge Control Ag Cd Cells, and Ag. Zn Cells. Procedures of the 20th Annual Power Sources Conference, 24, 25, and 26 May 1966.

5. Vette, James: Models of the Trapped Radiation Environment. Aerospace Corporation, NASA SP-3024.

6. Modisette, Jerry; et al.: Model Solar Proton Environments for Manned Spacecraft Design. NASA TN D-2746, April 1965.

7. Fichtel, C.F.; Guss, H.E.; and Malitson, H.H.: Solar Proton Manual. NASA TR R-169, December 1963.

8. Rosenzweig: Radiation Damage Studies. Photovoltaic Specialists Conference (Washington, D.C.), 10-11 April 1963.

9. Campbell, F.J.: Effects of Shielding on Electron Damage to Solar Cells. Proceedings of the 4th Photovoltaic Specialists Conference (Cleveland, Ohio), 2 June 1964.

10. Haynes, G.A.; and Patterson, J.L.: Effects of High-Energy Electron Radiation on Solar Cell Shields. Transcript of the Photovoltaic Specialists Conference, Vol. II, Report on Systems Experience, Applications and Design, 11 April 1963, pp. D-1-1, D-1-2.

11. Hagnos, Joseph G.: Investigation of Resinous Materials for Use as Solar Cell Cover Glass Adhesive. NASA Goddard Space Flight Center, September 1965.

12. Air Force Systems Command: Space Planners Guide. USGPO, 1965, 0-774-405, 1 July 1965.

13. Garrett, P.G.; and Pomroy, S.E.A.: Continuous Charge-Discharge Cycling Studies on Hermetically Sealed Nickel-Cadmium Cells Operating at Ten Percent Depth of Discharge. Technical Report No. 66045, Royal Aircraft Establishment, Farnborough-Hants, England, February 1966.

14. RCA Astro-Electronics Division: Tiros X Meteorological Satellite System Final Engineering Report. Vol. 1, AED-R-2801, 14 January 1966, p. II-28.

15. Harris, C.A.: Spacecraft Component Magnetic Field Restraints. U.S. Government Memorandum - Report No. 655-015, 12 August 1965.

16. Parsons, C. Leland: Magnetic Testing of Spacecraft. U.S. Government Memorandum - Report No. 655-016, 13 June 1966.

17. Smith, G. Louis: A Theoretical Study of the Torques Induced by a Magnetic Field on Rotating Cylinders and Spinning Thin-Wall Cones, Frustums and General Body of Revolution. NASA TR R-129, 1962.

18. Haynes, Gilbert A.; and Miller, William E.: Effects of 1.2 and 0.30 MEV Electrons on the Optical Transmission Properties of Several Transparent Materials. NASA TN D-2620. March 1965.

19. Rosenzweig, W.: Space Radiation Effects in Silicon Devices. IEEE Transactions on Nuclear Science, Vol. NS 12, October 1965, pp. 18 - 29.

May 1967

NASA CR-66378

CONCEPTUAL MECHANIZATION STUDIES FOR A HORIZON DEFINITION SPACECRAFT ELECTRICAL POWER SUBSYSTEM

By Otto L. Jourdan, Honeywell Inc.
Jay A. Cox, Gulton Industries, Inc.
John D. Gum, Spectrolab
Karl Preusse, Gulton Industries, Inc.
James J. Baltes, Honeywell Inc.
David J. Hartman, Honeywell Inc.
Fred E. Betz, Gulton Industries, Inc.
Burton J. McComb, Gulton Industries, Inc.

ABSTRACT

A solar cell-battery electrical power subsystem was developed which is compatible with the Horizon Definition Study spacecraft. This subsystem is capable of delivering 70 watts ot continuous electrical power for one year in a sun-synchronous, 3 o'clock nodal crossing, 500 km orbit.